Discovering and Using Patterns for Countering Security Challenges

by

Ziming Zhao

A Dissertation Presented in Partial Fulfillment
of the Requirements for the Degree
Doctor of Philosophy

Approved September 2014 by the
Graduate Supervisory Committee:

Gail-Joon Ahn, Chair
Stephen S. Yau
Dijiang Huang
Raghu Santanam

ARIZONA STATE UNIVERSITY

December 2014

ProQuest LLC.
789 East Eisenhower Parkway
P.O. Box 1346
Ann Arbor, MI 48106 - 1346

ABSTRACT

Most existing security decisions for both defending and attacking are made based on some deterministic approaches that only give binary answers. Even though these approaches can achieve low false positive rate for decision making, they have high false negative rates due to the lack of accommodations to new attack methods and defense techniques. In this dissertation, I study how to discover and use patterns with uncertainty and randomness to counter security challenges. By extracting and modeling patterns in security events, I am able to handle previously unknown security events with quantified confidence, rather than simply making binary decisions. In particular, I cope with the following four real-world security challenges by modeling and analyzing with pattern-based approaches: 1) How to detect and attribute previously unknown shellcode? I propose instruction sequence abstraction that extracts coarse-grained patterns from an instruction sequence and use Markov-chain-based model and support vector machines to detect and attribute shellcode; 2) How to safely mitigate routing attacks in mobile ad hoc networks? I identify routing table change patterns caused by attacks, propose an extended Dempster-Shafer theory to measure the risk of such changes, and use a risk-aware response mechanism to mitigate routing attacks; 3) How to model, understand, and guess human-chosen picture passwords? I analyze collected human-chosen picture passwords, propose selection function that models patterns in password selection, and design two algorithms to optimize password guessing paths; and 4) How to identify influential figures and events in underground social networks? I analyze collected underground social network data, identify user interaction patterns, and propose a suite of measures for systematically discovering and mining adversarial evidence. By solving these four problems, I demonstrate that discovering and using patterns could help deal with challenges in computer security, network security, human-computer interaction security, and social network security.

Dedicated to my family

ACKNOWLEDGEMENTS

First, I want to thank my wife Yiqi Zhao, my parents Dejun Zhao and Youjun Yuan, my mother-in-law Rong Zhao, my cousins Ye Yuan and Xin Yuan. I am the person I am today because of them. Without the support, understanding, and encouragement from them, I could never finish this degree.

I am grateful to my PhD advisor Prof. Gail-Joon Ahn. Prof. Ahn supported me to pursue my own research interest professionally, financially, and emotionally. He is an extremely visionary researcher, and discussions with him have always been rewarding. He helped me with every step of the way to my dissertation and my degree. Prof. Ahn is a true gentleman who treated me as an equal since the first day we met and opened a lot of doors for me in both academia and industry.

I am grateful to my PhD committee members, Prof. Stephen S. Yau, Prof. Dijiang Huang, and Prof. Raghu Santanam. I have learned so much from the classes they taught and the questions they asked for my comprehensive exam. I appreciate the assistance and guidance they provided in preparation of my dissertation proposal and this dissertation. I am grateful to Prof. Partha Dasgupta, Prof. Guoliang Xue, and Prof. Rida Bazzi for their guidance and encouragement.

This dissertation would not be possible without the support of many people at SEFCOM. I would like to express my gratitude to my coauthors, collaborators, labmates and friends at SEFCOM, in particular, Prof. Hongxin Hu (Clemson University), Ruoyu Wu, Yiming Jing, Michael Mabey, Jeong-Jin Seo, Wonkyu Han, Mukund Sankaran, Deepinder Mahi, Dr. Dae-il Jang, Darin Tupper, Dominic Chen, Justin Paglierani, Sowmya Challa, Monika Szalamacha, James Holmes, Clinton D'souza, Jeremy Whitaker, Carlos Rubio, Hadi Sharifi, Michael Sanchez, Patrick Trang, Pradeep Sekar, Ketan Kulkarni, Prof. Tae-Sung Kim (Chungbuk National University), Prof.

Namje Park (Jeju National University), Prof. Juan Wang (Wuhan University), Yusef Shaban, and Joshua Frisby.

I would like to thank my colleagues in ASU but outside of SEFCOM. The discussions with them have helped my research tremendously. They are Dr. Xi Fang, Prof. Dejun Yang (Colorado School of Mines), Dr. Jin Zhang, Dr. Qiang Zhang, Prof. Rui Zhang (University of Hawaii), Dr. Lingjun Li, Xinxin Zhao, Xiang Zhang, Yashu Liu, Jun Shen, and Chuan Huang.

I thank my friends who are not mentioned above. They are Yadong Shen, Fengze Xie, Prof. Su Dong (Fayetteville State University), Wu Li, Xinhui Hu, Wei Huang, Tianyi Xing, Yuan Wang, Abdullah Alshalan, Jian Cai, Heng Chen, Meng Chen, Ke Bai, Jing Lu, Jing Huang, Che Liu, Jie Zhu, Xiaoping Li, Ruozhou Yu, Albion Hargrave, and Jo-Nell Hargrave. Thank you for making my PhD journey very enjoyable.

TABLE OF CONTENTS

Page

LIST OF TABLES x

LIST OF FIGURES xi

CHAPTER

1 INTRODUCTION 1

1.1 Proposed Pattern-based Approach Framework 2

1.2 Contributions of This Dissertation 5

1.3 Previous Publications 9

2 MATHEMATICAL PREREQUISITES 11

2.1 Probability Theory 11

2.2 Dempster-Shafer Theory 13

2.3 Markov Models 15

2.4 Support Vector Machines 16

3 DETECTING AND ATTRIBUTING SHELLCODE 18

3.1 Introduction 18

3.2 Background 22

3.2.1 Differentiating Code from Data 22

3.2.2 IA-32 Instruction Format 23

3.3 Motivating Examples of Instruction Patterns 24

3.4 Overview of Extracting and Using Instruction Patterns 27

3.5 Automatic Extraction of Instruction Patterns 28

3.5.1 Customized Linear Sweep Disassembly 28

3.5.2 Feature Selection 29

3.5.3 Instruction Sequence Abstraction 33

3.6 Using Instruction Patterns to Detect and Attribute Shellcode 34

CHAPTER Page

3.6.1 Detecting Shellcode 35
3.6.2 Attributing Encoded Shellcode 36
3.7 Implementation 37
3.7.1 Data Collection and Implementation 37
3.7.2 Instruction Patterns Identification 39
3.8 Evaluation 39
3.8.1 Evaluation of Detecting Shellcode 39
3.8.2 Evaluation of Attributing Encoded Shellcode 42
3.8.3 The Strength of Encoding Engines 47
3.8.4 Performance Evaluation 50
3.9 Discussion 50
3.9.1 The Feasibility of Using One Model 50
3.9.2 Using Opcode Functionality Sequence to Detect Shellcode . . 51
3.9.3 The Arms Race and Future Work 52
3.10 Related Work 52
3.11 Summary 54
4 MITIGATING MANET ROUTING ATTACKS 56
4.1 Introduction 56
4.2 Background 58
4.2.1 OLSR Protocol 58
4.2.2 Routing Attack on OLSR 60
4.3 Extended Dempster-Shafer Theory of Evidence 61
4.3.1 Importance Factors and Belief Function 62

CHAPTER Page

4.3.2 Expected Properties for Our Dempster's Rule of Combination with Importance Factors 64
4.3.3 Dempster's Rule of Combination with Importance Factors . . 65
4.4 Overview of Risk-Aware Response Mitigation for MANET Routing Attacks 67
4.4.1 Response to Routing Attacks 69
4.5 Risk Assessment Based on Routing Table Change Patterns 70
4.5.1 Discovering Routing Table Change Patterns 71
4.5.2 Combination of Evidence 73
4.6 Adaptive Decision Making 74
4.7 Case Study and Evaluation 75
4.7.1 Methodology and Metrics 76
4.7.2 Case Study 78
4.7.3 Evaluation with Random Network Topologies 82
4.8 Related Work 83
4.9 Summary 85
5 GUESSING PICTURE PASSWORDS 86
5.1 Introduction 86
5.2 Background: Picture Gesture Authentication 88
5.3 User Choice Patterns in Picture Gesture Authentication Passwords . 90
5.3.1 Experiment Design 90
5.3.2 Findings 94
5.3.3 Memorability and Usability Analysis 100
5.4 Using User Choice Patterns to Attack PGA Passwords 101

CHAPTER Page

5.4.1 Attack Models . . . 101
5.4.2 Password and PoI Representations . . . 102
5.4.3 Location-dependent Gesture Selection Functions . . . 103
5.4.4 LdGSF Sequence List Generation and Ordering . . . 107
5.4.5 Password Dictionary Generation . . . 111
5.5 Implementation . . . 112
5.5.1 PoI Identification . . . 112
5.5.2 LdGSF Identification . . . 114
5.6 Attack Evaluation . . . 116
5.6.1 Nontargeted Attack Evaluation . . . 116
5.6.2 Targeted Attack Evaluation . . . 126
5.7 Discussion . . . 128
5.7.1 Picture-Password-Strength Meter . . . 128
5.7.2 Other Attacks on PGA . . . 129
5.7.3 Limitations of Our Study . . . 129
5.8 Related Work . . . 130
5.9 Summary . . . 131
6 DISCOVERING UNDERGROUND INTELLIGENCE . . . 132
6.1 Introduction . . . 132
6.2 Patterns in Cybercrime . . . 135
6.3 Using Social Interaction Patterns to Discover Intelligence . . . 138
6.3.1 Online Underground Social Dynamics Model . . . 139
6.3.2 Principles of Metric Design and Definitions . . . 141
6.3.3 Ranking Metrics . . . 144

CHAPTER Page

6.4 System Design and Implementation 147
6.4.1 Challenges from Real-world Data 147
6.4.2 System Architecture and Implementation 148
6.4.3 Visualization Interfaces of Our Tool 150
6.5 Experiments on Synthetic Social Dynamics Data 151
6.6 A Case Study on Real-world Online Underground Social Dynamics . 153
6.6.1 Post, User and Group Analysis 154
6.6.2 Evidence Mining by Correlating Social Dynamics with Adversarial Events 158
6.6.3 Comparison with HITS Algorithm 162
6.7 Related Work 164
6.8 Summary 165
7 CONCLUSION 166
7.1 Contributions 166
7.2 Future Work 168
REFERENCES 169

LIST OF TABLES

Table Page

3.1 Shellcode Dataset Comparison 36

3.2 Top 50 Opcode Transition Patterns 40

3.3 The Strength of Encoders 48

3.4 Shellcode Attribution Time Cost (millisecond) 49

4.1 Risk Assessment and Decision Making 80

5.1 Survey Question: Which of the following best describes what you are considering when you choose locations to perform gestures? 93

5.2 Attributes of Most Frequently Used PoIs 96

5.3 Numbers of Gesture-order Patterns 98

5.4 Numbers of Gesture Type Combinations and Average Time Spent on Creating Them 99

5.5 Top 10 Identified LdGSFs Using $P^2_{L\text{-}15}$ 115

5.6 Top 10 Identified LdGSFs Using $P^2_{A\text{-}40}$ 116

6.1 Top Five Influential/Active Users 155

6.2 Top Five Influential/Active Groups 155

6.3 Results from Our Tool for Queries 159

6.4 Selected Top Relevant Articles 160

6.5 Selected Articles by crx_ur and Her/His Information 161

6.6 Information about dx_ur 161

6.7 Selected Top Relevant Articles 163

6.8 Top Five Authorities and Hubs by HITS 163

LIST OF FIGURES

Figure		Page
1.1	The Security Cycle (a) Defenders' Perspective (b) Attackers' Perspective	3
1.2	Proposed Pattern-based Approach Framework	4
3.1	IA-32 Architecture Instruction Format	24
3.2	Motivating Examples of Instruction Patterns	25
3.3	Overview of the Approach of Using Instruction Patterns to Detect and Attribute Shellcode	27
3.4	Instruction Sequence Abstraction Example	34
3.5	Encoded Shellcode Samples Collection	38
3.6	The S-score Distribution with Different k	41
3.7	Shellcode Radar Charts	43
3.8	Attribution Accuracy with Four Kernel Functions	45
3.9	Accuracy with Increasing Number of Shellcode Classes	47
4.1	Risk-Aware Response Mechanism	69
4.2	An Example of Link Spoofing Attack	70
4.3	Adaptive Decision Making	75
4.4	Routing Tables	76
4.5	Performance Results in Three Stages Comparing DRCIF with Binary Isolation and DRC	79
4.6	Performance Results in Five Random Topologies Comparing DRCIF with Binary Isolation and DRC	81
5.1	Background Pictures Used in *Dataset-2*	92
5.2	Two Versions of *Starry Night* and Corresponding Passwords	97
5.3	Memorability and Usability	100

Figure Page

5.4 (a) Background Picture and Password (b) User's Selection Processes that Were Taken From Pace (2011b) (c) Corresponding LdGSFs that Simulate User's Selection Processes 104

5.5 (a) Background Picture and Identified PoIs (b) Identified PoIs (c) Password Representations (Colors are used to indicate the connections between the PoIs in (b) and LdGs in (c)) 105

5.6 PoI Identification on Example Pictures in *Dataset-2*: (a) Original Pictures (b) Circle Detection with Hough Transform (c) Contour Detection (d) Objectness Measure (e) Object Detection 113

5.7 (a) Percentage of passwords cracked vs. number of password guesses, per condition. (b) Percentage of LdGs cracked vs. number of password guesses, per condition. For *Dataset-1*, there are 86 passwords that include 258 LdGs. For *Dataset-2*, there are 10,039 passwords that have 30,117 LdGs. 117

5.8 (a) Percentage of passwords cracked vs. number of password guesses, per condition. (b) Percentage of LdGs cracked vs. number of password guesses, per condition. Only the first chosen password by each subject in *Dataset-2* was considered. There are 762 passwords that have 2,286 LdGs. 119

5.9 (a) Percentage of passwords cracked vs. number of password guesses, per condition. (b) Percentage of LdGs cracked vs. number of password guesses, per condition. Only passwords for pictures 243, 1116, 2057, 4054, 6467, and 9899 were considered. There are 4,003 passwords that have 12,009 LdGs. 120

Figure Page

5.10 Online attacks. (a) Number of passwords cracked within five guesses, per condition. (b) Number of LdGs cracked within five guesses, per condition. 122

5.11 (a) Average number of passwords cracked vs. different training data sizes. (b) Average number of LdGs cracked vs. different training data sizes. $P^2_{A\text{-}40}$ is used for this analysis. Average over 3 analyses, with one standard deviation shown. 123

5.12 (a) pictures with fewer PoIs (b) portraits (c) pictures with people in them (d) pictures with lots of PoIs. Unbiased algorithm on $P^2_{A\text{-}40}$ is used for this analysis. 125

5.13 Average runtime in seconds to order LdGSF sequences using BestCover and Unbiased. Average over 15 pictures in *Dataset-2* with one standard deviation shown. 126

5.14 Offline attacks. There are 9,974 passwords from 697 accounts in this experiment. The average size of training data sets is around 13. (a) Percentage of passwords cracked vs. number of password guesses, per condition. (b) Passwords cracked per account. Each horizontal bar represents a condition. Regions within each bar show the fraction of accounts for which the indicated number of passwords were cracked. . . . 127

6.1 Cybercrime Workflow 135

6.2 Motivating Example of Malware Distribution and Evolution in Social Dynamics (All screenshots taken from Holt (2008)) 137

6.3 Online Underground Social Dynamics Model: Entities and Relationships 139

6.4 SocialImpact: Systematic Ranking Indices 144

Figure Page

6.5 System Architecture of Our Tool 149
6.6 Screenshots of Our Tool 150
6.7 An OUSD Scenario 152
6.8 Indices According to Our Solution and PageRank 153
6.9 Comparison of Normalized Indices for Each User 153
6.10 Correlation Coefficient of UserActiveness & UserInfluence and GroupActiveness & GroupInfluence 156
6.11 Temporal Pattern Analysis 157

Chapter 1

INTRODUCTION

Discovering and using patterns in data is the process of discovering *regularities* in either a manual or an automatic way and using discovered regularities as supporting *evidence* to assist decision making such as predicting the outcomes of available actions. Patterns are everywhere, and the history of discovering and using patterns has been successful long before the invention of computers. The most famous story about the discovery of patterns in all times may be how Issac Newton defined the law of universal gravitation which was inspired by the *observations* of falling apples. Unfortunately, not all patterns can be described by a deterministic equation such as the equation of the law of universal gravitation. Most patterns follow a *skewed probability distribution* and their representations need the mathematical foundations of multiple theories. After we entered the era of computers, algorithms have been designed to automate the process of both discovering and using patterns with randomness and uncertainty. The research fields to improve such algorithms are known as pattern recognition, data mining, and machine learning which have achieved successes in many domains, such as face recognition, voice control, and text search.

The typical workflow of discovering patterns starts from observing the behaviors of the targets, a process known as signal acquisition. After signals are collected, preprocessing and feature extraction take place to remove redundant data and highlight salient characteristics, respectively. Even though there exists some pure statistical ways to do preprocessing and feature extraction, both of them require some *domain knowledge* of the targets and their signals to obtain more reliable and explainable results. The next step, which requires domain knowledge as well, is to select and build

models to best fit the extracted features. The generated models are used for future predictions and decision making, aka using patterns. Through the process of pattern discovery and modeling, regularities are encoded as mathematical models which are ready for using.

Security researchers and practitioners have been using two types of approaches to discover and use patterns in security events to solve security problems for decades. The first type of approaches uses predetermined patterns. Commercially popular anti-virus systems and intrusion detection systems are using malware signatures, a predefined sequence of bits, to tell if the captured samples are known malwares. Even if such misuse-based systems could minimize the false positive rate of malware detection, they could not detect new malware variants that do not contain that predefined bit sequences; hence they introduce high false negative rate. The other type of approaches uses statistical patterns. The first instance may be the intrusion detection model Denning (1986) proposed in 1986 by Dorothy E. Denning who designed to monitor a system's audit records and detect abnormal patterns of system usages with statistical models. However, pure statistical approaches overlook the root cause of the problems, and their results are usually inexplicable.

1.1 Proposed Pattern-based Approach Framework

In order to find out stages where discovering and using patterns might be applicable and beneficial in the security cycles, it is important to model the defense and attack processes from defenders' and attackers' perspectives. As shown in Figure 1.1(a), we model the security cycle of defenders as three stages for simplicity: *protection*, *detection*, and *response*. Protection is the stage where security policies are enforced. Detection is used to check if the protection mechanisms are breached and security policies are violated. When policy violations are confirmed, responses are

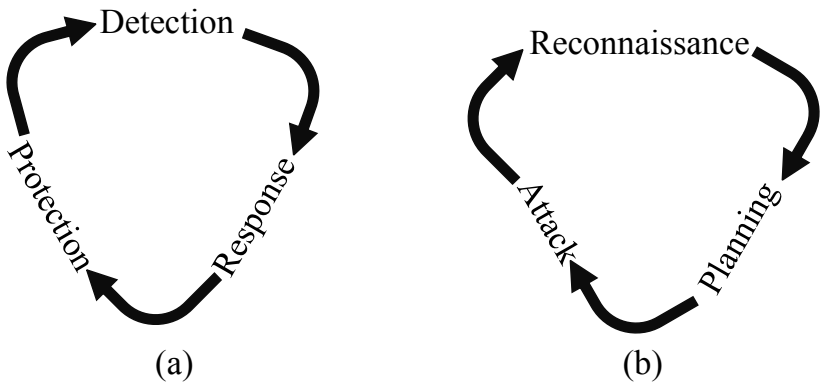

Figure 1.1: The Security Cycle (a) Defenders' Perspective (b) Attackers' Perspective

taken place to mitigate the threats. Obviously, patterns can be discovered and used in the detection stage, which is the practice adopted in Denning (1986). In Chapter 3, we show how to discover and use instruction patterns for shellcode *detection* and attribution. In Chapter 4, we show that routing table change patterns can be used to measure the risk of MANET attacks and guide *response*.

On the other hand, the security cycle of attackers consists of *reconnaissance*, *planning*, and *attack* as shown in Figure 1.1(b). Reconnaissance is the process that attackers gather information of potential targets and choose targets based on it. Planning is the stage where attack tactics and approaches are designed and prepared. The actual attacks are then carried out on the targets for attackers' benefits. Since direct intelligence is not available in many cases, patterns in side channel information are used to infer target intelligence in reconnaissance Al-Saleh and Crandall (2011). In Chapter 5, we show that user-choice patterns in picture passwords can be used by attackers for *planning*. In Chapter 6, we show that how to use social interaction patterns in the underground dynamics for *reconnaissance*.

We propose a pattern-based approach framework as shown in Figure 1.2, whose goal is to handle previously unknown security events by considering their root causes, randomness and uncertainty and at the same time quantify the confidence of decision

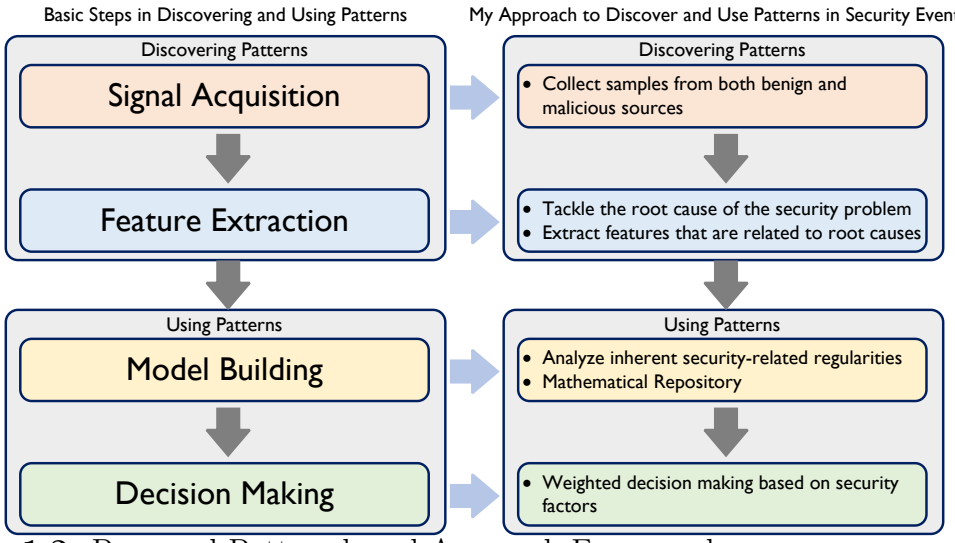

Figure 1.2: Proposed Pattern-based Approach Framework

making. Different from pre-determined pattern-based approaches, our approach does not rely on fixed bit sequences, but considers randomness and uncertainty. Thus, our approach can cope with previously unknown security events. Different from statistical pattern-based approaches that leave the feature discovery to statistical methods, our pattern-based approaches focuses on using the domain knowledge in each security problem to discover regularities and tackle root causes directly. Therefore, the reasons for such regularities to occur are explainable and interpreted in a security-related way. Our pattern-based approach framework has four major steps: i) signal acquisition, in which we collect samples from both benign and malicious sources. The instances of applying this step to solve different challenges can be found in Section 3.3, Section 4.5, Section 5.3, and Section 6.2; ii) feature extraction, in which we extract the features that are related to the root cause of each problem. The instances of applying this step to solve different challenges can be found in Section 3.5.3, Section 4.5.1, Section 5.3, and Section 6.3; iii) model building, in which we use the tools in our mathematical repository to describe the discovered security-related regularities. The instances of applying this step to solve different challenges can be found in Section 3.6, Section 4.3,

Section 5.4.3, and Section 6.3.1; and iv) decision making, in which we design weighted decision making to quantify our decision confidence. The instances of applying this step to solve different challenges can be found in Section 3.6, Section 4.6, Section 5.4.4, and Section 6.3.3.

1.2 Contributions of This Dissertation

This dissertation studies and addresses four security challenges: i) how to detect and attribute shellcode; ii) how to safely mitigate network routing attacks; iii) how to guess picture passwords; and iv) how to discover underground social intelligence. These four problems represent security challenges in four different domains: computer security, network security, human-computer interaction security, and human social network security. The common thread throughout the research on these different problems is applying the techniques of discovering and using patterns to model, analyze, and solve security-related issues. A brief introduction of each problem and the contributions from this dissertation are summarized as follows:

Among the list of 2011 CWE/SANS most widespread and dangerous software errors, fifteen out of twenty-five could lead to remote code injection and execution attacks Mitre (2011). Among all kinds of code injection attacks, binary code injection is the most destructive one. A successfully exploited system gives the direct control of its CPU, the binary code interpreter, to the adversaries that have all the privileges of the subverted processes One (1996). The malicious injected codes in this category is also named shellcode since they used to return a command shell to the attackers. For shellcode detection and attribution, we apply the proposed pattern-based approach framework and make the following contributions:

- (Signal Acquisition) We collect benign and malicious binary code samples and look into the instruction patterns shown in these sample.

- (Feature Extraction) We analyze the reason for such patterns and propose instruction sequence abstraction, a coarse-grained feature extraction method on the instruction sequence that reduces the size of input data dimension, removes confusing byte characteristics, and keeps distinguishable instruction features.

- (Model Building and Decision Making) We design a Markov-chain-based model to capture the observed sequential patterns for shellcode detection. Our detection approach is location-independent and length-independent, hence it supports on-line shellcode detection on suspicious data streams.

- (Model Building and Decision Making) We apply support vector machines to capture distributional patterns shown in the instruction sequence abstraction for understanding encoded shellcode attribution.

Mobile Ad hoc Networks (MANET) are utilized to set up wireless communication in improvised environments without a predefined infrastructure or centralized administration. The network topologies of MANET are frequently changed due to the unpredictable mobility of nodes. Furthermore, each mobile node in MANET plays a router role while transmitting data over the network. Hence, any compromised nodes under an adversary's control could cause significant damage to the functionality and security of its network since the impact would propagate in performing routing tasks. For mobile ad hoc network routing attack mitigation, we apply the proposed pattern-based approach framework and make the following contributions:

- (Signal Acquisition) We look into the routing table change patterns when routing attacks happen in MANET environment.

- (Feature Extraction) We identify several categories of routing table change patterns and measure the impact of each pattern category.

- (Model Building) We propose an extended Dempster-Shafer evidence model with importance factors and articulate expected properties for Dempster's rule of combination with importance factors. Our Dempster's rule of combination with importance factors is nonassociative and weighted.

- (Decision Making) We propose an adaptive risk-aware response mechanism with the extended D-S evidence model, considering damages caused by both attacks and countermeasures. The adaptiveness of our mechanism allows us to systematically cope with MANET routing attacks.

Picture Gesture Authentication Johnson (2012) has been recently introduced as an alternative login experience to text-based password on such devices. In particular, the new Microsoft Windows 8™ operating system adopts such an alternative authentication to complement traditional text-based authentication. This new authentication mechanism hit the market with miscellaneous computing devices including personal computers and tablets Microsoft (2013). Consequently, it is imperative to examine and explore potential attacks on picture gesture authentication in such a prevalent operating system for further understanding user experiences and enhancing this commercially popular picture password system. For picture gesture password guessing, we apply the proposed pattern-based approach framework and make the following contributions:

- (Signal Acquisition) We compile two datasets of PGA usage from user studies and perform an empirical analysis on collected data to understand user choice in background picture, gesture location, gesture order, and gesture type.

- (Feature Extraction) We identify the most popular user-choice patterns in gesture location, gesture order, and gesture type.

- (Model Building) We introduce the concept of selection function that abstracts and models users' selection processes when selecting their picture passwords. We demonstrate how selection functions can be automatically identified from training datasets.

- (Decision Making) We propose a novel attack framework that is able to generate ranked password dictionaries based on selection functions.

Existing research on net-centric attacks has focused on the detection of attack events on network side and the removal of rogue programs from client side. However, such approaches largely overlook the way on how attack tools and unwanted programs are developed and distributed. Recent studies in underground economy reveal that suspicious attackers heavily utilize online social networks to form special interest groups and distribute malicious code. Consequently, examining social dynamics, as a novel way to complement existing research efforts, is imperative to systematically identify attackers and tactically cope with net-centric threats. For underground social intelligence discovery, we apply the proposed pattern-based approach framework and make the following contributions:

- (Signal Acquisition) We study the role of underground social dynamics in the whole underground economy. We collect a dataset of user interactions of an underground social network.

- (Feature Extraction and Model Building) We study the user interactions in this dataset. And, we formulate an online underground social dynamics model considering both social relationships and user-generated contents.

- (Model Building and Decision Making) We propose a suite of measures to systematically quantify social impacts of individuals and groups along with their

online conversations which facilitate adversarial evidence acquisition and investigation.

1.3 Previous Publications

This dissertation incorporates materials from several of my previous conference papers, a journal paper and a book chapter. The concepts and techniques of using instruction patterns to detect and attribute shellcode in Chapter 3 were discussed in conference papers:

- Ziming Zhao, Gail-Joon Ahn, and Hongxin Hu. Automatic Extraction of Secrets from Malware. In *Proceedings of the 2011 Working Conference on Reverse Engineering*.

- Ziming Zhao, Gail-Joon Ahn. Using Instruction Sequence Abstraction for Shellcode Detection and Attribution. In *Proceedings of the 2013 IEEE Conference on Communications and Network Security*.

The ideas of using routing table change patterns to assess and mitigate routing attack risks in Chapter 4 were discussed in a conference and a journal paper:

- Ziming Zhao, Hongxin Hu, Gail-Joon Ahn, and Ruoyu Wu. Risk-aware Response for Mitigating MANET Routing Attacks. In *Proceedings of the 2010 IEEE Global Telecommunications Conference*.

- Ziming Zhao, Hongxin Hu, Gail-Joon Ahn, and Ruoyu Wu. Risk-Aware Mitigation for MANET Routing Attacks. In *IEEE Transactions on Dependable and Secure Computing*, 2012.

The ideas of using user choice patterns to guess picture passwords in Chapter 5 were presented in a conference paper:

- Ziming Zhao, Gail-Joon Ahn, Jeong-Jin Seo, and Hongxin Hu. On the Security of Picture Gesture Authentication. In *Proceedings of the 2013 USENIX Security Symposium*.

The ideas of using social interaction patterns to model underground social dynamics and predict future cyber attacks in Chapter 6 were discussed in two conference papers and a book chapter:

- Ziming Zhao, Gail-Joon Ahn, and Hongxin Hu. Examining Social Dynamics for Countering Botnet Attacks. In *Proceedings of the 2011 IEEE Global Communications Conference*.

- Ziming Zhao, Gail-Joon Ahn, Hongxin Hu, and Deepinder Mahi. SocialImpact: Systematic Analysis of Underground Social Dynamics. In *Proceedings of the 2012 European Symposium on Research in Computer Security*.

- Ziming Zhao and Gail-Joon Ahn. Examining Social Dynamics and Malware Secrets to Mitigate Net-centric Attacks in *Hackers and Hacking: A Reference Handbook*, 2013.

The rest of this dissertation is organized as follows. In Chapter 2, we overview the mathematical foundations of our research. In Chapter 3, we present how to detect and attribute shellcode using patterns extracted from instruction sequences. In Chapter 4, we present how to mitigate MANET routing attacks using evidence collected and combined from routing tables. In Chapter 5, we present how to guess picture gesture passwords by modeling the user-choices patterns exhibited in collected passwords. In Chapter 6, we present how to discover underground social intelligence using social patterns. Chapter 7 concludes this dissertation.

Chapter 2

MATHEMATICAL PREREQUISITES

There are many theories to model and describe patterns with uncertainty and randomness. This chapter is not meant to be a comprehensive introduction or summary of all existing techniques of discovering and using patterns. For more comprehensive coverage of existing techniques, please refer to Bishop and Nasrabadi (2006); Tan *et al.* (2007); Theodoridis and Koutroumbas (2008). This chapter only introduces the mathematical foundations for the techniques we will use and we will develop in this dissertation.

2.1 Probability Theory

Probability theory uses the concept of random variable to describe a variable whose value is subject to variations due to chance. A random variable can take on a set of discrete or continuous values, each with an associated probability.

In this dissertation, we denote the probability that a random variable X will take the value x_i as $Pr(X = x_i)$ for discrete random variables. In the cases where two discrete random variables are involved, we use $Pr(X = x_i, Y = y_i)$ to denote the probability that X will take the value x_i and Y will take the value y_i. Since this probability describes multiple random variables, it is called joint probability of X and Y. We use $Pr(Y = y_i|X = x_i)$ to denote the conditional probability that Y will take y_i given X takes x_i.

Suppose X and Y are two random variables, the sum rule states that

$$Pr(X) = \sum_{Y} Pr(X, Y) \tag{2.1}$$

Suppose X and Y are two random variables, the product rule states that

$$Pr(X, Y) = Pr(Y|X)Pr(X) \tag{2.2}$$

Since $Pr(X, Y) = Pr(Y, X)$, Bayes' theorem states that

$$Pr(Y|X) = \frac{Pr(X|Y)Pr(Y)}{Pr(X)} \tag{2.3}$$

Probability theory uses the concept of mathematical expectation to denote the value of a random variable one would expect to find if one could repeat the random variable process an infinite number of times and take the average of the values obtained. Obviously, the random variable could be some mathematical transformation from other random variable represented as $f(x)$. The expectation of $f(x)$ denoted as $\mathbb{E}[f]$ under a discrete probability distribution $Pr(X)$ is given by

$$\mathbb{E}[f(x)] = \sum_{x} Pr(x)f(x) \tag{2.4}$$

The variance of $f(x)$ that provides a measure of how much variability there is in $f(x)$ around its expectation $\mathbb{E}[f]$ is given by

$$var[f(x)] = \mathbb{E}[(f(x) - \mathbb{E}[f(x)])^2] \tag{2.5}$$

For two random variables, the covariance that expresses the extent to which two variables vary together is defined by

$$cov[x, y] = \mathbb{E}_{x,y}[(x - \mathbb{E}[x])(y - \mathbb{E}[y])] \tag{2.6}$$

If X and Y are said to be independent of each other,

$$Pr(X, Y) = Pr(X)Pr(Y) \tag{2.7}$$

and

$$Pr(Y|X) = Pr(Y) \tag{2.8}$$

When X and Y are independent to each other, their covariance $cov[X, Y]$ vanishes and is equal to 0. This means X and Y vary independently. When X and Y are not independent, we use Pearson's product-moment coefficient, a normalized representation of covariance, to denote how related they are.

$$\rho_{x,y} = \frac{cov[x, y]}{\sqrt{var(x)}\sqrt{var(y)}} = \frac{\mathbb{E}_{x,y}[(x - \mathbb{E}[x])(y - \mathbb{E}[y])]}{\mathbb{E}[(x - \mathbb{E}[x])^2]\mathbb{E}[(y - \mathbb{E}[y])^2]} \tag{2.9}$$

2.2 Dempster-Shafer Theory

The Dempster-Shafer theory begins with the familiar idea of using a number between zero and one to indicate the degree of support a body of evidence provides for a proposition. But unlike past attempts to develop this idea, the theory does not focus on the act of judgment by which such a number is determined. It focuses instead on something more amenable to mathematical analysis: the combination of degrees of belief or support based on one body of evidence with those based on an entirely distinct body of evidence. The heart of the theory is Dempster's rule for effecting this combination.

Mathematically, Dempster's rule is simply a rule for computing, from two or more belief functions over the same set Θ, a new belief function called their orthogonal sum. The burden of this theory is that this rule corresponds to the pooling of evidence: if the belief functions being combined are based on entirely distinct bodies of evidence and the set Θ discerns the relevant interaction between those bodies of evidence, then the orthogonal sum gives degrees of belief that are appropriate on the basis of the combined evidence.

In Dempster-Shafer theory, propositions are represented as subsets of a given set. Suppose Θ is a finite set, and let 2^{Θ} denote the set of all subsets of Θ. Θ will acquire its meaning from what we know or think we know. In order to emphasize this epistemic nature of the set of possibilities Θ, Θ will be called frame of discernment. When a proposition corresponds to a subset of a frame of discernment, it is said that the frame discerns that proposition.

If Θ is a frame of discernment, then a function $m : 2^{\Theta} \rightarrow [0, 1]$ is called a basic probability assignment whenever

$$m(\phi) = 0 \tag{2.10}$$

and

$$\sum_{A \subset \Theta} m(A) = 1 \tag{2.11}$$

The quantity $m(A)$ is called A's basic probability number, and it is understood to be the measure of the belief that is committed exactly to A. Condition (1) reflects the fact that no belief ought to be committed to ϕ, while (2) reflects the convention that one's total belief has measure one. To obtain the measure of the total belief committed to A, one must add to $m(A)$ the quantities $m(B)$ for all proper subsets B of A.

A function $Bel : 2^{\Theta} \rightarrow [0, 1]$ is called a belief function over Θ if it is given by (3) for some basic probability assignment $m : 2^{\Theta} \rightarrow [0, 1]$.

$$Bel(A) = \sum_{B \subset A} m(B) \tag{2.12}$$

Given several belief functions over the same frame of discernment but based on distinct bodies of evidence, Dempster's rule of combination enables us to compute their orthogonal sum, a new belief function based on the combined evidence. Suppose Bel_1 and Bel_2 are belief functions over the same frame Θ, with basic probability

assignments m_1 and m_2. Then the function $m : 2^{\Theta} \to [0, 1]$ defined by $m(\phi) = 0$ and

$$m(A) = \frac{\sum_{A_i \bigcap B_j = A} m_1(A_i) m_2(B_j)}{1 - \sum_{A_i \bigcap B_j = \phi} m_1(A_i) m_2(B_j)} \tag{2.13}$$

for all non-empty $A \subset \Theta$ is a basic probability assignment.

2.3 Markov Models

Markov models are used to treat sequential data by assuming it has Markov property. Markov property states that the conditional probability distribution of future states of the process depends only the most recent states, not on the sequence of events that preceded them. Assume $x_1, ..., x_N$ are N consecutive states of a process, $Pr(x_1, ..., x_N)$ represents the joint probability for a sequence of observations. According to the product rule, we have

$$Pr(x_1, ..., x_N) = \prod_{n=1}^{N} Pr(x_n | x_1, ..., x_{n-1}) \tag{2.14}$$

If we assume the process has first-order Markov property, which means only the most recent state contributes to the future state. We can rewrite the joint probability for a sequence of observations to

$$Pr(x_1, ..., x_N) = Pr(x_1) \prod_{n=2}^{N} Pr(x_n | x_{n-1}) \tag{2.15}$$

Transition matrix is a matrix used to describe the transitions of a Markov chain. Each of its entries is a nonnegative real number representing a probability. Taking first-order Markov model as an example, $Pr(i|j) = p_{i,j}$ is the probability of state

moving from j to i. The transition matrix looks like

$$P = \begin{pmatrix} p_{1,1} & p_{1,2} & \cdots & p_{1,j} & \cdots \\ p_{2,1} & p_{2,2} & \cdots & p_{2,j} & \cdots \\ \vdots & \vdots & \ddots & \vdots & \cdots \\ p_{i,1} & p_{i,2} & \cdots & p_{i,j} & \cdots \\ \vdots & \vdots & \vdots & \vdots & \ddots \end{pmatrix} \tag{2.16}$$

for which $\Sigma_j p_{i,j} = 1$.

2.4 Support Vector Machines

Support vector machines are decision machines that became popular for solving problems in classification, regression, and detection. Support vector machine approaches the problem of classification through the concept of margin, which is defined as the smallest distance between the decision boundary and any of the samples. In support vector machines, the decision boundary, that is determined by model parameters, is chosen to be the one for which the margin is maximized. Therefore, determination of the model parameters is transformed to a convex optimization problem.

There are many support vector machine variants.Here we only discuss C-support vector classification. Given l training vectors $\{\mathbf{x}_i, y_i\},\ i = 1, ..., l$ in two classes, where each vector is represented as $\mathbf{x}_i$, and a class label y_i with one of two values {-1|1}. The SVM requires the solution of the following optimization problem Boser *et al.* (1992); Cortes and Vapnik (1995); Chang and Lin (2011):

$$\min_{\mathbf{w},b,\xi} \frac{1}{2}\mathbf{w}^T\mathbf{w} + C\sum_{i=1}^{l}\xi_i$$
$$\text{Subject to } y_i(\mathbf{w}^T\phi(\mathbf{x}_i) + b) \geq 1 - \xi_i,$$
$$\xi_i \geq 0 \tag{2.17}$$

where feature vectors $\mathbf{x}_i$ are mapped to higher dimensional space by a function ϕ and $C > 0$ is the penalty parameter of the error term. In SVM, $K(\mathbf{x}_i, \mathbf{x}_j) = \phi(\mathbf{x}_i)^T\phi(\mathbf{x}_i)$, called the kernel function, determines how the feature vector maps data to higher dimensional space.

We list some popular kernel functions here. The first is radial basis function (RBF). A RBF kernel takes the form of

$$K(\mathbf{x}_i, \mathbf{x}_j) = exp(-\gamma \parallel \mathbf{x}_i - \mathbf{x}_j \parallel^2),\ \gamma > 0 \tag{2.18}$$

Therefore, there are two parameters to tune: the penalty parameter C and γ.

Linear function. A linear function takes the form of

$$K(\mathbf{x}_i, \mathbf{x}_j) = \mathbf{x}_i^T\mathbf{x}_j \tag{2.19}$$

Therefore, the only parameter for tuning is C.

Sigmoid function. A sigmoid function takes the form of

$$K(\mathbf{x}_i, \mathbf{x}_j) = tanh(\gamma\mathbf{x}_i^T\mathbf{x}_j + r),\ \gamma > 0 \tag{2.20}$$

Therefore, there are three parameters to tune: the penalty parameter C, γ and r.

Polynomial function. A polynomial function takes the form of

$$K(\mathbf{x}_i, \mathbf{x}_j) = (\gamma\mathbf{x}_i^T\mathbf{x}_j + r)^d,\ \gamma > 0 \tag{2.21}$$

Therefore, there are four parameters to tune: the penalty parameter C, γ, r, and d.

Chapter 3

DETECTING AND ATTRIBUTING SHELLCODE

3.1 Introduction

Malicious code injection is still an unsolved problem that threatens critical net-centric production systems. According to the recent report from SANS, fifteen out of twenty-five most widespread and dangerous software errors could lead to remote code injection and execution attacks Mitre (2011). Even though research efforts have been invested on such a devastating issue, production systems, where known vulnerabilities are not mitigated and potential vulnerabilities are introduced with newly-deployed modules, remain highly vulnerable to these threats.

The targets of code injection attacks could be both script and native language interpreters which depends on the type of the inserting code. HTML injection, cross-site scripting (XSS), SQL injection, and PHP inclusion fall into the first category where the corresponding language interpreter, such as browser, JavaScript engine, database management system and etc., is a software application. Therefore, code injection in this catalog is also called script injection, which could result in malicious manipulation of privileges and resources accessible within the environment, such as session record and account information Vogt *et al.* (2007).

Compared with script injection, binary code injection is the most destructive injection attack. A successfully exploited system gives the direct control of its CPU, the binary code interpreter, to the adversaries that have all the privileges of the subverted processes One (1996). If the underlying operating system or privileged processes are broken down, adversaries could take full control of the entire system

which renders all the active services unreliable and distrust. The injected malicious binary code is also known as shellcode since they used to return a command shell to the attackers.

Misuse of informational data as executable code is the root cause of code injection attacks. Sanitization techniques that remove and escape reserved characters in the corresponding programming language are proven to be effective and efficient in scripting languages Weinberger *et al.* (2011). However, these techniques are less successful in defending against binary code injection attacks due to the fact that there is no special meaningful token in binary to differentiate code from data. For instance, in IA-32 instruction set, the only invalid byte to start an instruction is `0xF1` and all other 255 possible values could be interpreted as the starting byte of a valid encoding Chinchani and Van Den Berg (2006).

One research body in defeating malicious code injection is concerned about the prevention of its execution in an architectural way rather than the detection of its existence. Instruction set randomization Barrantes *et al.* (2003), data execution prevention, and address space layout randomization, and structural exceptional handler overwrite protection all fall into this category by disrupting the successful running of shellcode. Data execution prevention (DEP) is intended to prevent a process from executing code from non-executable memory regions, such as process stack and system heap Microsoft (2006). Address space layout randomization (ASLR) randomly arranges the locations of data sections such as position of libraries, stack and heap for each process and makes it difficult for injected code to execute itself Shacham *et al.* (2004). Even if these prevention solutions are effective, widely supported by modern hardware, and popularly adopted in state-of-the-art operating systems, they could only be triggered after the attack event occurred. There is no way for these techniques to predict and detect exploit attempts before it reaches the real attack

surface. The reason behind this shortcoming is that these solutions are not able to address the aforementioned root cause of code injection attacks. Although they could serve as the last line of code injection defense, it is imperative to have other defense techniques which are able to gather tactical intelligence for future shellcode detection and response.

Although signature-based methods remain the most effective ways to defeat known malware, they could be effective only when malicious samples have been acquired and signatures have been obtained. It is less useful against new samples and may be vulnerable to code encoding techniques, such as polymorphism and metamorphism. Several static analysis solutions Toth and Kruegel (2002a); Christodorescu *et al.* (2005); Chinchani and Van Den Berg (2006); Wang *et al.* (2006b) construct some distinguishable criteria, such as the length of the instruction sequence, to identify previously unknown malicious code. Since the heuristics in these methods are dependent on the existing knowledge of shellcode, they fail to accommodate the new trends of shellcode evolution. There also exist some discussions about utilizing both sequential and distributional byte patterns to model malicious code Wang *et al.* (2006a); Kolter and Maloof (2006). However, statistically modeling the byte patterns is vulnerable to deliberate byte cramming Detristan (2003) and blending attacks Fogla *et al.* (2006). Moreover, quantitative analysis of the byte strength of different shellcode engines presented in Song *et al.* (2007) concludes that modeling the byte patterns in shellcode is infeasible.

Besides all the investments on binary code detection, it is important to discover binary code attribution that automatically attributes binary code to its originating tools. *Encoded shellcode attribution* that tells whether the newly-captured shellcode sample is generated by a known shellcode engine provides security analysts and practitioners with more intelligence about the attack event and the adversaries behind the

scene than simplistic detection approaches. However, existing work on this topic Kong *et al.* (2011) that utilize byte characteristics still face the same challenges as binary code detection with byte anomaly analysis does.

Consequently, systematic techniques that can *confront* the root cause of code injection, *detect* unseen malicious attacks and *attribute* newly-detected malicious code samples are imperative to cope with emerging rogue code threats and gather tactical intelligence for a more comprehensive knowledge base on cyberattacks. These solutions should be resilient to known attacks, such as byte cramming and blending, that undermine existing techniques. To achieve these goals, in this chapter, we propose a novel solution based on static analysis and supervised machine learning techniques. Instead of using byte patterns, we propose *instruction sequence abstraction* to extract coarse-grained but distinguishable features from disassembled instruction sequence.

We design a Markov-chain-based model and apply support vector machines for unknown shellcode detection and classification. The rest of this chapter is organized as follows. Section 3.2 discusses the background. Section 3.3 discusses the observed motivating instruction patterns. Section 3.4 presents the overview of our approach to extract and use instruction patterns. Section 3.5 illustrates instruction sequence abstraction to automatically extract instruction patterns. In Section 3.6, we propose two learning models for shellcode detection and attribution. Section 3.7 discusses the implementation details and automated identified instruction patterns. We show our experimental results in Section 3.8 and discuss some research issues in Section 3.9. Section 3.10 overviews the related work and Section 3.11 concludes the chapter.

3.2 Background

In this section, we address the theoretical limit in differentiating code from data in IA-32 architecture. We then briefly describe the instruction encoding method of IA-32. We discuss why byte pattern analysis on this architecture is difficult.

3.2.1 Differentiating Code from Data

Accurate and robust methodology for differentiating code from data in a static way has a profound value for both programming language and computer security research. Disassembler and decompiler could use such technique to determine the boundary between code and data in file and memory for better understanding of programs without source code. Intrusion detection system could also make use of it to alert unseen cyberattack. For some computer architectures, this problem is trivial due to their instruction representations and memory alignments. However, some CISC architectures, such as IA-32, adopt variable-length instruction sets and permit interleaving of code and data. That is, instructions and data are stored together in the memory and have indistinguishable representations. The problem is even harder to solve when we consider self-modifying code and indirect jump (`jmp eax`)–a control transfer approach whose destination can only be calculated at execution time–in binary. Therefore, statically separating code from data in such architectures may lead to the halting problem that is undecidable in general Cifuentes and Fraboulet (1997); Wartell *et al.* (2011); Horspool and Marovac (1980); Landi (1992).

A major reason for the failure of byte pattern analysis on binary code is that even a slight change on assembly syntax would cause tremendous changes in byte syntax. Consequently, pattern detection and recognition on byte level is not resilient to assembly-level syntax change that is prevalent in shellcode encoding. For example,

different shellcode instances from the same metamorphic engine could use different general registers to perform semantically equivalent operations. While one could use two instructions `pop edx; mov ebx, [edx]` (byte sequence: `5A8B1A`) to move a value from memory to register for computing, another may use `pop eax; mov esi, [eax]` (byte sequence: `588B30`). Even though the instruction sequences look similar, the byte sequences only share one single byte (`8B`). With more sophisticated encoding technique, this shared byte could be further avoided.

3.2.2 IA-32 Instruction Format

We briefly discuss the instruction encoding scheme in IA-32 architecture that serves as the cornerstone of our analysis. IA-32 instructions follow the encoding approach shown in Figure 3.1. Each instruction consists of up to 4 prefix bytes, up to 3 opcode bytes, and up to 10 operand bytes. The prefix bytes determine modifiers of this instruction, such as `lock` (`F0h`) and `repeat` (`F2h`). The opcode bytes define the operation of this instruction, such as `mov` or `add`. The operands part consists of optional ModR/M (Address-Form specifier), SIB (Scale-Index-Base), displacement and immediate that are used to specify the operand combinations. ModR/M byte contains fields of information to specify the address form of following operands: If required, a SIB byte follows to detail the scale, index, and base fields of base-plus-index and scale-plus-index addressing form. A displacement or an immediate follows if required. For instance, instruction `imul [ebp+esi+20], 616D2061` references a signed integer multiplication operation. The addressing mode specifies a `base-plus-index` form. A displacement `20` and immediate `616D2061` appear in this instruction as well.

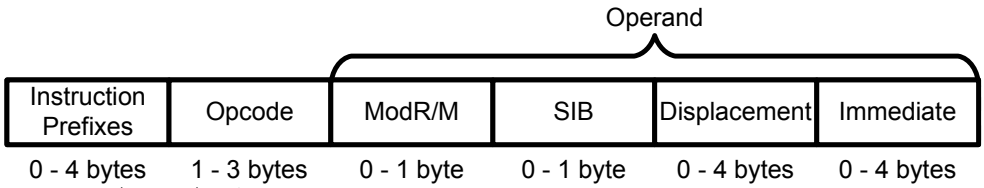

Figure 3.1: IA-32 Architecture Instruction Format

3.3 Motivating Examples of Instruction Patterns

We describe several motivating patterns observed in both benign and malicious binary samples as shown in 3.2. Different from previous solutions that concentrate on byte patterns, we pay more attention on the instruction patterns shown in disassembly. We address instruction patterns of both sequences and distributions. For patterns in the sequence, we focus on the ones that are found in binary code but less likely to be found in text string, video files, or any other forms of data. For patterns of distributions, we concentrate on the ones that are found across different shellcode instances generated by the same encoder. Note that these patterns only serve as the motivation of our approach that is not dependent on any specific pattern mentioned in this section, but has the ability to extract human-observable and unobservable patterns in binary disassembly.

A *push-call* sequential pattern consists of several `push` instructions followed by a `call` instruction. In IA-32 architecture, the parameters to a function call are stored temporarily on stack usually by a `push` operation. Depending on the prototype of the function, it is obvious to observe several `push` instructions before a `call` instruction. Therefore, in a valid sequence of instructions, the subsequent instruction of `push` is more likely to be another `push` or `call`. SigFree Wang *et al.* (2006b) used the number of *push-call* in the instruction sequence as threshold to determine whether a package has code.

A *function-prologue* sequential pattern normally exists in `bp`-based function, a

```
push [ebp+20h]
push eax
push ecx
call edx
```

(a) push-call pattern

```
xor [eax], edx
ror dword ptr [eax], 0BEh
xor [eax], edx
rol dword ptr [eax], 92h
sub dword ptr [eax], 0E2B3D1A9h
```

(b) group-of-arithmetic pattern

```
push ebp
mov ebp, esp
add esp, 0FFFFFFECh
```

(c) function prologue pattern

```
cmp edi, ebx
ja 40CA2Ah

test al, al
jnz 40E722h
```

(d) test-jmp pattern

```
push eax
push ecx
call 40E712h
pop ecx
pop ecx
mov [ebp+20h], eax
```

(e) function epilogue pattern

```
call 7h
pop esi
```

(f) getPC pattern

Figure 3.2: Motivating Examples of Instruction Patterns

procedure that uses `ebp` as the frame pointer to mark the bottom of stack for the called function and `esp` as the stack pointer to track the top of stack. Therefore, as the prologue of `bp`-based function, the frame pointer of the caller function is stored on stack by `push ebp` and then updated to the current frame pointer by `mov ebp, esp`.

Frequently, an `add esp, immediate` is followed to reserve bytes for local variables in this pattern.

A *function epilogue pattern* exists in `_cdecl` calling conventions. In `_cdecl` calling conventions, it is the caller's responsibility to clean the stack and maintain stack balance. Therefore, in this sample we observe that there are equal bytes of parameters pushed on stack before calling and popped from stack after calling. Also in IA-32, the return value of a function is normally stored in `EAX`, which is why `EAX` is access after function call.

A *group-of-arithmetic-shift* distributional pattern groups several bitwise and arithmetic instructions, such as `xor` (exclusive or) and `sub` (subtraction), to perform some sophisticated calculations. Instances of this pattern are mostly found in decryption routines that contain the inordinate number of such instructions to decode protected resources Caballero *et al.* (2009).

In a *test-jmp pattern*, there is a comparison or test instruction first, such as `cmp`, `test` which sets the corresponding bits of the `EFLAGS` register. Then, a conditional jump instruction, such as `ja` (jump if above), `jnz` (jump if not zero), is followed which transfers the control to different destinations based on the bit pattern set in `EFLAGS`.

A *getPC pattern* is widely adopted in shellcode Polychronakis *et al.* (2007). Since there is no way to predict the absolution address a shellcode would be located, shellcode always need methods to get its location in runtime. However, IA-32 does not provide any build-in method to retrieve the value of `EIP`, adversaries devise some techniques to get this value in runtime. In this example, `call 7h` pushes the absolute address of `pop esi` on stack, then `pop esi` stores this value to `esi` and restores stack balance at the same time.

A *alphabet* pattern is mostly found in shellcode generated by *English_shellcode* Mason *et al.* (2009) and *alpha_mixed _encoder* engines, whose outputs only consist of dis-

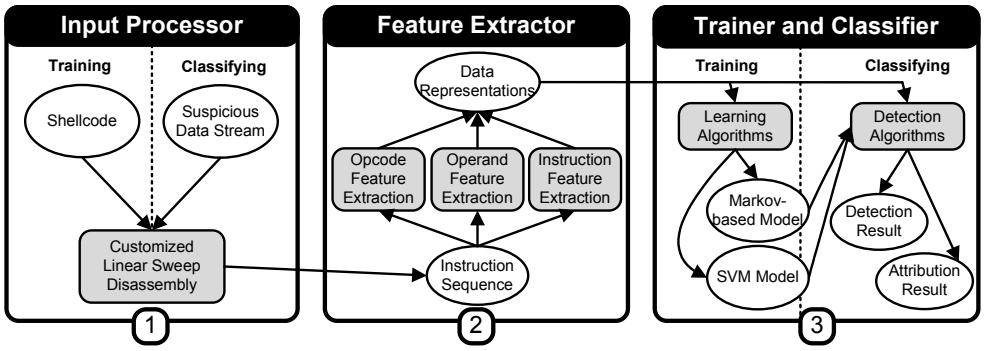

Figure 3.3: Overview of the Approach of Using Instruction Patterns to Detect and Attribute Shellcode

playable ASCII values, such as English letters, blank space and punctuation marks. Because of the narrow choices these engines have, generated shellcode have significantly more unconditional jumps, stack and arithmetic operations than samples generated by other encoders.

However, there are several obstacles in using these instruction observations directly in statistical models. For example, the trained model may overfit instruction patterns shown in the training set. Adversaries and encoding engines could easily choose other semantically-equivalent instructions to replace existing ones which render the modeling of any specific instruction ineffective. In order to solve these challenges, we propose *instruction sequence abstraction*, a coarse-grained feature extraction method, to tackle the problem of overfitting by mapping high-dimensional byte sequence representations to low-dimensional instances.

3.4 Overview of Extracting and Using Instruction Patterns

Our approach is based on static analysis and supervised machine learning as shown in Figure 3.3. Our solution consists of three major components: i) input processor, that is presented in Section 3.5, preprocesses binary code or suspicious data with customized linear disassembly that outputs the instruction sequence; ii) feature extrac-

tor, that is presented in Section 3.5, reveals distinguishable features from the instruction sequence and outputs its two corresponding data representations named opcode mnemonic sequence and binary finite-dimensional representation; and iii) trainer, that is presented in Section 3.6, utilizes Markov-chain-based model and support vector machines to train detection and classification models based on training set and classifiers that use trained models to detect and classify suspicious data.

3.5 Automatic Extraction of Instruction Patterns

In this section, we propose customized linear sweep disassembly algorithm. To remove any confusion between byte and instruction characteristics that hinder previous research efforts, we then present our feature selection and *instruction sequence abstraction* to extract representative characteristics from the instruction sequence.

3.5.1 Customized Linear Sweep Disassembly

The first step of our approach is to disassemble binary, a method that extracts semantics out of binary code and outputs machine-understandable disassembly. There exist two basic disassembly algorithms: i) linear sweep disassembly and ii) recursive descent disassembly. Linear sweep disassembly decodes new instruction at the location where the previous one ends. If the current byte could not be decoded as a valid starting byte of the instruction, linear sweep disassembly stops. The disadvantage of linear sweep disassembly is that it may mistakenly disassemble data as code if the starting location is wrong. Recursive descent disassembly determines whether a location should be decoded with the references by other instructions. In other words, recursive descent disassembly follows the control flow of the instruction sequence. Recursive descent disassembly stops when it could not determine the location of the next

instruction, such as when an indirect jump is encountered. The major disadvantage of recursive descent disassembly is that it cannot cover the entire code section.

In our solution, we need the most comprehensive coverage of disassembly. Therefore, we modify linear sweep disassembly and propose a customized linear sweep disassembly $CLSD : (b_1, ..., b_n) \rightarrow (i_1, ..., i_m)$ as shown in Algorithm 1. Unlike linear sweep disassembly, *CLSD* does not stop when it reaches an undecodable address. Instead, it moves to the next address and perform linear sweep until it reaches the end of file. The complexity of this algorithm is $O(n)$. Although *CLSD* may mistakenly decode some data section, such as encrypted payload in polymorphic shellcode, and incorrectly disassemble some instructions with a wrong starting location, this algorithm would disassemble the major portion of code over the data stream with the help of the self-repairing ability of IA-32 instruction set Linn and Debray (2003).

3.5.2 Feature Selection

In this section, we present our coarse-grained feature extraction method to reveal representative features from the instruction sequence $(i_1, ..., i_m)$ generated from *CLSD*. We try to introduce as many features as possible to reduce the possibility that the learned model is over-fitting the training dataset. We inspect both opcode and operand of an instruction as the sources for features. The opcode part of an instruction reveals the functionality of the disassembly statement, while operand part tells which object the effect is enforced on. We design opcode features based on two aspects: functionality and origin. Functionality captures the basic behavior and effect of a given opcode, and origin describes the source of instruction set that a given opcode was first introduced. Although the operand part of an instruction includes several fields such as addressing form and immediate, for simplicity, we only analyze the usage of eight general purpose registers in an instruction as representative char-

Algorithm 1: *CLSD*

Input: **Byte sequence b** $= (b_1, ..., b_n)$ with n bytes

Output: **Instruction sequence i** $= (i_1, ..., i_m)$

```
Initially i is empty;
Set p = 1;
while p is not greater than n do
    if b_p is a valid instruction starting byte then then
        Do linear sweep disassembly on b_p;
        When its stops, append its output (i_1, ..., i_k) to i;
        Set p;
    else
        Set p = p + 1;
    end
end
return the instruction sequence i
```

acteristics for operand features. We also use the length of instruction as a feature that represents the instruction in general.

Opcode functionality: We categorize each opcode into one of the following ten groups in terms of its functionality:

1. *Arithmetic.* Opcodes that provide arithmetic operations, such as addition, multiplication, and some miscellaneous conversion instructions. Examples include `add`, `adc`, `sub`, `sbb`, `mul`, and `imul`.

2. *Shift, rotate and logical.* Opcodes that provide shift, rotate and logical operations, such as bitwise and left shift with the carry-over. Examples include `and`, `or`, `ror`, and `xor`.

3. *Unconditional data transfer.* Operations that move data among memory locations and registers without querying flag register. Examples include `mov, in,` and `out`;

4. *Conditional data transfer.* Operations that move data among memory locations and registers based on the status indicated in a flag register. Examples include `seta` and `setnl`;

5. *Processor control.* Opcodes that manipulate the status of processor by modifying flag, loading and saving system registers, and synchronizing external devices. Examples include `arpl, hlt,` and `lgdt`;

6. *Stack operation.* Opcodes that manipulate a program stack. Examples include `push`, `pop`, `enter`, and `leave`;

7. *Unconditional program transfer.* Opcodes that change the program counter register without querying flag register. Examples include `call, int, jmp,` and `ret`;

8. *Conditional program transfer.* Opcodes that make transfer decisions based on specific bit combinations in flag register. Examples include `ja`, `jne`, and `loopw`;

9. *Test and compare.* Opcodes that compare the values of operands and store the result in some predefined register. Examples include `test`, `cmp`, and `scas`;

10. *Other operation.* Opcodes that are not included in the aforementioned categories.

Opcode origin: We also categorize each opcode into one of the following six instruction sets:

1. *8086 set*, a group of instructions that were introduced with 8086 family CPUs Intel (1979);

2. *80286, 80386, and 80486 sets.* We combine these three instruction sets together because there do not exist many instances in each of these instruction sets;

3. *Pentium and Pentium II sets*;

4. *80387 and MMX,* instruction sets that control and manipulate floating point coprocessors and MMX processors;

5. *Pentium III and Pentium IV*; and

6. *Other sets.*

General register usage: For each instruction i in the instruction sequence, we analyze whether any of the eight general registers or any part of them is explicitly used in this instruction. These eight general registers are: 1) `eax`; 2) `ebx`; 3) `ecx`; 4) `edx`; 5) `esi`; 6) `edi`; 7) `ebp`; and 8) `esp`. For instance, in an instruction `pop eax`, the only explicitly mentioned general register is `eax`. We do not count the usage of `esp` because it is not explicitly mentioned in the operand part. For an instruction `mov esi, [eax]`, both `esi` and `eax` appear in this statement. For an instruction `add al, ch`, we count one occurrence for both `eax` and `ecx` in this statement for the reason that `al` is part of `eax` and `ch` is part of `ecx`.

Length of instruction: For each instruction i in the instruction sequence, we calculate its length. This feature is necessary because even instructions with the same opcode may vary in length. We split instructions into eight categories: Instructions are categorized into the first seven categories by using the length as an identifier if their lengths are not greater than seven bytes and instructions with longer than seven bytes fall into the eighth category. For example, `mov ebp, esp` (`8BEC`) is 2-byte long

and classified in category 'two', and `mov dword ptr [eax+ebp+14h], 0CCCCCCCCh` (`C7442814CCCCCCCC`) is 8-byte long and falls into category 'eight'.

3.5.3 Instruction Sequence Abstraction

We now present *instruction sequence abstraction* which includes two representation methods to model instruction sequence: opcode mnemonic sequence (OMS) and binary finite-dimensional representation (BFR). Since both methods map n-byte data sequence into much lower dimensional space as coarse-grained feature extraction approaches, they are abstractions of the original byte and the instruction sequence. While OMS maps instances in 256^n byte sequence space to their counterparts in a^m space (a is the number of mnemonics in IA-32 instruction set and m is the length of the instruction sequence), BFR represents instances in $\mathbb{Z}^{32}$ space. For the mathematical notations, we use lower case bold roman letters such as $\mathbf{f}$ to denote vectors, subscript such as f_i to denote the i-th component of $\mathbf{f}$, superscript such as $\mathbf{f}^{(i)}$ to denote the i-th sample in dataset, and $f_j^{(i)}$ to denote the i-th sample's j-th component. We assume all vectors to be column vectors and a superscript T to denote the transposition of a matrix or vector.

Definition 3.1. *Opcode Mnemonic Sequence (OMS). For a given instruction sequence* $\mathbf{i} = (i_1, ..., i_m)$*, its opcode mnemonic sequence is represented as* $\mathbf{o}^T = (o_1, ..., o_m)$*, where* $o_k \in \{$`aaa`*,* `aad`*, ...}, which is the valid opcode mnemonic set of IA-32 architecture.*

Definition 3.2. *Binary Finite-dimensional Representation (BFR). For a given instruction sequence* $\mathbf{i} = (i_1, ..., i_m)$*, its binary finite-dimensional representation is a 32-dimensional vector* $\mathbf{f}^T = (f_1, ..., f_{32})$*, where* f_i*,* $i \in \{1, ..., 10\}$*, is the number of instructions in the i-th opcode functionality category,* f_i*,* $i \in \{11, ..., 16\}$*, is the num-*

55	push ebp
8BEC	mov ebp, esp
8B7608	mov esi, dword ptr [ebp+08]
85F6	test esi, esi
743B	je 401045
8B7E0C	mov edi, dword ptr [ebp+0c]
09FF	or edi, edi
7434	je 401045
31D2	xor edx, edx

(a) Byte sequence (b) Instruction sequence

$$\mathbf{o}^T = (\mathsf{push}, \mathsf{mov}, \mathsf{mov}, \mathsf{test}, \mathsf{je}, \mathsf{mov}, \mathsf{or}, \mathsf{je}, \mathsf{xor})$$

(c) OMS

$$\mathbf{f}^T = (0, 2, 3, 0, 0, 1, 0, 2, 1, 0, 9, 0, 0, 0, 0, 0, 0, 0, 0, 2, 3, 3, 4, 1, 1, 5, 2, 0, 0, 0, 0, 0)$$

(d) BFR

Figure 3.4: Instruction Sequence Abstraction Example

ber of instructions from the corresponding opcode origins, f_i, $i \in \{17, ..., 24\}$, *is the occurrence of corresponding general register, and* f_i, $i \in \{25, ..., 32\}$, *is the number of instructions with the corresponding length. Figure 3.4(b) shows the* CLSD *output of the byte sequence shown in Figure 3.4(a), and Figures 3.4(c) and 3.4(d) show the OMS and BFR representations of the example.*

3.6 Using Instruction Patterns to Detect and Attribute Shellcode

In this section, we articulate our approach to detect and attribute suspicious byte sequences. We propose two classifiers for shellcode detection and attribution, respectively.

3.6.1 Detecting Shellcode

Based on the observation that certain instruction sequences are more likely to exist in some binary code rather than others, we propose to use the existence possibility of opcode mnemonic sequence to identify whether the suspicious byte stream contains shellcode. We choose first-order Markov chain, which is a discrete random process, to model the opcode mnemonic sequence by assigning each opcode mnemonic as a Markov state and computing the transition matrix of this Markov chain.

Like other supervised machine learning techniques, our method has training and evaluation phases. Given OMSs of l shellcode training samples $\{\mathbf{o}^{(i)}\},\ i = \{1, ..., l\}$, a transition matrix $\mathbf{P} \in \mathbb{R}^{a \times a}$ can be trained, with the (i, j)-th element of $\mathbf{P}$ implies $p_{ij} = Pr(o_{k+1} = j | o_k = i)$ indicating the probability of opcode state transition from o_k to o_{k+1}. In the evaluation phase, we calculate shellcode probability score (*S-score*) of suspicious data stream, which is defined in Definition 3 and determine whether it contains shellcode based on a threshold value t, which is also learned from the training set.

Definition 3.3. *Shellcode Probability Score (*S-score*). Given the transition matrix* $\mathbf{P}$ *trained from shellcode dataset and a suspicious OMS* $\mathbf{o}^T = (o_1, ..., o_m)$*, the* S-score *of this OMS is defined as follows:*

$$S\text{-}score(\mathbf{o}) = \sqrt[k]{\max_{i=1,...,m-k} \prod_{j=i}^{i+k} Pr(o_{j+1} | o_j)} \tag{3.1}$$

where k is the length of calculation window. To calculate the *S-score* of $\mathbf{o}$, a value for each of $m - k$ opcode mnemonic subsequences with k-length is computed as the multiplications of the transition probabilities. Then, the maximum value among all $m - k$ opcode mnemonic subsequences is chosen whose k-th root is defined as the

Table 3.1: Shellcode Dataset Comparison

Criteria \ Projects	*styx*	SigFree	Song	STILL	SA[3]	Our Work
# of shellcode engines	2	2	6	10	6	14
# of shellcode samples	2	200	60,000	12,000	N/A	13,176

S-score of $\mathbf{o}$. If *S-score*$(\mathbf{o}) > t$, we say the byte sequence where $\mathbf{o}$ is generated from is a shellcode and *vice versa*.

Our shellcode detection approach is length-independent and location-independent on the byte sequence for two reasons: i) *CLSD* outputs the most comprehensive coverage of code, hence it has the ability to disassemble most shellcode bytes in a package, no matter where it is started; and ii) only the subsequent k instructions are used to calculate the *S-score*, hence the length of the byte sequence is not vital. Therefore, our approach is able to monitor on-line data stream, where the length and location of interesting points are unknown.

3.6.2 Attributing Encoded Shellcode

We propose to use support vector machines (SVM) to attribute encoded shellcode's BFR to its originating encoding engine. SVM maps feature vectors into a higher dimensional space and computes a hyperplane to separate instances from different groups by maximizing the margin between them. Therefore, SVM is the largest margin classifier. The problem of attributing shellcode to its originating engine is a multi-class classification problem. However, the basic SVM only supports binary classification problems. Therefore, we use algorithms that supports a one-vs-all approach to extend SVM for classifying multi-class problems. Here, we only discuss how to use SVM for the binary classification problem that checks whether a shellcode sample is from a specific engine e.

Given l shellcode training samples $\{\mathbf{f}^{(i)}, y^{(i)}\},\ i = 1, ..., l$, where each sample is denoted by its BFR that has 32 features, represented as $\mathbf{f}^{(i)}$, and a class label y_i with one of two values {-1|1}. -1 means it is not generated by an engine e, while 1 confirms a specific engine. The SVM requires the solution of the following optimization problem Boser *et al.* (1992); Cortes and Vapnik (1995); Chang and Lin (2011):

$$\begin{aligned} \min_{\mathbf{w},b,\xi} \frac{1}{2}\mathbf{w}^T\mathbf{w} + C\sum_{i=1}^{l}\xi_i \\ \text{Subject to } y_i(\mathbf{w}^T\phi(\mathbf{f}^{(i)}) + b) \geq 1 - \xi_i, \\ \xi_i \geq 0 \end{aligned} \tag{3.2}$$

where feature vectors $\mathbf{f}^{(i)}$ are mapped to higher dimensional space by a function ϕ and C is the penalty parameter of the error term. In SVM, $K(\mathbf{f}^{(i)}, \mathbf{f}^{(j)}) = \phi(\mathbf{f}^{(i)})^T\phi(\mathbf{f}^{(i)})$, called the kernel function, determines how the feature vector maps data to higher dimensional space. It can be noted that the kernel function maps feature vectors into higher dimensional space only to search for a separate hyperplane so it does not rebuild more complicated features. Hence, it does not conflict with our approach to abstract features from the instruction sequence.

3.7 Implementation

We first discuss the data collection and implementation details of our proof-of-concept system. Then, we present the automatically identified sequential instruction patterns in shellcode.

3.7.1 Data Collection and Implementation

We utilized Metasploit Moore (2009)–a penetration framework that hosts exploits and tools from a variety of sources–to collect shellcode samples. We collected 140

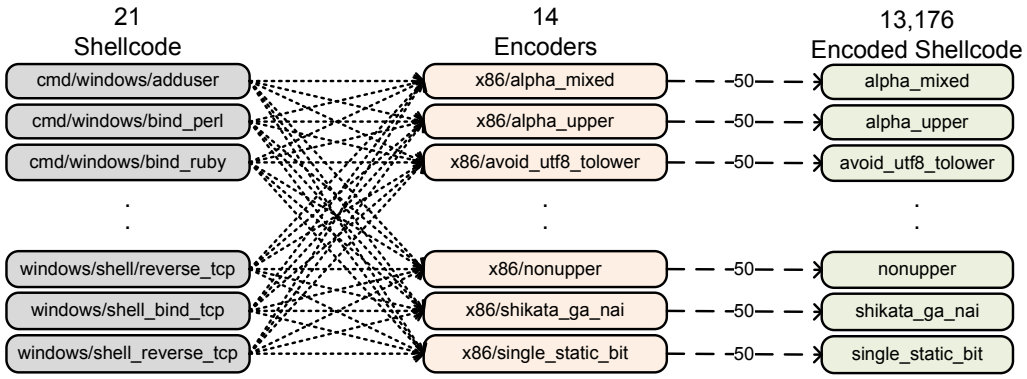

Figure 3.5: Encoded Shellcode Samples Collection

unencoded shellcode samples, all of which are executable on IA-32 architecture, across different operating system platforms including Windows (85), Unix (11), Linux (21), FreeBSD (10), OSX (12), and Solaris (1). These samples are used to train our Markov-chain-based model and test the effectiveness of our approach. For the evaluation of *encoded shellcode* attribution, we chose 21 different payloads that are targeted at Windows, then used 14 different engines to encode these payloads (see Table 3.3 for the full list of engines). We tried to generate 50 unique shellcode instances for each pair of payload and encoder. Even though some payloads are not compatible with specific encoders, we successfully collected 13,176 encoded shellcode samples for attribution analysis. Compared with existing research bodies in both shellcode detection and attribution Chinchani and Van Den Berg (2006); Wang *et al.* (2006b); Song *et al.* (2007); Wang *et al.* (2008); Kong *et al.* (2011), our shellcode dataset covers a more comprehensive set of samples in term of underlying platform, payload functionality, and encoder class.

We implemented the customized linear sweep disassembly algorithm and feature extractor as an IDA Pro Rescue (2006) plug-in that outputs the OMS and BFR in separate files for each byte sequence input. We also developed the shellcode detection

module with Matlab and shellcode attribution module with `LIBSVM` Chang and Lin (2011).

3.7.2 Instruction Patterns Identification

In the learning phase, we trained our Markov model with aforementioned shellcode samples to generate the transition matrix of opcode. The top 50 highest opcode transition probabilities are shown in Table 3.2. Some transition patterns, such as $Pr(\texttt{xor|aaa})= 1.00$, $Pr(\texttt{push|push})= 0.61$, $Pr(\texttt{jz|test})= 0.57$, and $Pr(\texttt{jnz|cmp})= 0.56$, can be human-observable as we mentioned in Section 2.3 but other patterns cannot be easily identified. The results show that our approach is able to extract underlying and implicit machine code characteristics.

3.8 Evaluation

We show shellcode detection and attribution results followed by an analysis approach for measuring the strength of 14 popular shellcode encoding engines. We conclude our evaluation with the performance of our system.

3.8.1 Evaluation of Detecting Shellcode

In the detection phase, *S-score* uses a calculation window k to compute the shellcode probability of the given input. A threshold value t is also used to determine if a given byte sequence is executable or not. To find out the appropriate length of calculation window and threshold value, we tested 140 shellcode samples, 1,280 random data samples, 250 gif files, 250 png files, and 660 benign code pieces (we split `ntoskrnl.exe` which is the kernel image of Windows NT into 660 pieces). For a given sample, its *S-score* decreases as the calculation window increases, because $Pr(o_{j+1}|o_j)$ is always less than or equal to 1. We calculated the *S-score* of all of the collected

Table 3.2: Top 50 Opcode Transition Patterns

Top 1 - 17		Top 18 - 34		Top 35 - 50	
Pr(xor|aaa)	1.00	Pr(adc|fst)	1.00	Pr(push|jp)	0.71
Pr(push|aam)	1.00	Pr(cmps|fistp)	1.00	Pr(cld|in)	0.67
Pr(sal|cwde)	1.00	Pr(cmp|fadd)	1.00	Pr(into|iret)	0.67
Pr(std|clc)	1.00	Pr(in|fsubr)	1.00	Pr(outs|jbe)	0.67
Pr(sbb|cmps)	1.00	Pr(in|fdivp)	1.00	Pr(cdq|sal)	0.67
Pr(jmp|hlt)	1.00	Pr(fstenv|fldpi)	1.00	Pr(jmp|sti)	0.67
Pr(std|idiv)	1.00	Pr(xor|fstenv)	1.00	Pr(xchg|stos)	0.67
Pr(dec|jecxz)	1.00	Pr(add|ror)	0.92	Pr(push|xchg)	0.66
Pr(add|jg)	1.00	Pr(sub|jl)	0.89	Pr(pop|popa)	0.64
Pr(outs|jge)	1.00	Pr(xor|movzx)	0.87	Pr(push|shl)	0.62
Pr(outs|jle)	1.00	Pr(push|lea)	0.86	Pr(push|push)	0.61
Pr(cli|loope)	1.00	Pr(push|jns)	0.86	Pr(in|retf)	0.61
Pr(push|mul)	1.00	Pr(call|out)	0.80	Pr(jnz|scas)	0.60
Pr(loope|neg)	1.00	Pr(mov|pusha)	0.78	Pr(jz|test)	0.57
Pr(push|or)	1.00	Pr(add|nop)	0.78	Pr(cld|retn)	0.57
Pr(cli|sgdt)	1.00	Pr(push|jno)	0.75	Pr(jnz|cmp)	0.56
Pr(cmc|fcomip)	1.00	Pr(push|loop)	0.72		

samples with the length of calculation windows from 8 to 40 to find the appropriate value.

Figure 3.6 presents the *S-score* distribution of each sample category with three different values of the calculation window length. Figure 3.6(a) shows that if the length of calculation window k is set to 8, all shellcodes' *S-score* is greater than 0.1, and a significant portion of shellcode have *S-score* greater than 0.3. However, only a small number of random data samples have *S-score* greater than 0 as shown in Figure 3.6(d). Figures 3.6(g),(j) show the *S-score* distribution of gif and png files,

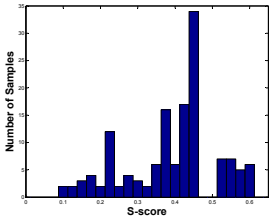

(a) Shellcode, $k = 8$

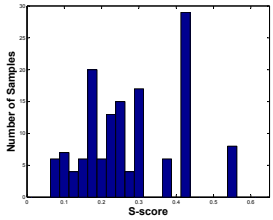

(b) Shellcode, $k = 20$

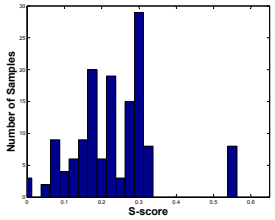

(c) Shellcode, $k = 28$

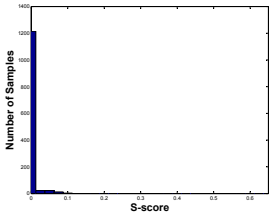

(d) Data, $k = 8$

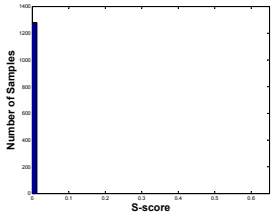

(e) Data, $k = 20$

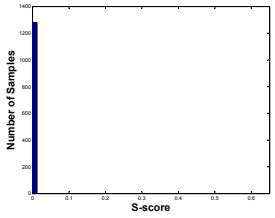

(f) Data, $k = 28$

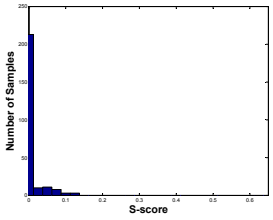

(g) Gif, $k = 8$

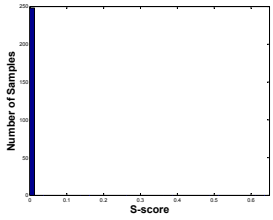

(h) Gif, $k = 20$

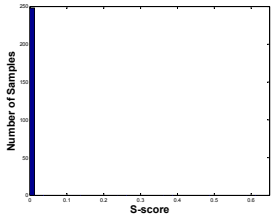

(i) Gif, $k = 28$

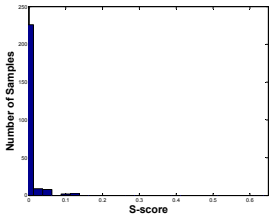

(j) Png, $k = 8$

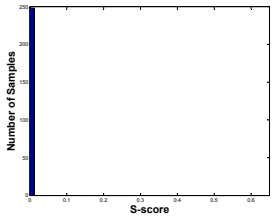

(k) Png, $k = 20$

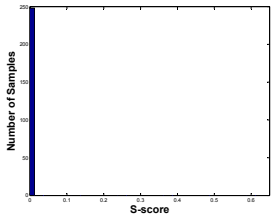

(l) Png, $k = 28$

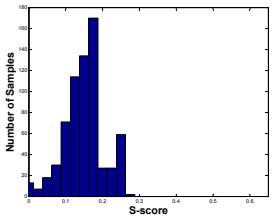

(m) Benign code, $k = 8$

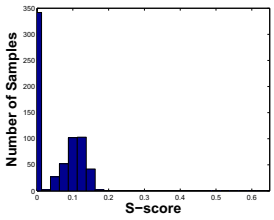

(n) Benign code, $k = 20$

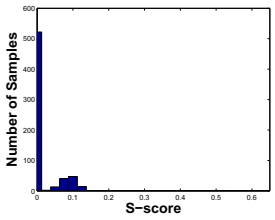

(o) Benign code, $k = 28$

Figure 3.6: The S-score Distribution with Different k

where only a small portion of samples have *S-score* greater than 0.1. By comparing Figure 3.6(a) and Figure 3.6(m), it is clear that benign code samples have much lower *S-score* than shellcode. Figure 3.6(b) shows that if the length of calculation window k is set to 20, the *S-score* of every shellcode reduces. But, most shellcode samples still have *S-score* greater than 0.1. However, as shown in Figure 3.6(c), if the length of calculation window is set to 28, 3 shellcode samples have *S-score* with 'null'. On the other hand, the *S-score* of all other samples are reduced close to 0 if k is greater than 20, as shown in Figure 3.6. The results suggest that the combination of calculation window length $k = 28$ and threshold $t = 0.1$ be sufficient to identify shellcode with 97.9% accuracy and 0.82% false positive rate in our dataset.

3.8.2 Evaluation of Attributing Encoded Shellcode

We evaluate our shellcode representation and attribution analysis technique from several different aspects including visualization, correlation analysis of selected features, accuracy of attributing, and quantification of encoder strength.

Data Visualization

The visualization of shellcode samples could tell us the differences of shellcode generated from various engines in an intuitive way. We propose to visualize shellcode sample in BFR form with a radar chart graph, in which a circle is equally divided by 32 invisible lines. Each of these 32 lines represents an axis for each corresponding feature in BFR form, where the center of circle represents 0 and the periphery represents 1. Since, in the BFR form, a shellcode sample is represented as $\mathbf{f} \in \mathbb{Z}^{32}$, we used data scaling on all the samples in our dataset to transform each feature into the range of $[0, 1]$. The value of each feature is marked by a dot on its corresponding line.

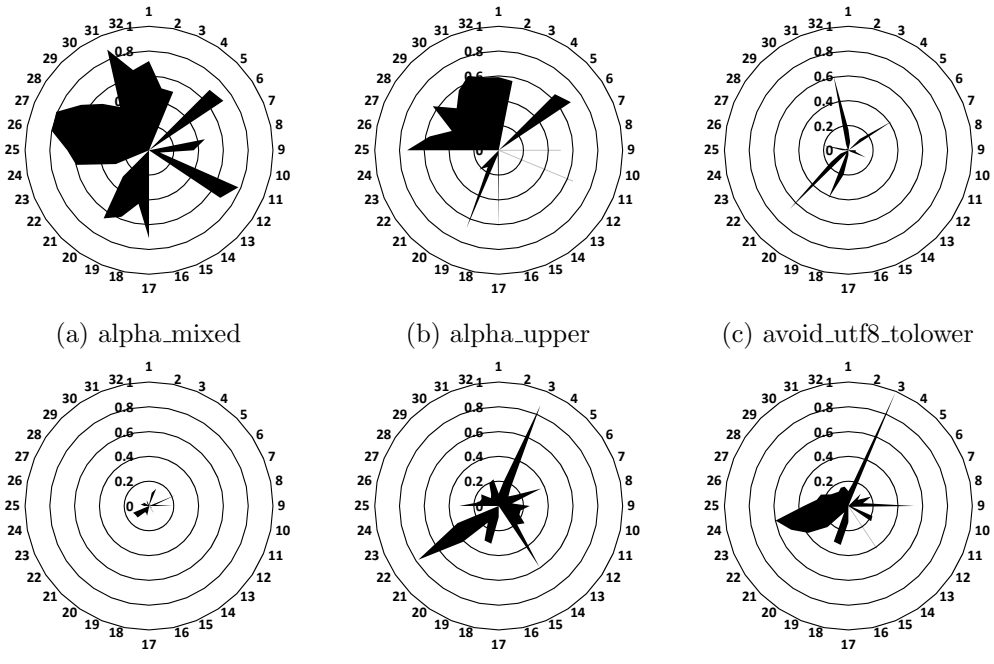

(a) alpha_mixed (b) alpha_upper (c) avoid_utf8_tolower

(d) call4_dword_xor (e) context_time (f) fnstenv_mov

Figure 3.7: Shellcode Radar Charts

Then, the dots from each pair of consequent features are connected together and the contained area is marked black.

Figure 3.7 shows six radar charts of instances from six different shellcode engines. As we can notice, the shellcode generated by *alpha_mixed* has strong similarity with the shellcode generated by *alpha_upper*. They both generate shellcode with longer instructions (features 25 to 32). Shellcode generated by *context_time* or *fnstenv_mov* has more unconditional data transfer instructions than others (feature 3). *fnstenv_mov* tends to use registers `esi, edi` and `ebp` more often (features 21, 22, and 23), while *alpha_mixed* prefers `eax, ecx`, and `edx` (feature 17, 19, and 20). Because the data scaling is performed over the whole dataset, we could also notice that the size of black area differs significantly. The major reason behind this phenomenon is that some engines tend to generate much longer data sequence even if the input payload is

the same. Obviously, the shellcode generated by *call_dword_xor* or *avoid_utf8_tolower* is smaller than its counterpart generated by *alpha_mixed* in size.

Effectiveness of Feature Selection

In order to prove our feature selection approach in BFR is effective and the extracted features are not redundant, we utilize *Pearson product-moment correlation coefficient* to measure the linear relationships between each pair of features in BFR form. Given two features f_i and f_j in BFR, the correlation coefficient ρ_{f_i,f_j} is a measure of the linear dependency between them that is defined as $\rho_{f_i,f_j} = \frac{E[(f_i-\mu_{f_i})(f_j-\mu_{f_j})]}{\sigma_{f_i}\sigma_{f_j}}$, where μ_{f_i} is the mean and σ_{f_i} is the standard deviation of this feature value over our dataset.

The maximum value for correlation coefficient, which is 1, represents a perfect positive correlation between two variables, and the minimum value -1 indicates a perfect negative correlation. If $|\rho_{f_i,f_j}|$ is close to 1, it means one of the selected features could be linearly represented by another one, hence it clearly indicates redundancy. We calculated the correlation coefficient for each pair of features over our dataset, and computed the average of their absolute values defined as $P = \frac{\sum_{i\neq j}|\rho_{f_i,f_j}|}{496}$, where 496 is the number of feature pairs $(32 \times 31)/2$. The result was $P = 0.3428$ that indicates our feature selection is not redundant.

Parameter Tuning

In the SVM model, the factors that affect the classification result include the penalty parameter C, the kernel function, and corresponding parameters in the kernel function. We randomly divided our shellcode dataset into a training set and a testing set, which is a standard approach in machine learning. The training set has 60% of samples from each class and the testing set consists of the rest of samples, 40% of samples. To find the best kernel function and parameters, we used a grid-search for

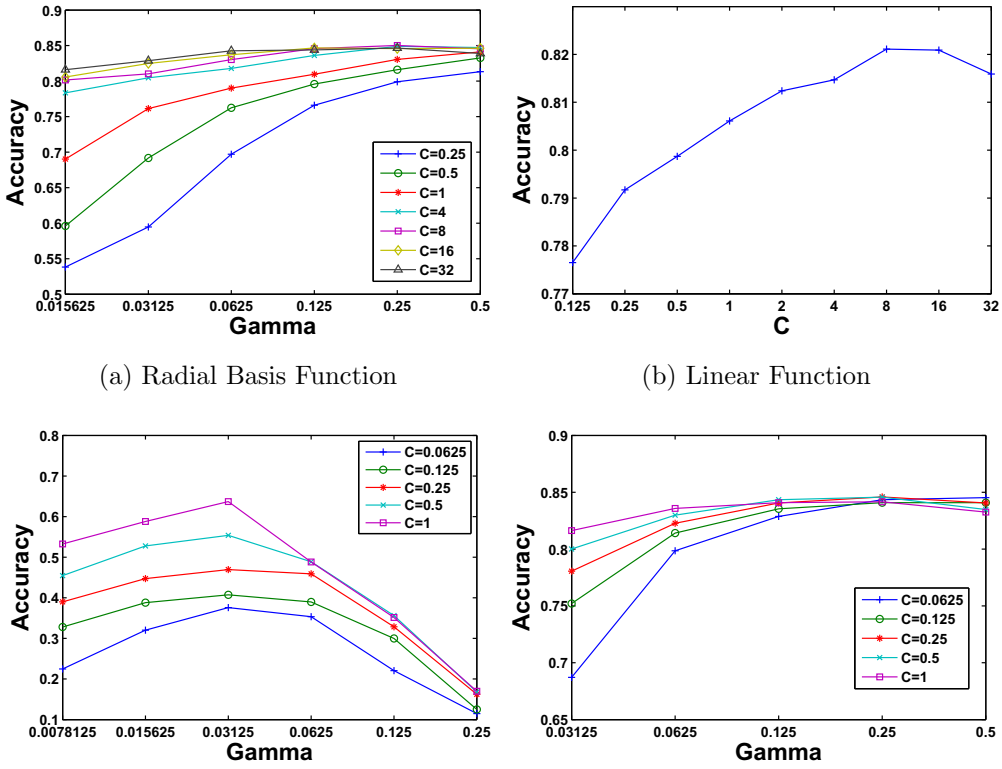

(a) Radial Basis Function

(b) Linear Function

(c) Sigmoid Function

(d) Polynomial Function

Figure 3.8: Attribution Accuracy with Four Kernel Functions

possible parameter combinations on the training set to learn SVM model with four popular kernel functions Chang and Lin (2011) and to evaluate it on the testing set.

Radial basis function (RBF): A RBF kernel takes the form of $K(\mathbf{f}^{(i)}, \mathbf{f}^{(j)}) = exp(-\gamma \parallel \mathbf{f}^{(i)} - \mathbf{f}^{(j)} \parallel^2)$, $\gamma > 0$. Therefore, there are two parameters to tune: the penalty parameter C and γ. We used a grid-search to test exponentially growing sequence of $C = 2^{-3}, 2^{-2}, ..., 2^{8}$ and $\gamma = 2^{-7}, 2^{-6}, ..., 2^{5}$. Figure 3.8(a) shows the accuracy of testing when different parameter combinations are used. The results show that, when C is fixed, the best r is in the range $[2^{-4}, ..., 2^{-2}]$. On the other hand, when r is fixed, the best C is above 8. We found the best (C, γ) combination $(8, 0.25)$ with the accuracy of 85.02% in attributing testing samples to its class;

Linear function: A linear function takes the form of $K(\mathbf{f}^{(i)}, \mathbf{f}^{(j)}) = \mathbf{f}^{(i)T}\mathbf{f}^{(j)}$. There-

fore, the only parameter for tuning is C. We tested $C = 2^{-3}, ..., 2^5$ and found the best penalty parameter $C = 8$ with 82.11% accuracy as shown in Figure 3.8(b);

Sigmoid function: A sigmoid function takes the form of $K(\mathbf{f}^{(i)}, \mathbf{f}^{(j)}) = tanh(\gamma \mathbf{f}^{(i)T} \mathbf{f}^{(j)} + r),\ \gamma > 0$. We found the best (C, γ, r) combination $(2^{-4}, 2^{-5}, -2^{-3})$ with the accuracy of 63.70% in attributing testing samples to its class as shown in Figure 3.8(c);

Polynomial function: A polynomial function takes the form of $K(\mathbf{f}^{(i)}, \mathbf{f}^{(j)}) = (\gamma \mathbf{f}^{(i)T} \mathbf{f}^{(j)} + r)^d,\ \gamma > 0$. We evaluated the combinations of $C = 2^{-1}, ..., 2^3,\ \gamma = 2^{-5}, ..., 2^{-1},\ r = 2^{-3}, ..., 2^{-1}$ and $d = 2, 3, 4$. We found the best (C, γ, r, d) combination $(4, 0.25, 0.125, 3)$ with the accuracy of 84.57% as shown in Figure 3.8(d). In summary, our results suggest that RBF, linear, and polynomial kernels be appropriate for attributing shellcode samples in terms of accuracy. However, the computation cost for each kernel is different. We discuss the system performance using different kernels in Section 3.8.4.

The Hardness of Multi-class Attributing

We tested a radius basis function–the kernel function with the highest accuracy–with parameter combination $C = 8, \gamma = 0.25$ in subsets of our dataset to find out whether increasing the number of shellcode engines for the classification makes the problem harder to solve. We performed the same testing procedure mentioned in the previous section to test the accuracy of our model for $2, ..., 13$ shellcode classes. Our model can achieve 100% classification accuracy for up to 6 shellcode engines and 95.0% classification accuracy for 11 classes, which is higher than previous efforts Kong *et al.* (2011). Note that, compared with Kong *et al.* (2011) in which a specific model is built for each shellcode class, our approach only use one model to classify instances

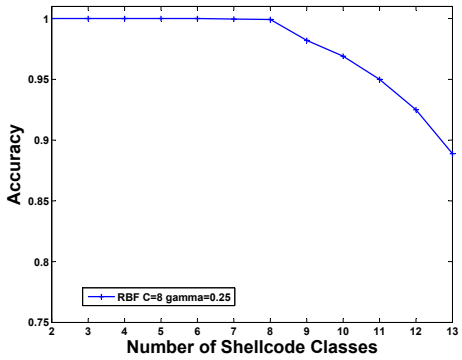

Figure 3.9: Accuracy with Increasing Number of Shellcode Classes

from all kinds of classes, hence does not need different parameter settings for each model.

3.8.3 The Strength of Encoding Engines

In Song *et al.* (2007), the authors introduced variation strength, propagation strength and overall strength on the byte sequence of shellcode to measure polymorphic engines' strength. We redefine these measures to accommodate our binary representation form.

Variation strength: The variation strength of an encoding shellcode engine measures the engine's ability to generate shellcodes that span a sufficiently large portion of 32-dimensional BFR space. We make use of covariance matrix to recover the hyper-ellipsoidal bound on the dataset of each engine. The matrix is defined as $\Sigma(e) = \frac{1}{N}\sum_{i=1}^{N}(\mathbf{f}^{(i)} - \mu)(\mathbf{f}^{(i)} - \mu)^T$, where N is the number of samples generated by an engine e in our dataset. $\Sigma \in \mathbb{R}^{32\times32}$ describes the shape of a 32-dimensional ellipsoid. Then, the problem of calculating the spanned set is transformed to an eigenvector decomposition problem. Thus, $\mathbf{v}$ and λ, such as $\Sigma\mathbf{v} = \mathbf{v}\lambda$, are recovered where λ is a 32-dimensional vector. We define $\Psi(e) = \frac{1}{32}\sum_{i=1}^{32}\sqrt{|\lambda_i|}$ as the variation strength of an encoder e; *Euclidean distance*: Given two BFRs $\mathbf{f}^{(i)}$ and $\mathbf{f}^{(j)}$ which represent two samples in our dataset, the Euclidean distance between these

Table 3.3: The Strength of Encoders

Engine	Variation Strength	Propagation Strength	Overall Strength
alpha_mixed	1.91	26.07	49.91
alpha_upper	1.42	22.50	31.86
avoid_utf8_tolower	1.29	14.53	18.70
call4_dword_xor	2.17	25.82	55.96
context_cpuid	0.27	4.66	1.25
context_stat	0.93	12.53	11.65
context_time	0.94	12.51	11.73
countdown	0.80	10.42	8.33
fnstenv_mov	2.29	26.11	59.71
jmp_call_additive	1.46	15.74	22.91
nonalpha	0.74	9.91	7.36
nonupper	0.98	11.93	11.71
shikata_ga_nai	1.58	16.78	26.46
single_static_bit	1.22	15.87	19.34
random_data_generator	3.31	49.07	162.59

BFRs is defined as $\delta(\mathbf{f}^{(i)}, \mathbf{f}^{(j)}) = \sqrt{\sum_{k=1}^{32}(f_k^{(i)} - f_k^{(j)})^2}$; *Propagation strength*: Given N samples labeled as outputs of an engine e, the propagation strength of this engine describes the average Euclidean distance between all sample pairs defined as $\Phi(e) = \frac{2}{N(N-1)} \sum_{i \neq j} \delta(\mathbf{f}^{(i)}, \mathbf{f}^{(j)})$; *Overall strength*: The overall strength of an encoder e is defined as the multiplication of its variation strength and propagation strength $\Pi(e) = \Phi(e) \times \Psi(e)$. The higher overall strength of an engine indicates that its shellcode instances are more obscured and harder to be correctly attributed.

In order to remove the differences introduced by different payloads, we only took

Table 3.4: Shellcode Attribution Time Cost (millisecond)

Kernel Function	Parameter Combination	Training[1] Time	Classification[2] Time
Radial Basis function	$C = 8, \gamma = 0.25$	2,760	1,720
Linear function	$C = 8$	1,840	1,320
Sigmoid function	$C = 2^{-4}, \gamma = 2^{-5}$ $r = -2^{-3}$	15,640	7,240
Polynomial function	$C = 8, \gamma = 0.25$ $r = 0.125, d = 3$	3,120	1,230

[1] Training set includes 7,906 shellcode samples

[2] Testing set includes 5,270 shellcode samples

the shellcode instances generated by different engines from the same payload into account. Table 3.3 shows the strength of these engines based on our metrics. *random_data_generator* refers to a generator that outputs a group of randomly generated strings with the value of each byte in $\{0, ..., 255\}$. The lengths of these strings are also randomly generated with the value from 160 to 400 bytes, which is the length range of shellcode we mostly observed. It is not surprising to discover that *random_data_generator* is the strongest 'encoder' with the overall strength of 162.59. Among all the encoders, we also noticed that *fnstenv_mov* and *call4_dword_xor* are two of strongest engines based on our metrics, while *context_cpuid* is the weakest one. *alpha_mixed* (49.91) is stronger than *alpha_upper* (31.86), because it could output both upper and lower case alphabets. However, the strength is not doubled because the size of output character set is doubled. Similar observation can be found between *nonalpha* and *nonupper* where *nonupper* shows a little bit stronger obfuscation.

3.8.4 Performance Evaluation

We conducted experiments on a machine with Intel Core2 Duo CPU 3.16 GHz 3.25 GB RAM running Windows 7, IDA Pro 5.6 and Matlab R2010a. We used Windows API `GetTickCount` to measure the performance of our program in C language and `cputime` to measure the elapsed time in Matlab program. The training phase of Markov-chain-based model only took less than 15 milliseconds to learn from 140 shellcode samples. The detection phase with the calculation window length of 20 took less than a second to calculate the *S-score* of 1,200 data streams with variable-length from 160 bytes to 400 bytes.

Table 3.4 shows the time cost for shellcode attribution in training and testing with different kernel functions. We evaluated the performance of the parameter combination with the accuracy of each kind of kernel function. Linear function is the most efficient kernel with 1,840 milliseconds in training for 7,906 samples and 1,320 milliseconds in classifying 5,270 samples. Radial basis function that has 85.02% accuracy in classifying 14 shellcode classes is also efficient, taking 2,760 milliseconds in training and 1,720 milliseconds in classification.

3.9 Discussion

In this section, we discuss other possible ways to model, detect, and attribute shellcode samples.

3.9.1 The Feasibility of Using One Model

It is possible to use one unified model to detect and attribute encoded shellcode in a single step. However, we choose not to adopt such an approach due to the following issues: i) the problem of differentiating code from data and the problem of

attributing detected attack are two separate issues. By separating these two research issues, we could achieve the most accurate results for each group. However, we have to balance the detection rate and attribution rate if these two problems are mixed together; ii) we only consider sequential information to detect and attribute shellcode and we use Markov-chain-based model to fulfill this requirement. In the training phase, we need to train a specific sequential model for each shellcode class instead of modeling all shellcode samples together. Correspondingly, in the detection phase, the given suspicious data stream has to be evaluated by all trained models. With the increased number of shellcode class, the evaluation process will be slow and infeasible for on-line detection; and iii) we also consider a standard classifier, such as SVM and neural networks, to perform detection and attribution. Most standard classifiers do not support modeling of sequential knowledge that may render valuable 'ordering' information useless.

3.9.2 Using Opcode Functionality Sequence to Detect Shellcode

In our experimental evaluation, we also considered to use opcode functionality sequence to detect shellcode instead of opcode mnemonic sequence. For a given instruction sequence $\mathbf{i} = (i_1, ..., i_m)$, its opcode functionality sequence is represented as $\mathbf{s}^T = (s_1, ..., s_m)$, where $s_k \in \{1, ..., 10\}$ that is the set of the opcode functionality category. While opcode mnemonic sequence maps encoded shellcode instances into a a^m dimensional space, opcode functionality sequence maps them into an even lower dimensional space, 10^m. However, the evaluation results show that both false negative and false positive rate are high with this representation. We believe the reason is that the 10^m dimensional space is not sufficient to capture the difference between code and data.

3.9.3 The Arms Race and Future Work

It is possible for malicious code distributors to disturb our shellcode detection method by permutating the locations of instructions in a sequence. For instance, the sequence 1: `mov eax, 1;` 2: `add eax, 1;` 3: `mov ebx, 1;` 4: `add ebx, 1` has different transition probabilities from the sequence 3; 1; 2; 4. However, their permutation choices are limited in which the semantics of the instruction sequence has to be maintained. For example, permutation to 2; 4; 3; 1 is not possible. To cope with this potential arms race, we could integrate machine code slicing Cifuentes and Fraboulet (1997) into our approach. The previous example could be sliced into two independent pieces 1; 2 and 3; 4, and only intra-piece transition probabilities are considered for learning and detection. In addition, higher order Markov chain may be utilized to enhance the accuracy of our approach but might need to minimize unexpected performance overhead. For the attribution part, attackers may deliberately cram garbage instructions to interfere the distribution patterns used in BFR. Fortunately, this issue is easier to solve than byte cramming attacks with the awareness of semantics in disassembly. We could perform data flow analysis Wang *et al.* (2006b) on machine code first to prune useless instructions in a sequence to handle this challenge.

3.10 Related Work

On the signature generation side, Newsome et al. Newsome and Song (2005) proposed TaintCheck that performs dynamic taint analysis by implementing binary rewrite at run time. Newsome et al. introduced Polygraph Newsome *et al.* (2005), a mechanism that is robust to generate signatures for polymorphic code. Li et al. Li *et al.* (2006) proposed Hamsa, a noise-tolerant and attack-resilient network-based automated signature generation system for polymorphic worms. Approaches to gen-

erate vulnerability-based signatures Brumley *et al.* (2006); Li *et al.* (2007) were also proposed on the network level without any host-level analysis of execution. However, Chung et al. Chung and Mok (2007) showed that all of these signature generation schemes are vulnerable to advanced allergy attacks.

Several emulation and execution-based approaches were proposed to detect exploit, shellcode, and worm. Polychronakis et al. Polychronakis *et al.* (2007) proposed a heuristic detection method to execute and monitor suspicious data stream captured in network traffic. However, setting up such a runtime environment that fits every exploit and shellcode is extremely difficult. To solve this problem, Gu et al. Gu *et al.* (2010) proposed to dump the process's virtual memory before any input data are consumed and use the dumped image to instantiate a runtime environment that emulates the target process's input data consumption to monitor shellcode behaviors. In addition, Spector Borders *et al.* (2007) used symbolic execution to reveal high-level application programming interface calls from shellcode for a better understanding of what it does.

APE Toth and Kruegel (2002a) calculated the maximum execution length of a byte sequence, and learned threshold for detecting possible malicious packages. Stride Akritidis *et al.* (2005) complemented the previous effort by adding new criteria including non-privileged instruction in a byte sequence to identify sled in shellcode. Chinchani et al. Chinchani and Van Den Berg (2006) and Kruegel et al. Kruegel *et al.* (2006) proposed to utilize the control and data flow information in binary to detect polymorphic code. Wang et al. Wang *et al.* (2006b) first used data flow anomaly to prune useless instructions then compared the number of useful instructions with a certain threshold to determine if it has any code.

Wang et al. Wang *et al.* (2006a) compared the byte frequency of normal network packages with malicious ones to figure out the byte patterns that could lead to

attack detection. However, their solutions were vulnerable to byte cramming Detristan (2003) and polymorphic blending attacks Fogla *et al.* (2006). Recently, Kong et al. Kong *et al.* (2011) proposed to take advantage of semantic analysis and sequential models on n-gram data bytes to analyze the attribution of exploits. Wartell et al. Wartell *et al.* (2011) developed machine learning-based algorithms to differentiate code from data. Rosenblum et al. Rosenblum *et al.* (2010) proposed to use conditional random field to extract compiler provenance from code. While most of these work focus on the byte patterns identified in binary code, Song et al. Song *et al.* (2007) presented quantitative analysis of the byte strength of polymorphic shellcode and claimed that modeling the byte patterns in shellcode is infeasible.

Besides the aforementioned research efforts, several new binary encoding schemes were proposed in recent years. Mason et al. Mason *et al.* (2009) proposed English shellcode engine that transforms arbitrary shellcode to a representation that is similar to English prose. Wu et al. Wu *et al.* (2010) proposed mimimorphism to transform binary into mimicry counterpart that exhibits high similarity to benign programs in terms of statistical properties and semantic characteristics.

3.11 Summary

In this chapter, we proposed a technique for modeling shellcode detection and attribution through a novel feature extraction method, called *instruction sequence abstraction*, that extracts distinguishable features from suspicious data stream by reducing the size of input data dimension and removing ambiguous byte patterns. We also presented a Markov-chain-based model for shellcode detection and adopted support vector machines for shellcode attribution. Our experiments showed that our approach does not require any signature and is only based on static analysis and supervised machine learning. The evaluation results also suggested that our solution

detect and attribute shellcode to its originating engines with high accuracy and lower false positive rate.

Chapter 4

MITIGATING MANET ROUTING ATTACKS

4.1 Introduction

Mobile Ad hoc Networks (MANET) are utilized to set up wireless communication in improvised environments without a predefined infrastructure or centralized administration. Therefore, MANET has been normally deployed in adverse and hostile environments where central authority point is not necessary. Another unique characteristic of MANET is the dynamic nature of its network topology which would be frequently changed due to the unpredictable mobility of nodes. Furthermore, each mobile node in MANET plays a router role while transmitting data over the network. Hence, any compromised nodes under an adversary's control could cause significant damage to the functionality and security of its network since the impact would propagate in performing routing tasks.

Several work Sun *et al.* (2006b); Refaei *et al.* (2010) addressed the intrusion response actions in MANET by isolating uncooperative nodes based on the node reputation derived from their behaviors. Such a simple response against malicious nodes often neglects possible negative side effects involved with the response actions. In MANET scenario, improper countermeasures may cause the unexpected network partition, bringing additional damages to the network infrastructure. To address the above-mentioned critical issues, more flexible and adaptive response should be investigated.

The notion of risk can be adopted to support more adaptive responses to routing attacks in MANET Cheng *et al.* (2007). However, risk assessment is still a non-

trivial, challenging problem due to its involvements of subjective knowledge, objective evidence and logical reasoning. Subjective knowledge could be retrieved from previous experience and objective evidence could be obtained from observation while logical reasoning requires a formal foundation. Wang et al. Wang *et al.* (2007) proposed a naïve fuzzy cost-sensitive intrusion response solution for MANET. Their cost model took subjective knowledge and objective evidence into account but omitted a seamless combination of two properties with logical reasoning. In this chapter, we seek a way to bridge this gap by using Dempster-Shafer mathematical theory of evidence (D-S theory), which offers an alternative to traditional probability theory for representing uncertainty Shafer (1976).

D-S theory has been adopted as a valuable tool for evaluating reliability and security in information systems and by other engineering fields Sun *et al.* (2006a); Mu *et al.* (2008), where precise measurement is impossible to obtain or expert elicitation is required. D-S theory has several characteristics. First, it enables us to represent both subjective and objective evidence with basic probability assignment and belief function. Second, it supports Dempster's rule of combination to combine several evidence together with probable reasoning. However, as identified in Sentz and Ferson (2002); Zadeh (1984); Yager (1987); Wu *et al.* (2002); Zhao *et al.* (2010, 2012c), Dempster's rule of combination has several limitations, such as treating evidence equally without differentiating each evidence and considering priorities among them. To address these limitations in MANET intrusion response scenario, we introduce a new Dempster's rule of combination with a notion of *importance factors* in D-S evidence model.

In this chapter, we propose a risk-aware response mechanism to systematically cope with routing attacks in MANET, and propose an adaptive time-wise isolation method. Our risk-aware approach is based on the extended D-S evidence model.

In order to evaluate our mechanism, we perform a series of simulated experiments with a proactive MANET routing protocol, Optimized Link State Routing Protocol (OLSR) Clausen and Jacquet (2003). In addition, we attempt to demonstrate the effectiveness of our solution.

The rest of this chapter is organized as follows. Section 4.2 overviews a MANET routing protocol OLSR and routing attacks against OLSR. Section 4.3 describes how our extended D-S evidence model can integrate *importance factors*. Section 4.4 overviews our risk-aware response mechanism to cope with MANET routing attacks. Section 4.5 illustrates how to assess the risk by leveraging routing table change evidence. Section 4.6 illustrates how to adaptively make risk mitigation decisions. The evaluations of our approach are discussed in Section 4.7. Section 4.8 provides the related work in MANET intrusion detection and response systems, also reviews risk-aware approaches in different fields. Section 4.9 concludes this paper.

4.2 Background

In this section, we overview the OLSR and routing attacks on OLSR.

4.2.1 OLSR Protocol

The major task of the routing protocol is to discover the topology to ensure that each node can acquire a recent map of the network to construct routes to its destinations. Several efficient routing protocols have been proposed for MANET. These protocols generally fall into one of two major categories: reactive routing protocols and proactive routing protocols. In reactive routing protocols, such as Ad hoc On Demand Distance Vector (AODV) protocol Perkins *et al.* (2003), nodes find routes only when they must send data to the destination node whose route is unknown. In contrast, in proactive routing protocols, such as OLSR, nodes obtain routes by periodic

exchange of topology information with other nodes and maintain route information all the time.

OLSR protocol is a variation of the pure Link-state Routing (LSR) protocol and is designed specifically for MANET. OLSR protocol achieves optimization over LSR through the use of multipoint relay (MPR) to provide an efficient flooding mechanism by reducing the number of transmissions required. Unlike LSR, where every node declares its links and forwards messages for their neighbors, only nodes selected as MPR nodes are responsible for advertising, as well as forwarding an MPR selector list advertised by other MPRs.

In OLSR, a node selects its MPR set that can reach all its two-hop neighbors. In case there are multiple choices, the minimum set is selected as an MPR set. A node learns about its one-hop and two-hop neighbors from its one-hop neighbors' HELLO messages. HELLO message is used for neighbor discovery and MPR selection. In OLSR, each node generates a HELLO message periodically. A node's HELLO message contains its own address and the list of its one-hop neighbors. By exchanging HELLO messages, each node can learn a complete topology up to two hops. HELLO messages are exchanged locally by neighbor nodes and are not forwarded further to other nodes. In addition to HELLO message, Topology Control (TC) message is used for route calculation. In OLSR, each MPR node advertises TC messages periodically. A TC message contains the list of the sender's MPR selector. Only MPR nodes are responsible for forwarding TC messages. Upon receiving TC messages from all of the MPR nodes, each node can learn the network topology and then build a route to every node in the network.

4.2.2 Routing Attack on OLSR

Based on the behavior of attackers, attacks against MANET can be classified into passive or active attacks. Attacks can be further categorized as either outsider or insider attacks. With respect to the target, attacks could be also divided into data packet or routing packet attacks. In routing packet attacks, attackers could not only prevent existing paths from being used, but also spoof non-existing paths to lure data packets to them. Several studies Deng *et al.* (2002); Hu and Perrig (2004); Kannhavong *et al.* (2007); Karlof and Wagner (2003) have been carried out on modeling MANET routing attacks. Typical routing attacks include black-hole, fabrication, and modification of various fields in routing packets (route request message, route reply message, route error message, etc.). All these attacks could lead to serious network dysfunctions.

In terms of attack vectors, a malicious node can disrupt the routing mechanism in the following simple ways: first, it changes the contents of a discovered route, modifies a route reply message and causes the packet to be dropped as an invalid packet; then it validates the route cache in other nodes by advertising incorrect paths, and refuses to participate in the route discovery process; and finally, it modifies the contents of a data packet or the route via which the data packet is supposed to travel or behave normally during the route discovery process but is dropped.

In OLSR, any node can either modify the protocol messages before forwarding them, or create false messages or spoof an identity. Therefore, the attacker can abuse the properties of the selection algorithm to be selected as MPR. The worst case is the possible selection of the attacker as the only MPR of a node. Or, the attackers can give wrong information about the topology of a network (TC message) in order to disturb the routing operation.

Typical routing attacks methods against OLSR are:

- Link spoofing attack. A malicious node advertises it has a direct link, which does not really exist, with non-neighbors to disrupt routing and application data operations related to this node. In OLSR, an attacker can advertise a fake link with a victim's two-hop neighbors. This results in the victim node selecting the attacker as its MPR. As an MPR node, the attacker can manipulate routing traffic and data later on by modifying, dropping, recording and delaying.

- Link withholding attack. A malicious node refuses to advertise the existing link to specific nodes or a group of nodes, which can make these nodes unreachable for others. Specific to OLSR, the malicious node may disclaim the existence of its one-hop neighbors by modifying its HELLO message.

- Replay attack. A malicious node could record other nodes' valid routing control message and replay them later. Because of the unpredictable mobility of MANET nodes, replaying control massage could advertise some topology which does not exist anymore, and then cause network routing chaos.

- Colluding misrelay attack. Multiple attackers collude to modify or drop routing packets to disrupt MANET routing process. This kind of attack can disrupt up to 100% data packets in OLSR.

4.3 Extended Dempster-Shafer Theory of Evidence

The Dempster-Shafer mathematical theory of evidence is both a theory of evidence and a theory of probable reasoning. The degree of belief models the evidence, while Dempster's rule of combination (DRC) is the procedure to aggregate and summarize a corpus of evidence. However, previous research efforts identify several limitations of the Dempster's rule of combination:

1. *Associative.* For DRC, the order of the information in the aggregated evidence does not impact the result. As shown in Yager (1987), a non-associative combination rule is necessary for many cases.

2. *Non-weighted.* DRC implies that we trust all evidence equally Wu *et al.* (2002). However, in reality, our trust on different evidence may differ. In other words, it means we should consider various factors for each evidence.

Yager Yager (1987) and Yamada et al. Yamada and Kudo (2004) proposed rules to combine several evidence presented sequentially for the first limitation. Wu et al. Wu *et al.* (2002) suggested a weighted combination rule to handle the second limitation. However, the weight for different evidence in their proposed rule is ineffective and insufficient to differentiate and prioritize different evidence in terms of security and criticality. Our extended Dempster-Shafer theory with importance factors can overcome both of the aforementioned limitations.

4.3.1 Importance Factors and Belief Function

In D-S theory, propositions are represented as subsets of a given set. Suppose Θ is a finite set of states, and let 2^{Θ} denote the set of all subsets of Θ. D-S theory calls Θ, a frame of discernment. When a proposition corresponds to a subset of a frame of discernment, it implies that a particular frame discerns the proposition. First, we introduce a notion of *importance factors*.

Definition 4.1. *Importance factor (IF) is a positive real number associated with the importance of evidence. IFs are derived from historical observations or expert experiences.*

Definition 4.2. *An evidence E is a 2-tuple $\langle m, IF \rangle$, where m describes the basic probability assignment Shafer (1976). Basic probability assignment function m is*

defined as follows:

$$m(\phi) = 0 \tag{4.1}$$

and

$$\sum_{A \subseteq \Theta} m(A) = 1 \tag{4.2}$$

According to Shafer (1976), a function $Bel : 2^{\Theta} \rightarrow [0, 1]$ is a belief function over Θ if it is given by (3) for some basic probability assignment $m : 2^{\Theta} \rightarrow [0, 1]$.

$$Bel(A) = \sum_{B \subseteq A} m(B) \tag{4.3}$$

for all $A \in 2^{\Theta}$, $Bel(A)$ describes a measure of the total beliefs committed to the evidence A.

Given several belief functions over the same frame of discernment and based on distinct bodies of evidence, Dempster's rule of combination, which is given by (4.4), enables us to compute the orthogonal sum, which describes the combined evidence.

Suppose Bel_1 and Bel_2 are belief functions over the same frame Θ, with basic probability assignments m_1 and m_2. Then the function $m : 2^{\Theta} \rightarrow [0, 1]$ defined by $m(\phi) = 0$ and

$$m(C) = \frac{\sum_{A_i \cap B_j = C} m_1(A_i) m_2(B_j)}{1 - \sum_{A_i \cap B_j = \phi} m_1(A_i) m_2(B_j)} \tag{4.4}$$

for all non-empty $C \subseteq \Theta$, $m(C)$ is a basic probability assignment which describes the combined evidence.

Suppose IF_1 and IF_2 are importance factors of two pieces of independent evidence named E_1 and E_2 respectively. The combination of these two pieces of evidence implies that our total belief to these two pieces of evidence is 1, but in the same time, our belief to either of evidence is less than 1. This is straightforward since if our belief to one evidence is 1, it would mean our belief to the other is 0, which models

meaningless evidence. And we define the importance factors of the combination result equals to $(IF_1 + IF_2)/2$.

Definition 4.3. *Extended D-S evidence model with importance factors: Suppose* $E_1 = \langle m_1, IF_1 \rangle$ *and* $E_2 = \langle m_2, IF_2 \rangle$ *are two pieces of independent evidence. Then, the combination of* E_1 *and* E_2 *is* $E = \langle m_1 \oplus m_2, (IF_1 + IF_2)/2 \rangle$*, where* $\oplus$ *is Dempster's rule of combination with* importance factors*.*

4.3.2 Expected Properties for Our Dempster's Rule of Combination with Importance Factors

The proposed rule of combination with *importance factors* should be a superset of Dempster's rule of combination. In this section, we describe four properties that a candidate Dempster's rule of combination with *importance factors* should follow. Property 1 and Property 2 ensure that the combined result is valid evidence. Property 3 guarantees that the original Dempster's Rule of Combination is a special case of Dempster's Rule of Combination with *importance factors*, where the combined evidence have the same priority. Property 4 ensures that importance factors of the evidence are also independent from each other.

Property 4.1. *No belief ought to be committed to* ϕ *in the result of our combination rule.*

$$m'(\phi) = 0 \tag{4.5}$$

Property 4.2. *The total belief ought to be equal to* 1 *in the result of our combination rule.*

$$\sum_{A \subseteq \Theta} m'(A) = 1 \tag{4.6}$$

Property 4.3. *If the* importance factors *of each evidence are equal, our Dempster's rule of combination should be equal to Dempster's rule of combination without* im-

portance factors.

$$m'(A, IF_1, IF_2) = m(A),\ if\ IF_1 = IF_2 \tag{4.7}$$

for all $A \in \Theta$, where $m(A)$ is the original Dempster's Combination Rule.

Property 4.4. *Importance factors of each evidence must not be exchangeable.*

$$m'(A, IF_1, IF_2) \neq m'(A, IF_2, IF_1)\ \ if(IF_1 \neq IF_2) \tag{4.8}$$

4.3.3 Dempster's Rule of Combination with Importance Factors

In this section, we propose a Dempster's rule of combination with *importance factors*. We prove our combination rule follows the properties defined in the previous section.

Theorem 4.1. *Dempster's Rule of Combination with Importance Factors (DRCIF): Suppose Bel_1 and Bel_2 are belief functions over the same frame of discernment Θ, with basic probability assignments m_1 and m_2. The* importance factors *of evidence are IF_1 and IF_2. Then the function $m' : 2^\Theta \to [0, 1]$ defined by*

$$m'(\phi) = 0$$

and

$$m'(C, IF_1, IF_2)$$

$$= \frac{\sum_{A_i \cap B_j = C} [m_1(A_i)^{\frac{IF_1}{IF_2}} \cdot m_2(B_j)^{\frac{IF_2}{IF_1}}]}{\sum_{C \subseteq \Theta, C \neq \phi} \sum_{A_i \cap B_j = C} [m_1(A_i)^{\frac{IF_1}{IF_2}} \cdot m_2(B_j)^{\frac{IF_2}{IF_1}}]}$$

for all non-empty $C \subseteq \Theta$, m' is a basic probability assignment for the combined evidence.

It is obvious that our proposed $DRCIF$ holds Property 1 and Property 4. We prove our proposed $DRCIF$ also holds Property 2 and Property 3 here.

Property 2:

$$\sum_{A\subseteq\Theta} m'(A, IF_1, IF_2)$$

$$= \sum_{A\subseteq\Theta, A\neq\phi} \frac{\sum\limits_{A_i\cap B_j=A} [m_1(A_i)^{\frac{IF_1}{IF_2}} \cdot m_2(B_j)^{\frac{IF_2}{IF_1}}]}{\sum\limits_{A\subseteq\Theta, A\neq\phi} \sum\limits_{A_i\cap B_j=A} [m_1(A_i)^{\frac{IF_1}{IF_2}} \cdot m_2(B_j)^{\frac{IF_2}{IF_1}}]}$$

$$= \frac{\sum\limits_{A\subseteq\Theta, A\neq\phi} \sum\limits_{A_i\cap B_j=A} [m_1(A_i)^{\frac{IF_1}{IF_2}} \cdot m_2(B_j)^{\frac{IF_2}{IF_1}}]}{\sum\limits_{A\subseteq\Theta, A\neq\phi} \sum\limits_{A_i\cap B_j=A} [m_1(A_i)^{\frac{IF_1}{IF_2}} \cdot m_2(B_j)^{\frac{IF_2}{IF_1}}]}$$

$$= 1$$

Property 3:

$$m'(A, IF_1, IF_1)$$

$$= \frac{\sum\limits_{A_i\cap B_j=A} [m_1(A_i)^{\frac{IF_1}{IF_1}} \cdot m_2(B_j)^{\frac{IF_1}{IF_1}}]}{\sum\limits_{A\subseteq\Theta, A\neq\phi} \sum\limits_{A_i\cap B_j=A} [m_1(A_i)^{\frac{IF_1}{IF_1}} \cdot m_2(B_j)^{\frac{IF_1}{IF_1}}]}$$

$$= \frac{\sum\limits_{A_i\cap B_j=A} [m_1(A_i) \cdot m_2(B_j)]}{\sum\limits_{A\subseteq\Theta, A\neq\phi} \sum\limits_{A_i\cap B_j=A} [m_1(A_i) \cdot m_2(B_j)]}$$

$$= \frac{\sum\limits_{A_i\cap B_j=A} m_1(A_i)m_2(B_j)}{1 - \sum\limits_{A_i\cap B_j=\phi} m_1(A_i)m_2(B_j)}$$

$$= m(A)$$

Our proposed DRCIF is non-associative for multiple pieces of evidence. Therefore, for the case in which sequential information is not available for some instances, it is necessary to make the result of combination consistent with multiple pieces of evidence. Our combination algorithm supports this requirement and the complexity of our algorithm is $O(n)$, where n is the number of pieces of evidence. It indicates our extended Dempster-Shafer theory demands no extra computational cost compared to a naïve fuzzy-based method. The algorithm for combination of multiple pieces of evidence is constructed as follows:

Algorithm 2: MUL-EDS-CMB

Input: Evidence pool Ep

Output: One evidence

```
| Ep | = sizeof(Ep);
while | Ep |> 1 do
    Pick two pieces of evidence with the least IF in Ep, named E_1 and E_2;
    Combine these two pieces of evidence, E = ⟨m_1 ⊕ m_2, (IF_1 + IF_2)/2⟩;
    Remove E_1 and E_2 from Ep;
    Add E to Ep;
end
return the evidence in Ep
```

4.4 Overview of Risk-Aware Response Mitigation for MANET Routing Attacks

In this section, we articulate an adaptive risk-aware response mechanism based on quantitative risk estimation and risk tolerance. Instead of applying simple binary isolation of malicious nodes, our approach adopts an isolation mechanism in a tem-

poral manner based on the risk value. We perform risk assessment with the extended D-S evidence theory introduced in Section 4.5 for both attacks and corresponding countermeasures to make more accurate response decisions illustrated in Figure 4.1.

Because of the infrastructure-less architecture of MANET, our risk-aware response system is distributed, which means each node in this system makes its own response decisions based on the evidence and its own individual benefits. Therefore, some nodes in MANET may isolate the malicious node, but others may still keep in cooperation with due to high dependency relationships. Our risk-aware response mechanism is divided into the following four steps shown in Figure 4.1.

Evidence Collection. In this step, Intrusion Detection System (IDS) gives an attack alert with a confidence value, and then Routing Table Change Detector (RTCD) runs to figure out how many changes on routing table are caused by the attack.

Risk Assessment. Alert confidence from IDS and the routing table changing information would be further considered as independent evidence for risk calculation and combined with the extended D-S theory. Risk of countermeasures is calculated as well during a risk assessment phase. Based on the risk of attacks and the risk of countermeasures, the entire risk of an attack could be figured out.

Decision Making. The adaptive decision module provides a flexible response decision making mechanism, which takes risk estimation and risk tolerance into account. To adjust temporary isolation level, a user can set different thresholds to fulfill her goal.

Intrusion Response. With the output from risk assessment and decision making module, the corresponding response actions, including routing table recovery and node isolation, are carried out to mitigate attack damages in a distributed manner.

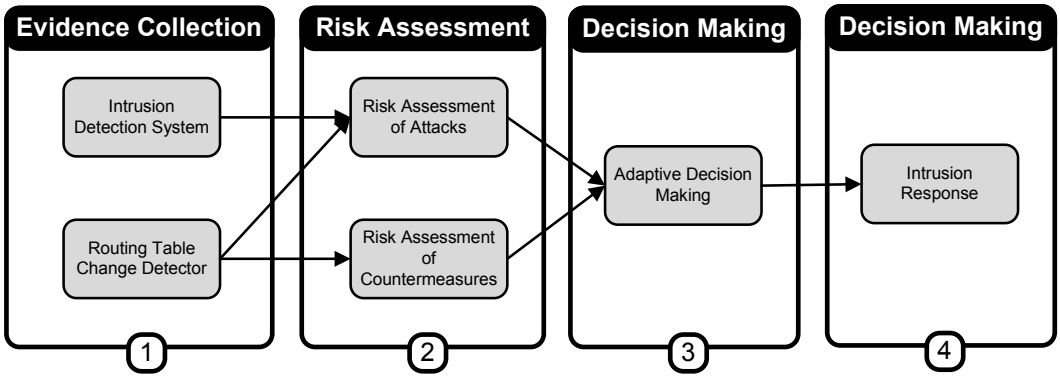

Figure 4.1: Risk-Aware Response Mechanism

4.4.1 Response to Routing Attacks

In our approach, we use two different responses to deal with different attack methods: *routing table recovery* and *node isolation*.

Routing table recovery includes local routing table recovery and global routing recovery. Local routing recovery is performed by victim nodes that detect the attack and automatically recover its own routing table. Global routing recovery involves with sending recovered routing messages by victim nodes and updating their routing table based on corrected routing information in real time by other nodes in MANET.

Routing table recovery is an indispensable response and should serve as the first response method after successful detection of attacks. In proactive routing protocols like OLSR, routing table recovery does not bring any additional overhead since it periodically goes with routing control messages. Also, as long as the detection of attack is positive, this response causes no negative impacts on existing routing operations.

Node isolation may be the most intuitive way to prevent further attacks from being launched by malicious nodes in MANET. To perform a node isolation response, the neighbors of the malicious node ignore the malicious node by neither forwarding packets through it nor accepting any packets from it. On the other hand, a binary

node isolation response may result in negative impacts to the routing operations, even bringing more routing damages than the attack itself.

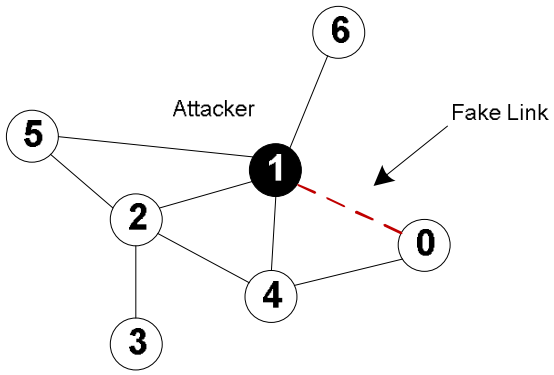

Figure 4.2: An Example of Link Spoofing Attack

For example, in Figure 4.2, Node 1 behaves like a malicious node. However, if every other node simply isolates Node 1, Node 6 will be disconnected from the network. Therefore, more flexible and fine-grained node isolation mechanism are required. In our risk-aware response mechanism, we adopt two types of time-wise isolation responses: *temporary isolation* and *permanent isolation*, which are discussed in Section 4.6.

4.5 Risk Assessment Based on Routing Table Change Patterns

Since the attack response actions may cause more damages than attacks, the risks of both attack and response should be estimated. We classify the security states of MANET into two categories: {Secure, Insecure}. In other words, the frame of discernment would be {ϕ, {Secure}, {Insecure}, {Secure, Insecure}}. Note that {Secure, Insecure} means the security state of MANET could be either secure or insecure, which describes the uncertainty of the security state. $Bel\{Insecure\}$ is used to represent the risk of MANET.

4.5.1 Discovering Routing Table Change Patterns

Our evidence selection approach considers subjective evidence from experts' knowledge and objective evidence from routing table modification. We propose a unified analysis approach for evaluating the risks of both attack ($Risk_A$) and countermeasure ($Risk_C$).

We take the confidence level of alerts from IDS as the subjective knowledge in *Evidence 1*. In terms of objective evidence, we analyze different routing table modification cases. There are three basic items in OLSR routing table (*destination*, *next hop*, *distance*). Thus, routing attack can cause existing routing table entries to be missed, or any item of a routing table entry to be changed. We illustrate the possible cases of routing table change and analyze the degrees of damage in *Evidence 2* through *5*.

Evidence 1: Alert Confidence. The confidence of attack detection by the IDS is provided to address the possibility of the attack occurrence. Since the false alarm is a serious problem for most IDSs, the confidence factor must be considered for the risk assessment of the attack. The basic probability assignments of *Evidence 1* are based on three equations 4.9–4.11:

$$m(Insecure) = c, c\ is\ confidence\ given\ by\ IDS \tag{4.9}$$

$$m(Secure) = 1 - c \tag{4.10}$$

$$m(Secure, Insecure) = 0 \tag{4.11}$$

Evidence 2: Missing Entry. This evidence indicates the proportion of missing entries in routing table. Link withholding attack or node isolation countermeasure can cause possible deletion of entries from routing table of the node.

Evidence 3: Changing Entry Type I. This evidence represents the proportion of changing entries in the case of *next hop being the malicious node*. In this case, the malicious node builds a direct link to this node. So it is highly possible for this node to be the attacker's target. Malicious node could drop all the packages to or from the target node, or it can behave as a normal node and wait for future attack actions. Note that isolating a malicious node cannot trigger this case.

Evidence 4: Changing Entry Type II. This evidence shows the proportion of changed entries in the case of *different next hop (not the malicious node) and the same distance*. We believe the impacts on the node communication should be very minimal in this case. Both attacks and countermeasures could cause this case.

Evidence 5: Changing Entry Type III. This evidence points out the proportion of changing entries in the case of *different next hop (not the malicious node) and the different distance*. Similar to Evidence 4, both attacks and countermeasures could result in this evidence. The path change may also affect routing cost and transmission delay of the network.

Basic probability assignments of Evidence 2 to 5 are based on Equations 4.12, 4.13 and 4.14. Equations 4.12, 4.13 and 4.14 are piecewise linear functions, where a, b, c, and d are constants and determined by experts. d is the minimum value of the belief that implies the status of MANET is insecure. On the other hand, *1-d* is the maximum value of the belief that means the status of MANET is secure. *a, b*, and c are the thresholds for minimum belief or maximum belief for each respective mass function.

$$m(Insecure) = \begin{cases} d & x \in [0, a] \\ (\frac{1-2d}{c-a})(x-a) & x \in (a, c] \\ 1-d & x \in (c, 1] \end{cases} \tag{4.12}$$

$$m(Secure) = \begin{cases} 1 - d + (\frac{2d-1}{b})x & x \in [0, b] \\ d & x \in (b, 1] \end{cases} \tag{4.13}$$

$$m(Secure, Insecure) = \begin{cases} \frac{1-2d}{b}x & x \in [0, a] \\ d - \frac{2d-1}{b}x - & \\ (\frac{1-2d}{c-a})(x-a) & x \in (a, b] \\ 1 - b - & \\ (\frac{1-2d}{c-a})(x-a) & x \in (b, c] \\ 0 & x \in (c, 1] \end{cases} \tag{4.14}$$

4.5.2 Combination of Evidence

For simplicity, we call the combined evidence for an attack, E_A and the combined evidence for a countermeasure, E_C. Thus, $Bel_A(Insecure)$ and $Bel_C(Insecure)$ represent risks of attack ($Risk_A$) and countermeasure ($Risk_C$), respectively. The combined evidence, E_A and E_C are defined in Equations 4.15 and 4.16. The entire risk value derived from $Risk_A$ and $Risk_C$ is given in Equation 4.17.

$$E_A = E_1 \oplus E_2 \oplus E_3 \oplus E_4 \oplus E_5 \tag{4.15}$$

$$E_C = E_2 \oplus E_4 \oplus E_5 \tag{4.16}$$

where $\oplus$ is *Dempster's rule of combination with important factors* defined in Theorem 1.

$$Risk = Risk_A - Risk_C = Bel_A(Insecure) - Bel_C(Insecure) \tag{4.17}$$

4.6 Adaptive Decision Making

Our adaptive decision making module is based on quantitative risk estimation and risk tolerance, which is shown in Figure 4.3. The response level is additionally divided into multiple bands. Each band is associated with an isolation degree, which presents a different time period of the isolation action. The response action and band boundaries are all determined in accordance with risk tolerance and can be changed when risk tolerance threshold changes. The upper risk tolerance threshold (UT) would be associated with permanent isolation response. The lower risk tolerance threshold (LT) would remain each node intact. The band between the upper tolerance threshold and lower tolerance threshold is associated with the temporary isolation response, in which the isolation time (T) changes dynamically based on the different response level given by Equations 4.18 and 4.19, where n is the number of bands and i is the corresponding isolation band.

$$i = \lceil \frac{Risk - LT}{UT - LT} \times n \rceil, \ Risk \in (LT, UT) \tag{4.18}$$

$$T = 100 \times i \ (milliseconds) \tag{4.19}$$

We recommend the value of lower risk tolerance threshold be 0 initially if no additional information is available. It implies when the risk of attack is greater than the risk of isolation response, the isolation is needed. If other information is available, it could be used to adjust thresholds. For example, *node reputation* is one of important factors in MANET security, our adaptive decision making module could take this factor into account as well. That is, if the compromised node has a high or low reputation level, the response module can intuitively adjust the risk tolerance thresholds accordingly. In the case that LT is less than 0, even if the risk of attack

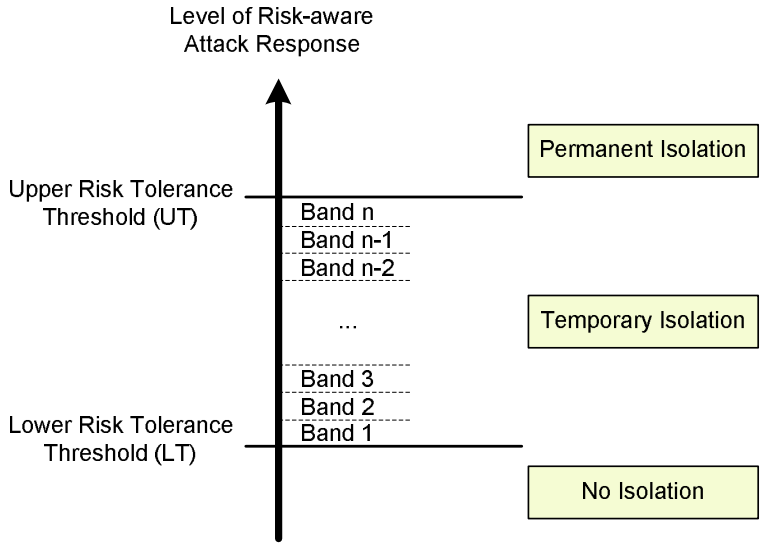

Figure 4.3: Adaptive Decision Making

is not greater than the risk of isolation, the response could also perform an isolation task to the malicious nodes.

The risk tolerance thresholds could also be dynamically adjusted by other factors, such as *attack frequency*. If the attack frequency is high, more severe response action should be taken to counter this attack. Our risk-aware response module could achieve this objective by reducing the values of risk tolerance threshold and narrowing the range between two risk tolerance thresholds.

4.7 Case Study and Evaluation

In this section, we first explain the methodology of our experiments and the metrics considered to evaluate the effectiveness of our approach. Then, we demonstrate the detailed process of our solution with a case study and also compare our risk-aware approach with binary isolation. In addition, we evaluate our solution with five random network topologies considering different size of nodes. The results show the effectiveness and scalability of our approach.

Des	Next	Dis
1	4	2
2	4	2
3	4	3
4	4	1
5	4	3
6	4	3

Before attack

Des	Next	Dis
1	1	1
2	1	2
3	1	3
4	4	1
5	1	2
6	1	2

After attack

Des	Next	Dis
2	4	2
3	4	3
4	4	1
5	4	3

After isolation

(a) Routing Table of Node 0

Des	Next	Dis
0	0	1
1	1	1
2	2	1
3	2	2
5	2	2
6	1	2

Before attack

Des	Next	Dis
0	0	1
1	1	1
2	2	1
3	2	2
5	2	2
6	1	2

After attack

Des	Next	Dis
0	0	1
2	2	1
3	2	2
5	2	2

After isolation

(b) Routing Table of Node 4

Des	Next	Dis
0	1	3
1	1	1
2	1	2
3	1	3
4	1	2
5	1	2

Before attack

Des	Next	Dis
0	1	2
1	1	1
2	1	2
3	1	3
4	1	2
5	1	2

After attack

Des	Next	Dis

After isolation

(c) Routing Table of Node 6

Figure 4.4: Routing Tables

4.7.1 Methodology and Metrics

The experiments were carried out using NS-2 as the simulation tool from VINT Project Fall and Varadhan (2010) with UM-OLSR Ros (2007). NS-2 is a discrete event network simulator which provides a detailed model of the physical and link layer behavior of a wireless network and allows arbitrary movement of nodes within the network. UM-OLSR is an implementation of Optimized Link State Routing protocol for the NS-2, which complies with Clausen and Jacquet (2003) and supports all core functionalities of OLSR plus the link-layer feedback option. In our experiments,

we constructed MANET scenarios in a topology of 1000m×1000m area. The total simulation time was set to 1200 seconds, and the bandwidth was set to 2 Mbps. Constant Bit Rate (CBR) traffic was used to send 512 byte-UDP packets between nodes. The queuing capacity of every node was set to 15. We adopted a random traffic generator in the simulation that chose random pairs of nodes and sent packets between them. Every node kept track of all packets sent by itself and the entire packet received from other nodes in the network.

In order to evaluate the effectiveness of our adaptive risk-aware response solution, we divided the simulation process into three stages and compared the network performance in terms of six metrics. The following describes the activities associated with each stage:

Stage 1 - Before attack: random packets were generated and transmitted among nodes without activating any of them as attackers. This simulation can present the traffic patterns under the normal circumstance.

Stage 2 - After attack: specific nodes were set as attackers which conducted malicious activities for their own profits. However, any detection or response is not available in this stage. This simulation process can present the traffic patterns under the circumstance with malicious activities.

Stage 3 - After response: response decisions for each node were made and carried out based on three different mechanisms.

We computed six metrics Hu *et al.* (2005) for each simulation run:

- *Packet Delivery Radio*: The ratio between the number of packets originated by the application layer CBR sources and the number of packets received by the CBR sink at the final destination.

- *Routing Cost*: The ratio between the total bytes of routing packets transmitted

during the simulation and the total bytes of packets received by the CBR sink at the final destination.

- *Packet Overhead*: The number of transmitted routing packets; for example, a HELLO or TC message sent over four hops would be counted as four packets in this metric.

- *Byte Overhead*: The number of transmitted bytes by routing packets, counting each hop similar to *Packet Overhead*.

- *Mean Latency*: The average time elapsed from "when a data packet is first sent" to "when it is first received at its destination."

- *Average Path Length*: This is the average length of the paths discovered by OLSR. It was calculated by averaging the number of hops taken by each data packet to reach the destination.

4.7.2 Case Study

Figure 4.2 shows our case study scenario, where packets from Node 5 to Node 0 are supposed to go through Node 2 and Node 4. Suppose a malicious Node 1 advertises it has a direct link (fake link) to Node 0 and it would cause every node to update its own routing table accordingly. As a result, the packets from Node 5 to Node 0 traverse Node 1 rather than Node 2 and Node 4. Hence, Node 1 can drop and manipulate the traffic between Node 5 and Node 0. We assume, as Node 1's one-hop neighbors, Node 0, Node 4 and Node 6 get the intrusion alerts with 80% confidence from their respective IDS modules. Figures 4.4(a)-(c) show the routing tables of Node 0, Node 4 and Node 6 before the attack, after the attack and after the isolation, respectively.

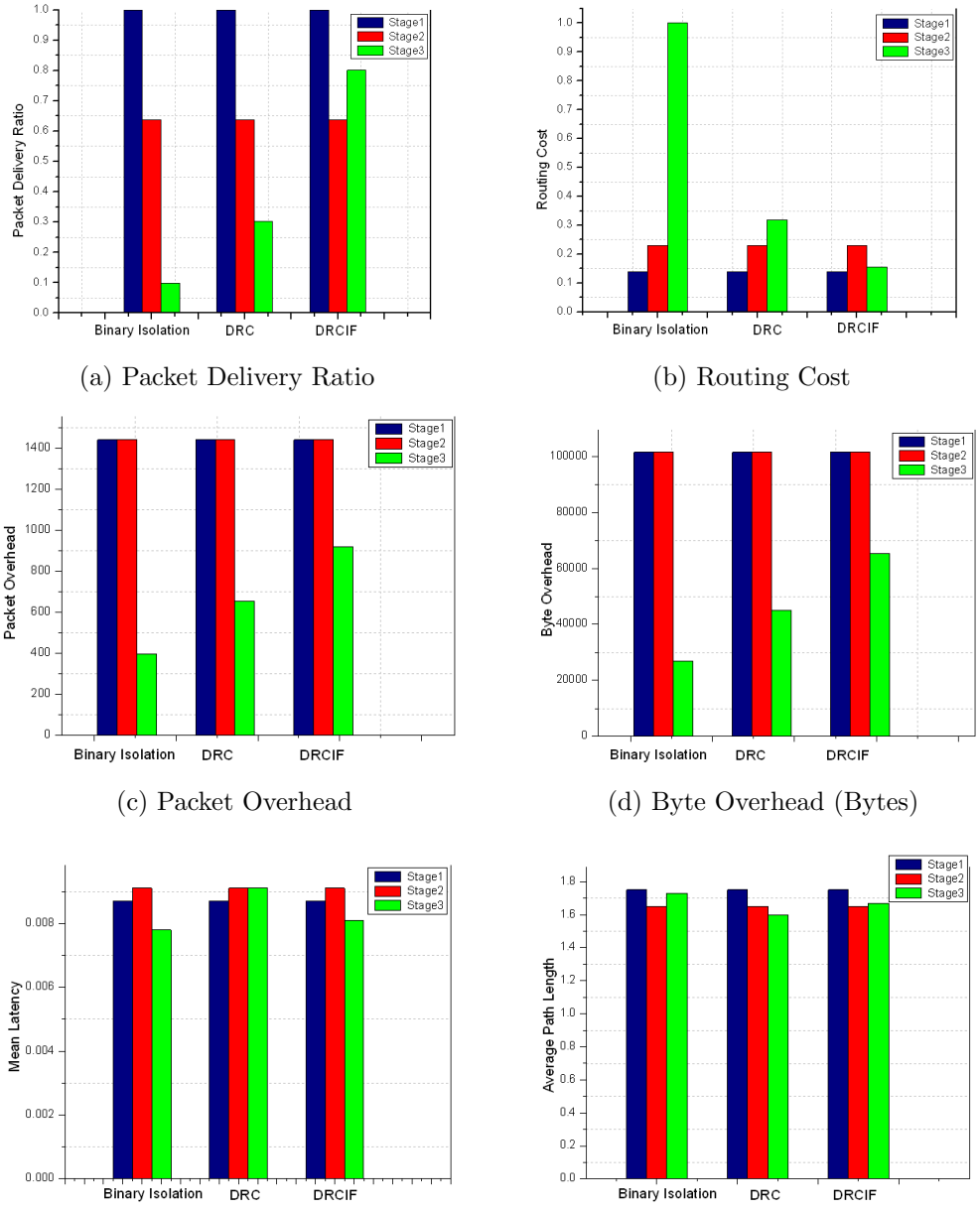

(a) Packet Delivery Ratio

(b) Routing Cost

(c) Packet Overhead

(d) Byte Overhead (Bytes)

(e) Mean Latency (Seconds)

(f) Average Path Length

Figure 4.5: Performance Results in Three Stages Comparing DRCIF with Binary Isolation and DRC

We set $a = 0.2$, $b = 0.7$, $c = 0.8$, $d = 0.05$, $IF_1 = 5$, $IF_2 = 7$, $IF_3 = 10$, $IF_4 = 3$, $IF_5 = 3$, $LT = -0.0017$, $UT = 1$, and $n = 5$ in our experiments.

We examine binary isolation approach, risk-aware approach with DRC, and risk-aware approach with DRCIF to calculate the response decisions for Node 0, Node

Table 4.1: Risk Assessment and Decision Making

		Node		
Approaches	Index	0	4	6
BINARY	*Decision*	*isolation*	*isolation*	*isolation*
DRC	$Risk_A$	0.00011	0.0000057	0.0000057
	$Risk_C$	0.00164	0.00164	0.0144
	Risk	-0.00153	-0.00163	-0.0143943
	Decision	*isolation*	*isolation*	*no isolation*
DRCIF	$Risk_A$	0.467	0.00355	0.00355
	$Risk_C$	0.0136	0.0136	0.1
	Risk	0.4534	-0.01005	-0.096
	Decision	*isolation*	*no isolation*	*no isolation*
	Time	300 *ms*	0	0

4 and Node 6. As shown in Table 4.1, binary isolation suggests all nodes to isolate the malicious one since it does not take countermeasure risk into account. With our risk-aware response mechanism based on our extended D-S theory, Node 1 should be isolated only by Node 0 while the original D-S theory would suggest that both Node 0 and Node 4 isolate Node 1.

In Figure 4.5(a), due to routing attacks, the packet delivery ratio decreases in *Stage 2*. After performing binary isolation and DRC risk-aware response in *Stage 3*, the packet delivery ratio even decreases more. This is because these two response mechanisms largely destroy the topology of network. However, the packet delivery ratio using our DRCIF risk-aware response in *Stage 3* is higher than those of the former two response mechanisms.

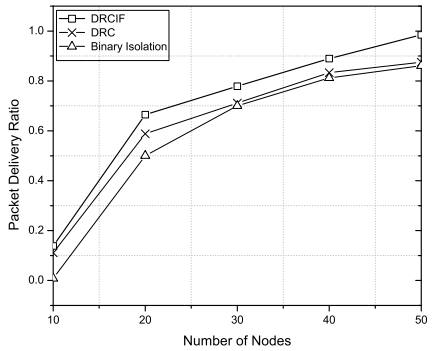

(a) Packet Delivery Ratio

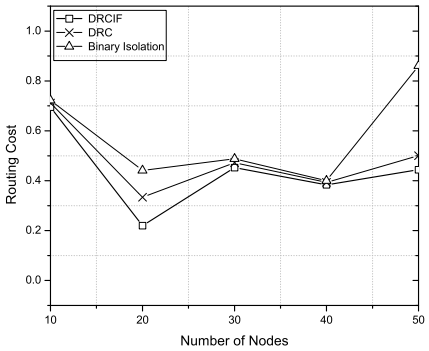

(b) Routing Cost

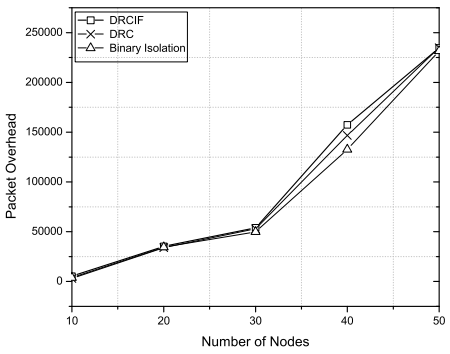

(c) Packet Overhead

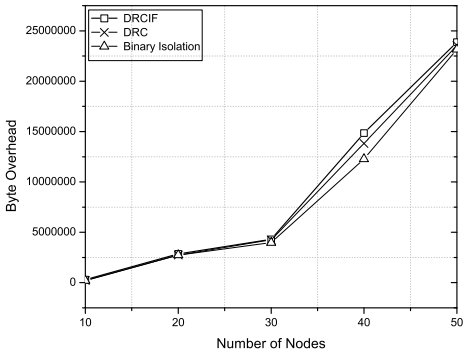

(d) Byte Overhead (Bytes)

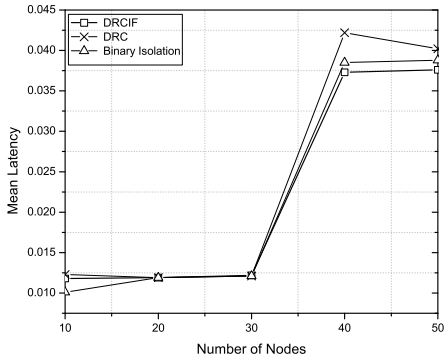

(e) Mean Latency (Seconds)

Figure 4.6: Performance Results in Five Random Topologies Comparing DRCIF with Binary Isolation and DRC

In Figure 4.5(b), the routing attacks increase the routing cost in *Stage 2*. Rather than recovering the routing cost in *Stage 3*, binary isolation and DRC risk-aware responses increase the routing cost. DRCIF risk-aware response, however, decreases

the routing cost. Compared with other two response mechanisms, it indicates our DRCIF risk-aware response effectively handles the attack.

Figures 4.5(c) and 4.5(d) show the packet and byte overhead, respectively. Since the routing attacks do not change the network topology further in the given case, the packet overhead and byte overhead remain almost the same in *Stage 2*. In *Stage 3*, however, they are higher when our DRCIF risk-aware response mechanism is applied. This result meet our expectation, because the number of nodes which isolate malicious node using binary isolation and DRC risk-aware response are greater than those of our DRCIF risk-aware response mechanism. As shown in Table 4.1, the number of isolated nodes for each mechanism varies.

In Figure 4.5(e), as a consequence of the routing attacks, the mean latency increases in *Stage 2*. After response, we notice the mean latencies in *Stage 3* for three different response mechanisms have approximately the same results.

In Figure 4.5(f), the average path length decreases in *Stage 2* due to the malicious action claiming a shorter path performed by Node 1. After response, the average path length using binary isolation is higher than those of the other two response mechanisms because more nodes isolated the malicious node based on the nature of binary isolation. Hence, some packets may be retransmitted by more hops than before.

4.7.3 Evaluation with Random Network Topologies

In order to test the effectiveness and scalability of our solution, we evaluated our risk-aware approach with DRCIF on five random network topologies. These five topologies have 10, 20, 30, 40 and 50 nodes respectively.

Figure 4.6 shows the performance results in these random network topologies of our risk-aware approach with DRCIF, risk-aware approach with DRC and binary

isolation approach. In Figure 4.6(a), as the number of nodes increases, the packet delivery ratio also increases because there are more route choices for the packet transmission. Among these three response mechanisms, we also notice the packets delivery ratio of our DRCIF risk-aware response is higher than those of the other two approaches.

In Figure 4.6(b), we can observe that the routing cost of our DRCIF risk-aware response is lower than those of the other two approaches. Note that the fluctuations of routing cost shown in Figure 4.6(b) are caused by the random traffic generation and random placement of nodes in our realistic simulation.

In our DRCIF risk-aware response, the number of nodes which isolate the malicious node is less than the other two response mechanisms. As shown in Figures 4.6(c) and 4.6(d), that is the reason why we can also notice that as the number of nodes increases, the packet overhead and the byte overhead using our DRCIF risk-aware response are slightly higher than those of the other two response mechanisms.

In Figure 4.6(e), the mean latency using our DRCIF risk-aware response is higher than those of the other two response mechanisms, when the number of nodes is smaller than 20. However, when the number of nodes is greater than 20, the mean latency using our approach is less than those of the other two response mechanisms.

4.8 Related Work

Intrusion Detection and Response in MANET. Some research efforts have been made to seek preventive solutions Hu *et al.* (2005); Levine *et al.* (2002); Hu *et al.* (2003); Awerbuch *et al.* (2008) for protecting the routing protocols in MANET. Although these approaches can prevent unauthorized nodes from joining the network, they introduce a significant overhead for key exchange and verification with the limited intrusion elimination. Besides, prevention-based techniques are less helpful to

cope with malicious insiders who possess the legitimate credentials to communicate in the network.

Numerous IDSs for MANET have been recently introduced. Due to the nature of MANET, most IDS are structured to be distributed and have a cooperative architecture. Similar to signatured-based and anomaly-based IDS models for the wired network, IDSs for MANET use specification-based or statistics-based approaches. Specification-based approaches, such as DEMEM Tseng *et al.* (2006b) and Tseng *et al.* (2006a); Mohammed *et al.* (2011); Felix *et al.* (2011), monitor network activities and compare them with known attack features, which are impractical to cope with new attacks. On the other hand, statistics-based approaches, such as Watchdog Marti *et al.* (2000), and Kurosawa *et al.* (2006), compare network activities with normal behavior patterns, which result in higher false positives rate than specification-based ones. Because of the existence of false positives in both MANET IDS models, intrusion alerts from these systems always accompany with alert confidence, which indicates the possibility of attack occurrence.

Intrusion response system (IRS) Hu *et al.* (2004) for MANET is inspired by MANET IDS. In Sun *et al.* (2006b) and Refaei *et al.* (2010), malicious nodes are isolated based on their reputations. Their work fails to take advantage of IDS alerts and simple isolation may cause unexpected network partition. Wang et al. Wang *et al.* (2007) brought the concept of cost-sensitive intrusion response which considers topology dependency and attack damage. The advantage of our solution is to integrate evidence from IDS, local routing table with expert knowledge, and countermeasures with a mathematical reasoning approach.

Risk-aware Approaches. When it comes to make response decisions Toth and Kruegel (2002b); Strasburg *et al.* (2009), there always exists inherent uncertainty which leads to unpredictable risk, especially in security and intelligence arena. Risk-

aware approaches are introduced to tackle this problem by balancing action benefits and damage tradeoffs in a quantified way. Cheng et al. Cheng *et al.* (2007) presented a fuzzy logic control model for adaptive risk-based access control. Teo et al. Teo *et al.* (2003) applied dynamic risk-aware mechanism to determine whether an access to the network should be denied or permitted. Jing et al. Jing *et al.* (2014) presented continuous and automated risk assessment of mobile applications.

However, risk assessment is still a non-trivial challenging problem due to its involvements of subjective knowledge, objective evidence and logical reasoning. Wang et al. Wang *et al.* (2007) proposed a naïve fuzzy cost-sensitive intrusion response solution for MANET. Their cost model took subjective knowledge and objective evidence into account but omitted a seamless combination of two properties with logical reasoning. Mu et al. Mu *et al.* (2008) adopted Dempster-Shafer theory to measure the risk of attacks and responses. However, as identified in Sentz and Ferson (2002), their model with Dempster's rule treats evidence equally without differentiating them from each other. To address this limitation, we propose a new Dempster's rule of combination with a notion of *importance factors* in D-S evidence model.

4.9 Summary

We have proposed a risk-aware response solution for mitigating MANET routing attacks. Especially our approach considered the potential damages of attacks and countermeasures. In order to measure the risks of both attacks and countermeasures, we extended Dempster-Shafer theory of evidence with a notion of *importance factors*. Based on several metrics, we also investigated the performance and practicality of our approach and the experiment results clearly demonstrated the effectiveness and scalability of our risk-aware approach.

Chapter 5

GUESSING PICTURE PASSWORDS

5.1 Introduction

Using text-based passwords that include alphanumerics and symbols on touch-screen devices is unwieldy and time-consuming due to small-sized screens and the absence of physical keyboards. Consequently, mobile operating systems, such as iOS and Android, integrate a numeric PIN and a draw pattern as alternative authentication schemes to provide user-friendly login services. However, the password spaces of these schemes are significantly smaller than text-based passwords, rendering them less secure and easy to break with some knowledge of device owners Bonneau *et al.* (2012).

To bring a fast and fluid login experience on touch-screen devices, the Windows 8™ operating system comes with a picture password authentication system, namely picture gesture authentication (PGA) Johnson (2012), which is also an instance of background draw-a-secret (BDAS) schemes Dunphy and Yan (2007). This new authentication mechanism hit the market with miscellaneous computing devices including personal computers and tablets. At the time of writing, over 60 million Windows 8™ licenses have been sold Foley (2013) and it is estimated that 400 million computers and tablets will run Windows 8™ with this newly introduced authentication scheme in one year Ovide (2012). Consequently, it is imperative to examine and explore potential attacks on picture gesture authentication in such a prevalent operating system for further understanding user experiences and enhancing this commercially popular picture password system.

Many graphical and gesture-based password schemes–including DAS Jermyn *et al.* (1999), Face Brostoff and Sasse (2000), Story Davis *et al.* (2004), PassPoints Wiedenbeck *et al.* (2005) and BDAS Dunphy and Yan (2007)–have been proposed in the past decade (for more, please refer to Dhamija and Perrig (2000); Thorpe and Van Oorschot (2004b); Suo *et al.* (2005); Chiasson *et al.* (2007); Gao *et al.* (2008); Bicakci *et al.* (2009); Biddle *et al.* (2011); Chiasson *et al.* (2012); Li *et al.* (2013c,b,a)). Amongst these schemes, click-based schemes, such as PassPoints, have attracted considerable attention and some research has analyzed the patterns and predictable characteristics shown in their passwords Chiasson *et al.* (2009); van Oorschot and Thorpe (2011). Furthermore, harvesting characteristics from passwords of a target picture and exploiting hot-spots and geometric patterns on the target picture have been proven effective for attacking click-based schemes Dirik *et al.* (2007); Thorpe and van Oorschot (2007); Salehi-Abari *et al.* (2008). However, PGA allows complex gestures other than a simple click. Moreover, a new feature in PGA, autonomous picture selection by users, makes it unrealistic to harvest passwords from the target pictures for learning. In other words, the target picture is previously *unseen* to any attack models. All existing attack approaches lack a generic knowledge representation of user choice in password selection that should be abstracted from specific pictures. The absence of this abstraction makes existing attack approaches impossible or abysmal (if possible) to work on previously unseen target pictures.

In this chapter, we provide an empirical analysis of user choice in PGA based on real-world usage data, showing interesting findings on user choice in selecting background picture, gesture location, gesture order, and gesture type. In addition, we propose a new attack framework that represents and learns users' password selection patterns from training datasets and generates ranked password dictionaries for previously unseen target pictures. To achieve this, it is imperative to build generic

knowledge of user choice from the abstraction of hot-spots in pictures. The core of our framework is the concept of a selection function that simulates users' selection processes in choosing their picture passwords. Our approach is not coupled with any specific pictures. Hence, the generation of a ranked password list is then transformed into the generation of a ranked selection function list which is then executed on the target pictures. We present two algorithms for generating the selection function list: one algorithm is to appropriately develop an optimal guessing strategy for a large-scale training dataset and the other deals with the construction of high-quality dictionaries even when the size of the training dataset is small. We also discuss the implementation of our attack framework over PGA, and evaluate the efficacy of our proposed approach with the collected datasets.

The rest of this chapter is organized as follows. Section 5.2 gives an overview of picture gesture authentication. Section 5.3 discusses our empirical analysis on picture gesture authentication. In Section 5.4, we illustrate our attack framework. Section 5.5 presents the implementation details and automated identified PoIs and gestures. Section 5.6 presents the evaluation results of the proposed attack framework. We discuss several research issues in Section 5.7 followed by the related work in Section 5.8. Section 5.9 concludes the chapter.

5.2 Background: Picture Gesture Authentication

Like other login systems, Windows 8™ Picture Gesture Authentication has two independent phases, namely registration and authentication. In the registration stage, a user chooses a picture from his or her local storage as the background. PGA does not force users to choose pictures from a predefined repository. Even though users may choose pictures from common folders, such as the `Picture Library` folder in Windows 8™, the probability for different users to choose an identical picture as the

background for their passwords is low. This phenomenon requires potential attack approaches to have the ability to perform attacks on previously unseen pictures. PGA then asks the user to draw exactly three gestures on the picture with his or her finger, mouse, stylus, or other input devices depending on the equipment he or she is using. A gesture could be viewed as the cursor movements between a pair of 'finger-down' and 'finger-up' events. PGA does not allow free-style gestures, but only accepts tap (indicating a location), line (connecting areas or highlighting paths), and circle (enclosing areas) Pace (2011a). If the user draws a free-style gesture, PGA will convert it to one of the three recognized gestures. For instance, a curve would be converted to a line and a triangle or oval will be stored as a circle. To record these gestures, PGA divides the longest dimension of the background image into 100 segments and the short dimension on the same scale to create a grid, then stores the coordinates of the gestures. The line and circle gestures are also associated with additional information such as directions of the finger movements.

Once a picture password is successfully registered, the user may login the system by drawing corresponding gestures instead of typing his or her text-based password. In other words, PGA first brings the background image on the screen that the user chose in the registration stage. Then, the user should reproduce the drawings he or she set up as his or her password. PGA compares the input gestures with the previously stored ones from the registration stage. The comparison is not strictly rigid but shows tolerance to some extent. If any of gesture type, ordering, or directionality is wrong, the authentication fails. When they are all correct, an operation is further taken to measure the distance between the input password and the stored one. For tapping, the gesture passes authentication if the predicate $12-d^2 \geq 0$ satisfies, where d denotes the distance between the tap coordinates and the stored coordinates. The starting

and ending points of line gestures and the center of circle gestures are measured with the same predicate Pace (2011a).

The differences between PGA and the first BDAS scheme proposed in Dunphy and Yan (2007) include: i) in PGA, a user uploads his or her picture as the background instead of choosing one from a predefined picture repository; ii) a user is only allowed to draw three specific types of gestures in PGA, while BDAS takes any form of strokes. The first difference makes PGA more secure than the previous scheme, because a password dictionary could only be generated after the background picture is acquired. However, the second characteristic reduces the theoretical password space from its counterpart. Pace et al. Pace (2011a) quantified the size of the theoretical password space of PGA which is $2^{30.1}$ with current length-three configuration in Windows 8™. For more details, please refer to Pace (2011a).

5.3 User Choice Patterns in Picture Gesture Authentication Passwords

In this section, we present an empirical analysis on user choice in PGA by analyzing data collected from our user studies. Our empirical study is based on human cognitive capabilities. Since human cognition of pictures is limited in a similar way to their cognition of texts, the picture passwords selected by users are probably constrained by human cognitive limits which would be similar to the ones in text-based passwords Yuille (1983).

5.3.1 Experiment Design

For the empirical study, we developed a web-based PGA system for conducting user studies. The developed system resembles Windows 8™ PGA in terms of its workflow and appearance. The differences between our implementation and Windows 8™ PGA include: i) our system works with major browsers in desktop PCs and

tablets whereas Windows 8™ PGA is a stand-alone program; ii) some information, such as the criterion for circle radius comparison, is not disclosed. In other words, our implementation and Windows 8™ PGA differ in some criteria (we regard radiuses the same if their difference is smaller than 6 segments in grid). In addition, our developed system has a tutorial page that includes a video clip educating how to use the system and a test page on which users can practice gesture drawings.

Our study protocol, including the type of data we plan to collect and the questionnaire we plan to use, was reviewed by our institution's IRB. The questionnaire consisted of four sections: i) general information of the subject (gender, age, level of education received, and race); ii) general feeling toward PGA (is it easier to remember, faster to input, harder to guess, and easier to observe than text-based password); iii) selection of background picture (preferred picture type); and iv) selection of password (preferred gesture location and type).

We started user studies after receiving the IRB approval letter in August 2012 and compiled two datasets from August 2012 to January 2013 using this system. *Dataset-1* was acquired from a testbed of picture password used by an undergraduate computer science class. *Dataset-2* was produced by advertising our studies in schools of engineering and business in two universities and Amazon's Mechanical Turk crowdsourcing service that has been used in security-related research work Kelley *et al.* (2012). Turkers who had finished more than 50 tasks and had an approval rate greater than 60% were qualified for our user study.

For registration, subjects in *Dataset-1* were asked to provide their student IDs for a simple verification after which they were guided to upload a picture, register a password and then use the password to access class materials including slides, homework, assignments, and projects. Subjects used this system for the Fall 2012 semester which lasted three and a half months at our university. If subjects forgot

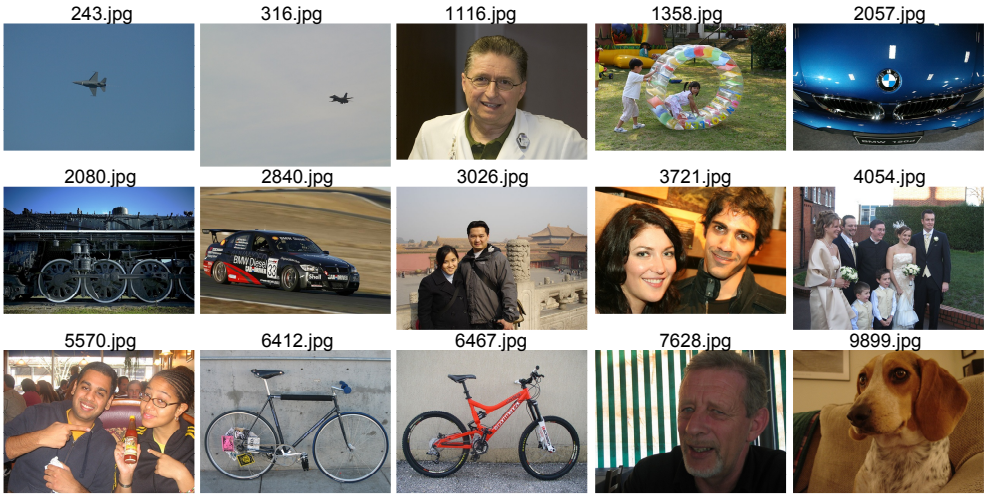

Figure 5.1: Background Pictures Used in *Dataset-2*

their passwords during the semester, they would inform the teaching assistant who reset their passwords. Subjects were allowed to change their passwords by clicking a change password link after login. There were 56 subjects involved in *Dataset-1* resulting in 58 unique pictures, 86 registered passwords, and 2,536 login attempts.

Instead of asking subjects to upload pictures for *Dataset-2*, we chose 15 pictures in advance from the PASCAL Visual Object Classes Challenge 2007 dataset Everingham *et al.* (2007). Figure 5.1 shows the 15 images that are used in *Dataset-2* as the background pictures for password selection. We chose these pictures because they represent a diverse range of pictures in terms of category (portrait, wedding, party, bicycle, train, airplane and car) and complexity (pictures with few and plentiful stand-out regions). Subjects were asked to choose one password for each picture by pretending that it was protecting their bank information. The 15 pictures were presented to subjects in a random order to reduce the dependency of password selection upon the picture presentation order. 762 subjects participated in the *Dataset-2* collection resulting in 10,039 passwords. The number of passwords for each picture in the *Dataset-2* varies slightly, with an average of 669, because some subjects quit the study without setting up passwords for all pictures.

Table 5.1: Survey Question: Which of the following best describes what you are considering when you choose locations to perform gestures?

Multi-choice Answers	Dataset		
	1	*2*	Overall
I try to find locations where special objects are, such as face, eye, clock, car, badge, etc.	24 (72.7%)	389 (59.6%)	413 (60.3%)
I try to find locations where some special shapes are, such as circle and line, etc.	8 (24.2%)	143 (21.9%)	151 (22.1%)
I try to find locations where colors are different from their surroundings, such as a red apple in a green lemon pile, etc.	0 (0%)	57 (8.7%)	57 (8.3%)
I randomly choose a location to draw without thinking about the background picture.	1 (3.0%)	66 (10.1%)	67 (9.8%)

For both datasets, subjects were asked to finish the aforementioned questionnaire to help us understand their experiences. We collected 685 (33 for *Dataset-1*, 652 for *Dataset-2*) copies of survey answers in total. According to the demographic-related inquiries in the exit survey, 81.8% subjects in *Dataset-1* are self-reported male and 63.6% are between 18 and 24 years old. While participants in *Dataset-2* are more diverse with 64.4% male, 37.2% among 18 to 24 years old, 45.4% among 25 - 34, and 15.0% among 35 - 50. Even though the subjects in our studies do not represent all possible demographics, the data collected from them represents the most comprehensive PGA usage so far. Their tendencies could provide us with significant insights into the user choice in PGA.

5.3.2 Findings

This section summarizes our empirical analysis on the above-mentioned datasets by presenting five findings.

Finding 1: Relationship Between Background Picture and User's Identity, Personality, or Interests

We analyzed all unique pictures in *Dataset-1*, and the background pictures chosen by subjects range from celebrity to system screenshot. We categorize them into six classes: i) people (27/58), ii) civilization (7/58), iii) landscape (3/58), iv) computer-generated picture (14/58), v) animals (6/58), and vi) others (1/58).

For the category of 'people', 6 pictures were categorized as 'me'; 12 pictures were subjects' families; 4 were pictures of subjects' friends; and 5 were celebrities. The analysis of answers to the survey question "*Could you explain why you choose such types of pictures?*" revealed two opposite attitudes towards using picture of people. The advocates for such pictures considered: i) it is more friendly. e.g. "*The image was special to me so I enjoy seeing it when I log in*"; ii) it is easier for remembering passwords. e.g. "*Marking points on a person is easier to remember*"; and iii) it makes password more secure. e.g. "*The picture is personal so it should be much harder for someone to guess the password*". However, other participants believed it may leak his or her identity or privacy. e.g. "*revealing myself or my family to anyone who picks up the device*". They preferred other types of pictures because "*less personal if someone gets my picture*" and "*landscape usually doesn't have any information about who you are*".

14 pictures in *Dataset-1* could be categorized as computer-generated pictures including computer game posters, cartoons, and some geometrical graphs. 24.1%

(14/58) of such pictures were observed in *Dataset-1* but the survey results indicated 6.4% (42/652) of participants were in such a usage pattern in *Dataset-2* based on the following survey question: "*Please indicate the type of pictures you prefer to use as the background*". We concluded the population characteristics (male, age 18-24, college students) in *Dataset-1* were the major reason behind this phenomenon. The answers to "*Could you explain why you choose such types of pictures?*" in *Dataset-1* supported this conjecture: "*computer game is something I am interested [in] it*" and "*computer games picture is personalized to my interests and enjoyable to look at*".

It is obvious that pictures with personally identifiable information may leak personal information. However, it is less obvious that even pictures with no personally identifiable information may provide some clues which may reveal the identity or persona of a device owner. Traditional text-based password does not have this concern as long as the password is kept secure. Previous graphical password schemes, such as Face and PassPoints, do not have this concern either because pictures are selected from a predefined repository.

Finding 2: Gestures on Points of Interest

The security of background draw-a-secret schemes mostly relies on the location distribution of users' gestures. It is the most secure if the locations of users' gestures follow a uniform distribution on any picture. However, such passwords would be difficult to remember and may not be preferable by users. By analyzing the collected passwords, we notice that subjects frequently chose standout regions (points of interest, PoIs) on which to draw. As shown in Table 5.1, only 9.8% subjects claimed to choose locations randomly without caring about the background picture. The observation is supported by survey answers to "*Could you explain the way you choose locations*

Table 5.2: Attributes of Most Frequently Used PoIs

Attributes	# Gesture	# Password	# Subject
Eye	36	20	19
Nose	21	13	10
Hand/Finger	6	5	4
Jaw	5	3	3
Face (Head)	4	2	2

to perform gestures?": "*If I have to remember it; it [would] better stand out.*" and "*Something that would make it easier to remember*".

Even though the theoretical password space of PGA is larger than text-based passwords with the same length, a background picture affects user choice in gesture location, reducing the feasible password space tremendously. We summarize three popular ways that subjects used to identify standout regions: i) finding regions with objects. e.g. "*I chose eyes and other notable features*" and "*I chose locations such as nose, mouth or whole face*"; ii) finding regions with remarkable shapes. e.g. "*if there is a circle there I would draw a circle around that*"; and iii) finding regions with outstanding colors. The detailed distribution of these selection processes is shown in Table 5.1. 60.3% of subjects prefer to find locations where special objects catch their eyes while 22.1% of subjects would rather draw on some special shapes.

Finding 3: Similarities Across Points of Interest

We analyzed the attributes of PoIs that users preferred to draw on. We paid more attention to the pictures of people because it was the most popular category. In the 31 registered passwords for the 27 pictures of people uploaded by 22 subjects in *Dataset-1*, we analyzed the patterns of PoI choice. As shown in Table 5.2, 36 gestures were drawn on eyes and 21 gestures were drawn on noses. Other locations that attracted

Figure 5.2: Two Versions of *Starry Night* and Corresponding Passwords

subjects to draw included hand/finger, jaw, face (head), and ear. Interestingly, 19 subjects out of 22 (86.3%) drew on eyes at least once, while 10 subjects (45.4%) performed gestures on noses. The tendencies to choose similar PoIs by different subjects are common in other picture categories as well. Figure 5.2 shows another example where two subjects uploaded two versions of *Starry Night* in *Dataset-1*. The passwords they chose show strikingly similar patterns with three taps on stars, even if there is no single gesture location overlap.

Finding 4: Directional Patterns in PGA Password

Salehi-Abari et al. Salehi-Abari *et al.* (2008) suggest many passwords in click-based systems follow some directional patterns. We are interested in whether PGA passwords show similar characteristics. For simplicity, we consider the coordinates of tap and circle gestures as their locations and the middle point of the starting and ending points of line as its location. If the x or y coordinate of a gesture sequence follows a consistent direction regardless of the other coordinate, we say the sequence follows a LINE pattern. We divide LINE patterns into four categories: i) H+, denoting left-to-right ($x_i \leq x_{i+1}$); ii) H-, denoting right-to-left ($x_i \geq x_{i+1}$); iii) V+, denoting top-to-bottom ($y_i \leq y_{i+1}$); and iv) V-, denoting bottom-to-top ($y_i \geq y_{i+1}$). If a se-

Table 5.3: Numbers of Gesture-order Patterns

	H+	H-	V+	V-	DIAG	Others
Dataset-1	43	5	16	4	22	18
	50.0%	5.8%	18.6%	4.6%	25.5%	20.9%
Dataset-2	3144	1303	1479	887	2621	3326
	31.3%	12.9%	14.7%	8.8%	26.1%	33.1%

quence of gestures follows a horizontal pattern and a vertical pattern at the same time, we say it follows a DIAG pattern.

We examined the occurrence of each LINE and DIAG pattern in the collected data. As shown in Table 5.3, more than half passwords in both datasets exhibited some LINE patterns, and a quarter of them exhibited some DIAG patterns. Among four LINE patterns, H+ (drawing from left to right) was the most popular one with 50.0% and 31.3% occurrences in *Dataset-1* and *Dataset-2*, respectively. And, V+ (drawing from top to bottom) was the second most popular with 18.6% and 14.7% occurrences in two datasets, respectively. This finding shows it is reasonable to use gesture-order patterns as one heuristic factor to prioritize generated passwords.

Finding 5: Time Disparity among Different Combinations of Gesture Types

We analyzed all registered passwords to understand the gesture patterns and the relationship between gesture type and input time. For 86 registered passwords (258 gestures) in *Dataset-1*, 212 (82.1%) gesture types were taps, 39 (15.1%) were lines, and only 7 (2.7%) were circles. However, the corresponding occurrences for 10,039 registered passwords (30,117 gestures) in *Dataset-2* were 15,742 (52.2%), 10,292 (34.2%), and 4,083 (13.5%), respectively. Obviously, subjects in *Dataset-2* chose more diverse gesture types than subjects in *Dataset-1*. As shown in Table 5.4, there was

Table 5.4: Numbers of Gesture Type Combinations and Average Time Spent on Creating Them

		3×t	3×l	3×c	2×t+l	2×t+c
Dataset-1	#	60	3	0	9	1
	Average Time (Seconds)	5.74	12.39	N/A	10.12	21.56
Dataset-2	#	3438	1447	253	1211	380
	Average Time (Seconds)	4.33	7.11	9.96	6.02	6.14
		2×l+t	2×l+c	2×c+t	2×c+l	t+l+c
Dataset-1	#	7	1	0	0	5
	Average Time (Seconds)	11.17	17.51	N/A	N/A	11.22
Dataset-2	#	1000	622	192	442	1054
	Average Time (Seconds)	7.72	9.98	8.78	10.19	9.37

a strong connection between the time subjects spent on reproducing passwords and the gesture types they chose. Three taps, the most common gesture combination, appeared in both datasets with the lowest average time (5.74 seconds and 4.33 seconds in corresponding dataset). On the other hand, the passwords with two circles and one line took the longest average input time (10.19 seconds in *Dataset-2*). In the user studies, subjects in *Dataset-2* were asked to set up the passwords by pretending they were protecting their bank information. However, subjects in *Dataset-1* actually used these passwords to access the class materials which they accessed more than four times a week on average. This may be a reason why subjects in *Dataset-1* prefer passwords with simpler gesture type combinations that are easier to reproduce in a timely manner.

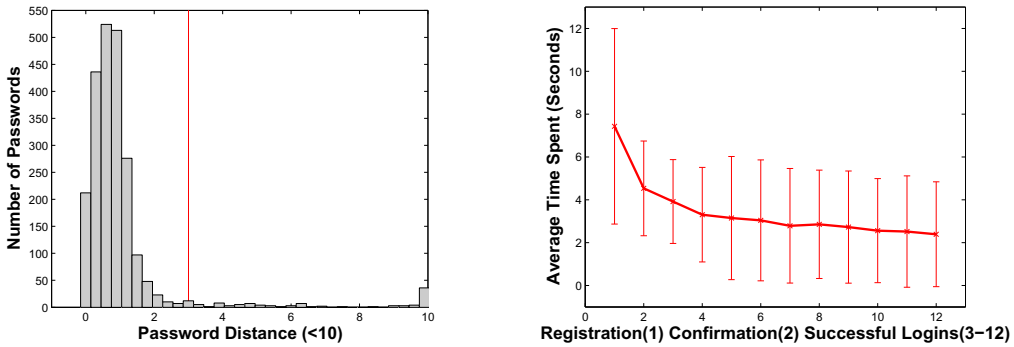

(a) Password Distance Histogram (b) Average Time Spent (Seconds)

Figure 5.3: Memorability and Usability

5.3.3 Memorability and Usability Analysis

The tolerance introduced in PGA is a trade-off between security and usability. In order to quantify this tradeoff, we calculate the distance between input PGA passwords with the registered ones. When the types or directions of gestures do not match, we regard input passwords incomparable with the registered ones. Otherwise, the distance is defined as the average distance of all gestures. We denote the password presented for the i-th attempt $\vec{\pi}^{(i)}$ and $\vec{\pi}^{(0)}$ as the password registered for the same picture.

In the 2,536 login attempts collected in *Dataset-1*, 422 are unsuccessful in which 146 are type or direction errors and 276 are distance errors. Figure 5.3(a) shows the distance distribution for the password whose distance is less than 10 and the red line denotes the threshold for being classified as successful. The result shows the current setup in our system is quite reasonable to capture most closely presented passwords.

Figure 5.3(b) shows the average time in seconds that subjects spent on registering, confirming, and reproducing passwords. $x = 1$ denotes the registration, $x = 2$ denotes the conformation, and all others denote the later login attempts. As we can notice, the average time for the registration is 7.43 seconds while 4.53 seconds are taken for the confirmation. With subjects getting used to the picture password system, the

average time spent for successful logins is reduced to as low as 2.51 seconds. On the other hand, the average time spent on all unsuccessful login attempts is 5.86 seconds.

5.4 Using User Choice Patterns to Attack PGA Passwords

In this section, we present an attack framework on Windows 8™ picture gesture authentication, leveraging the findings addressed in Section 5.3. Our attack framework takes the target picture's PoIs, a set of learning pictures' PoIs and corresponding password pairs as input, and produces a list of possible passwords, which is ranked in the descending order of the password probabilities.

Next, we first discuss the attack models followed by the representations of picture password and PoI. We then illustrate the idea of a selection function and its automatic identification. We also present two algorithms for generating a selection function sequence list and describe how it can generate picture password dictionaries for previously unseen target pictures.

5.4.1 Attack Models

Depending on the resources an attacker possesses, we articulate three different attack models: i) *Pure Brute-force Attack*: an attacker blindly guesses the picture password without knowing any information of the background picture and the users' tendencies. The password space in this model is $2^{30.1}$ in PGA Pace (2011a). ii) *PoI-assisted Brute-force Attack*: an attacker assumes the user only performs drawings on PoIs of the background picture and this model randomly guesses passwords on identified PoIs. The password space for a picture with 20 PoIs in this model is $2^{27.7}$ Pace (2011a). Salehi-Abari et al. Salehi-Abari *et al.* (2008) designed an approach to automatically identify hot-spots in a picture and generate passwords on them. iii) *Knowledge-based PoI-assisted Attack*: in addition to the assumption for PoI-assisted

brute-force attack, an attacker ought to have some knowledge about the password patterns learned from collected picture and password pairs (not necessarily from the target user or picture). The guessing space in this model is the same as the one in PoI-assisted brute-force attack. However, the generated dictionaries in this model are ranked with the higher possibility passwords on the top of the list.

Attack schemes could also be divided into two categories based on whether or not an attacker has the ability to attack previously unseen pictures. The method presented in Salehi-Abari *et al.* (2008) is able to attack previously unseen pictures for click-based graphical password. It uses click-order heuristics to generate partially ranked dictionaries. However, this approach cannot be applied directly to background draw-a-secret schemes because the gestures allowed in such schemes are much more complex and the order-based heuristics could not capture users' selection processes accurately. In contrast, our attack framework could abstract generic knowledge of user choice in picture password schemes. In addition, as a working *knowledge-based PoI-assisted* model, it is able to generate ranked dictionaries for previously unseen pictures.

5.4.2 Password and PoI Representations

We first formalize the representation of a password in PGA with the definition of a location-dependent gesture which represents a single gesture on some locations in a picture.

Definition 5.1. *A location-dependent gesture (LdG) denoted as π is a 7-tuple $\langle g, x_1, y_1, x_2, y_2, r, d\rangle$ that consists of gesture's type, location, and other attributes.*

In this definition, g denotes the type of LdG that must be one of tap, line, and circle. A tap LdG is further represented by the coordinates of a gesture $\langle x_1, y_1\rangle$. A

line LdG is denoted by the coordinates of the starting and ending points of a gesture $\langle x_1, y_1 \rangle$ and $\langle x_2, y_2 \rangle$. A circle LdG is denoted by the coordinates of its center $\langle x_1, y_1 \rangle$, radius r, and direction $d \in \{+, -\}$ (clockwise or not). We define the password space of location-dependent gesture as $\Pi = \Pi_{\mathsf{tap}} \bigcup \Pi_{\mathsf{line}} \bigcup \Pi_{\mathsf{circle}}$. A valid PGA password is a length-three sequence of LdGs denoted as $\vec{\pi}$, and the PGA password space could be denoted as $\vec{\Pi}$.

A point of interest is a standout region in a picture. PoIs could be regions with semantic-rich meanings, such as face (head), eye, car, clock, etc. Also, they could stand out in terms of their shapes (line, rectangle, circle, etc.) or colors (red, green, blue, etc.). We denote a PoI by the coordinates of its circumscribed rectangle and some describing attributes. A PoI is a 5-tuple $\langle x_1, y_1, x_2, y_2, D \rangle$, where $\langle x_1, y_1 \rangle$ and $\langle x_2, y_2 \rangle$ are the coordinates of the top-left and bottom-right points of the circumscribed rectangle, and $D \subseteq 2^{\mathcal{D}}$ is a set of attributes that describe this PoI. $\mathcal{D}$ has three sub-categories $\mathcal{D}_o, \mathcal{D}_s$ and $\mathcal{D}_c$ and four wildcards $*_o, *_s, *_c$, and $*$, where $\mathcal{D}_o = \{\mathsf{head}, \mathsf{eye}, \mathsf{nose}, ...\}$, $\mathcal{D}_s = \{\mathsf{line}, \mathsf{rectangle}, \mathsf{circle}, ...\}$, and $\mathcal{D}_c = \{\mathsf{red}, \mathsf{blue}, \mathsf{yellow}, ...\}$. Wildcards are used when no specific information is available. For example, if a PoI is identified with objectness measure Alexe *et al.* (2012) that gives no semantics about the identified region, we mark the PoI's describing attribute as $*$.

5.4.3 Location-dependent Gesture Selection Functions

A key concept in our framework is the location-dependent gesture selection function (LdGSF) which models and simulates the ways of thinking that users go through when they select a gesture on a picture. The motivation behind this abstraction is that the set of PoIs and their locations differ from picture to picture, but the ways that users think to choose locations for drawing a gesture exhibit certain patterns.

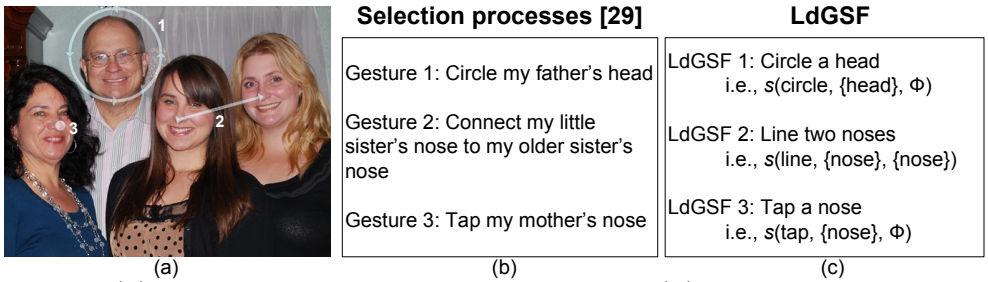

Figure 5.4: (a) Background Picture and Password (b) User's Selection Processes that Were Taken From Pace (2011b) (c) Corresponding LdGSFs that Simulate User's Selection Processes

This conjecture is supported by our observations from collected data and surveys discussed in Section 5.3. With the help of LdGSF, the PoIs and corresponding passwords in training pictures are used to generalize picture-independent knowledge that describes how users choose passwords.

Definition 5.2. *A location-dependent gesture selection function (LdGSF) is a mapping* $s : G \times 2^{\mathcal{D}} \times 2^{\mathcal{D}} \times \Theta \rightarrow 2^{\Pi}$ *which takes a gesture, two sets of PoI attributes, and a set of PoIs in the learning picture as input to produce a set of location-dependent gestures.*

The universal set of LdGSF is defined as S. A length-three sequence of LdGSF is denoted as $\vec{s}$, and a set of length-three LdGSF sequences is denoted as $\vec{S}$. $s(\mathsf{tap}, \{\mathsf{red}, \mathsf{apple}\}, \varnothing, \theta_k)$ is interpreted as 'tap a red apple in the picture p_k' and $s(\mathsf{circle}, \{\mathsf{head}\}, \varnothing, \theta_k)$ as 'circle a head in p_k'. Note that, no specific information of the locations of 'red apple' and 'head' is provided here which makes the representations independent from actual locations of objects in the picture.

One challenge we face is some PoIs may be big enough to take several unique gestures. Let us consider a picture with a big car image in it. Simply saying 'tap a car' could result in lots of distinct tap gestures in the circumscribed rectangle of the car. One solution to this problem is to divide the circumscribed rectangle into a grid with the scale of toleration threshold. However, this solution would result

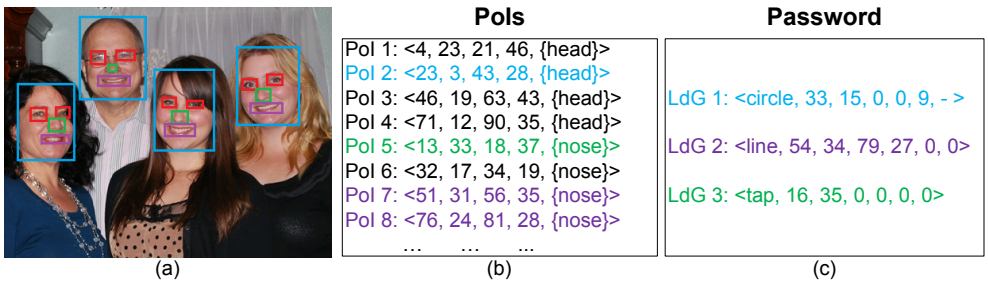

Figure 5.5: (a) Background Picture and Identified PoIs (b) Identified PoIs (c) Password Representations (Colors are used to indicate the connections between the PoIs in (b) and LdGs in (c))

in too many password entries in the generated dictionary. For simplicity, we introduce five inner points for one PoI, namely center, top, bottom, left, and right that denote the center of the PoI and four points of the center of two consecutive corners. Any gesture that falls into the proximities of these five points of a PoI would be considered as an action on this PoI. For some PoIs that are big enough to take an inner line gesture, we put $\varnothing$ as the input of the second set of PoI attributes. $s(\mathsf{line}, \{\mathsf{mouth}\}, \varnothing, \theta_k)$ denotes 'line from the left(right) to the right(left) on the same mouth'. While, $s(\mathsf{line}, \{\mathsf{mouth}\}, \{\mathsf{mouth}\}, \theta_k)$ means 'connect two different mouths'.

Figure 5.4 shows an example demonstrating how LdGSF simulates a user's selection processes that were taken from Pace (2011b). In reality, a user's selection process on a PoI and gesture selection may be determined by some subjective knowledge and cognition. For example, 'circle my father's head' and 'tap my mother's nose' may involve some undecidable computing problems. One solution to handle this issue is to approximate subjective selection processes in objective ways by including some modifiers. 'circle my father's head' may be transformed into 'circle the *uppermost* head' or 'circle the *biggest* head'. However, it is extremely difficult, if not impossible, to accurately approximate subjective selection processes in this way, and it may bring serious over-fitting problems in the learning stage. Instead, we choose to ignore subjective information by abstracting 'circle my father's head' to 'circle a head'. A

drawback of this abstraction is that an LdGSF may return more than one LdG and we have no knowledge to rank them directly, as they come from the same LdGSF. Using Figure 5.4(a) as an example, 'circle a head' outputs four different LdGs on each head in the picture. The LdGSF sequence shown in Figure 5.4(c) generates $4 \times (4 \times 3) \times 4 = 192$ passwords. To cope with this issue, we use gesture-order to rank the passwords generated by the same LdGSF sequence that will be detailed in Section 5.4.5. Next, we present an automated approach to extract users' selection processes from the collected data and represent them with LdGSFs.

Figure 5.5 shows an example demonstrating that how to extract users' selection processes from PoIs automatically. First, PoIs in the background picture are identified using mature computer vision techniques such as face detection and recognition Zhang and Li (2010, 2012), object detection Canny (1986), and objectness measure Alexe *et al.* (2012). Then, each LdG in a password is compared with PoIs based on their coordinates and sizes. If a match between PoIs and LdGs is found, a new LdGSF is created as the combination of the LdG's gesture type and PoI's attributes. For instance, the location and size of LdG 1 in Figure 5.5(c) matches PoI 2 in Figure 5.5(b) (the locations of the circle gesture and PoI center are compared first; then, the radius of the circle is compared with 1/2 of PoI's height and width). Then, an LdGSF $s(\mathsf{circle}, \{\mathsf{head}\}, \varnothing)$ is created which is equivalent to the LdG shown in Figure 5.4(c).

To choose a password in PGA, the user *selects* a length-three LdGSF sequence. With the definition of LdGSF, the generation of ranked password list is simplified into the generation of the ranked LdGSF sequence list. Let $\mathsf{order}\colon \vec{S} \to \{1..|\vec{S}|\}$ be a bijection which indicates the order LdGSF sequences should be performed. The objective of generating ranked LdGSF sequence list is to find such a bijection.

5.4.4 LdGSF Sequence List Generation and Ordering

Now we present our approach to find the aforementioned bijection that indicates the order that the LdGSF sequences should be performed on a target picture for generating the password dictionary. Our framework is not dependent on certain rules, but is adaptive to the tendencies shown by users who participate in the training set. The characteristic of adaptiveness helps our framework generate dedicated guessing paths for different training data. Next, we present two algorithms for obtaining such a feature.

BestCover LdGSF Sequence List Generation

We first propose an LdGSF sequence list generation algorithm named BestCover that is derived from $\mathcal{B}_{\mathsf{mssc}}$ Feige *et al.* (2004) and $\mathcal{B}_{\mathsf{emts}}$ Zhang *et al.* (2010). The objective of BestCover LdGSF sequence list generation is to optimize the guessing order for the sequences in the list by minimizing the expected number of sequences that need to be tested on a random choice of picture in the training dataset.

The problem is formalized as follows: *Instance*: The collection of LdGSF sequences $\vec{s_1}, ..., \vec{s_n}$ and corresponding picture password $\vec{\pi_1}$,...,$\vec{\pi_n}$, for which $\vec{s_i}(\theta_i) \ni \vec{\pi_i}, i \in \{1..n\}$ and $\theta_1, .., \theta_n$ are the sets of PoIs in pictures $p_1, .., p_n$. *Question*: Expected Min Selection Search (emss): The objective is to find order so as to minimize $\mathbb{E}(\min\{i : \vec{s_i}(\theta_r) \ni \vec{\pi_r}\}$, where $\vec{s_i} = \mathsf{order}^{-1}(i)$ and the expectation is taken with respect to a random choice of $r \leftarrow \{1..n\}$. We use $\mathsf{cover}_{emss}(k) = \min_{\vec{s}:\vec{s}(\theta_k) \ni \vec{\pi_k}}(\mathsf{order}_{emss}(\vec{s}))$ to compute the number of required guesses to break $\vec{\pi_k}$. Therefore, $\mathbb{E}(\min\{i : \vec{s_i}(\theta_r) \ni \vec{\pi_r}\}$ is equivalent to $\mathbb{E}(\mathsf{cover}_{emss}(r))$.

The hardness of this problem is that different LdGSFs and LdGSF sequences may generate the same list of LdGs and passwords. For instance, 'tap a red object' and

'tap an apple' turn out the same result on a picture in which there is a red apple. An overlap in different LdGSF results is similar to the coverage characteristics in the set cover problem. We can prove the NP-hardness of emss by reducing from mssc Feige *et al.* (2004); Zhang *et al.* (2010). Min Sum Set Cover (mssc) is formalized as follows: Given is a set U and a collection $\mathcal{C}$ of subsets of U where $\bigcup_{C\in\mathcal{C}} = U$. Let $\mathsf{order}_{mssc} : \mathcal{C} \to \{1..|\mathcal{C}|\}$ be a bijection, and let $\mathsf{cover}_{mssc} : U \to \{1..|\mathcal{C}|\}$ be defined by $\mathsf{cover}_{mssc}(j) = \min_{C\ni j}(\mathsf{order}_{mssc}(C))$. The problem is called min sum, because the object is to minimize $\sum_{j\in U}\mathsf{cover}_{mssc}(j)$.

Given any instance $(U,\mathcal{C})$ of mssc, denote $U = \{1..n\}$. We create a set of PoIs θ_j and a picture password $\vec{\pi_j}$ for each $j \in U$. θ_j and $\vec{\pi_j}$ must be different from θ_k and $\vec{\pi_k}$ respectively for any $k \neq j$. For each $C \in \mathcal{C}$, we create an LdGSF sequence $\vec{s_C}$ such that $\vec{s_C}(\theta_j) \ni \vec{\pi_j}$ if $j \in C$ and such that $\vec{s_C}(\theta_j) = \phi$ if $j \notin C$. We can always construct such an LdGSF sequence for each C by combining all $\theta_j, j \in C$ as a new PoI type in a wildcard representation. The set $\vec{S}$ consists of the set of $\vec{s_C}$ for different C. Set $\mathsf{order}_{mssc}(C) \leftarrow \mathsf{order}_{emss}(\vec{s_C})$, then

$$
\begin{aligned}
&\mathbb{E}(\mathsf{cover}_{emss}(r)) \\
&= \sum_{i=1}^{n} i \times Pr(\mathsf{cover}_{emss}(r) = i) \\
&= \sum_{i=1}^{n} i \times \frac{|k \in \{1..n\} : \mathsf{cover}_{emss}(k) = i|}{n} \\
&= \sum_{i=1}^{n} i \times \frac{|j \in U : \mathsf{cover}_{mssc}(j) = i|}{n} \\
&= \sum_{j\in U} \frac{\mathsf{cover}_{mssc}(j)}{n}
\end{aligned}
$$

The number of picture passwords that are cracked for the first time at the ith guess divided by the total number of picture passwords

Therefore, order_{emss} minimizes $\mathbb{E}(\mathsf{cover}_{emss}(r))$ if and only if order_{mssc} minimizes

$\sum_{j \in U} \mathsf{cover}_{mssc}(j)$. We give an approximation algorithm for emss in Algorithm 8 that is a modification from $\mathcal{B}_{\mathsf{mssc}}$ Feige *et al.* (2004) and $\mathcal{B}_{\mathsf{emts}}$ Zhang *et al.* (2010). The time complexity of BestCover is $O(n^2 + |\vec{S'}|log(|\vec{S'}|))$.

Algorithm 3: BestCover$((\vec{s_1}, .., \vec{s_n}),(\vec{\pi_1},...,\vec{\pi_n}))$

```
for i = 1..n do
    T_{s_i} ← {k : s_i(θ_k) ∋ π_k};
end
S' ← {s : |T_s| > 0};
for i = 1..|S'| do
    order^{-1}(i) ← s_k, that T_{s_k} has most elements that are not included in
    ⋃_{i'<i} order^{-1}(i');
end
return order
```

BestCover is good for a training dataset that consists of comprehensive and large scale password samples, because it assumes the target passwords exhibit same or at least very similar distributions to the training data. However, if the training dataset is small and biased, the results from BestCover may over-fit the training data and fail in testing data.

Unbiased LdGSF Sequence List Generation

The over-fitting problem in BestCover is brought about by the biased PoI attribute distributions in training data. For example, we have a training set with 9 pictures of apples and 1 picture of a car, and 5 corresponding passwords have circles on apples and 1 has a circle on car. In the generated LdGSF sequence list, BestCover will put sequences with 'circle an apple' prior to the ones with 'circle a car', because the

former ones have an LdGSF that was used in more passwords. However, we can see the probability for users to circle car (1/1) is higher than apples (5/9) if we consider the occurrences of apple and car in pictures.

Unbiased LdGSF sequence list generation copes with this issue by considering the PoI attribute distributions. It removes the biases from the training dataset by normalizing the occurrences of LdGSFs with the occurrences of their corresponding PoIs. Let $D_{\vec{s_k}} \subseteq \theta$ denote the event that θ contains enough PoIs that have attributes specified in $\vec{s_k}$. If a PoI with a specific type of attributes does not exist in a picture, the probability that a user select the PoI with such an attribute on this picture to draw a password is 0, denoted as $Pr(\vec{s_k}|\overline{D_{\vec{s_k}} \subseteq \theta}) = 0$, e.g. a user would not think and perform 'tap a red apple' on a picture without the existence of the red apple. We assume each LdGSF in a sequence is independent of each other and approximately compute $Pr(\vec{s_k}|D_{\vec{s_k}} \subseteq \theta)$ with Equation 5.1.

$$\begin{aligned} & Pr(\vec{s_k}|D_{\vec{s_k}} \subseteq \theta) \\ & = Pr(s_1 s_2 s_3 | D_{s_1} \subseteq \theta \wedge D_{s_2} \subseteq \theta \wedge D_{s_3} \subseteq \theta) \\ & = Pr(s_1|D_{s_1} \subseteq \theta) \times Pr(s_2|D_{s_2} \subseteq \theta) \times Pr(s_3|D_{s_3} \subseteq \theta) \end{aligned} \tag{5.1}$$

For each $s_i \in S$, we compute $Pr(s_i|D_{s_i} \subseteq \theta)$ with Equation 5.2:

$$Pr(s_i|D_{s_i} \subseteq \theta) = \frac{\sum_{j=1}^{n} count(D_{s_i}, \vec{\pi_j})}{\sum_{j=1}^{n} count(D_{s_i}, \theta_j)} \tag{5.2}$$

where $\sum_{j=1}^{n} count(D_{s_i}, \vec{\pi_j})$ denotes the number of LdGs in passwords of the training set that share the same attributes with s_i, and $\sum_{j=1}^{n} count(D_{s_i}, \theta_j)$ denotes the number of PoIs in the training set that share the same attributes with s_i. $Pr(s_i|D_{s_i} \subseteq \theta)$ describes the probability of using a certain LdGSF when there are enough PoIs with the required attributes.

The Unbiased algorithm generates an LdGSF sequence list by ranking $Pr(\vec{s_k}|D_{\vec{s_k}} \subseteq \theta)$ instead of $Pr(\vec{s_k})$ in descending order as shown in Algorithm 10. The time complexity of Unbiased is $O(n|S| + |\vec{S}|log(|\vec{S}|))$. The Unbiased algorithm would be better for the scenarios where fewer samples are available or samples are highly biased.

Algorithm 4: Unbiased(S)

```
for s ∈ S do
    Compute Pr(s|D_s ⊆ θ) with Equation 5.2;
end
for s⃗ ∈ S⃗ do
    Compute Pr(s⃗|D_s⃗ ⊆ θ) with Equation 5.1;
end
for i = 1..|S⃗| do
    order^{-1}(i)← s⃗_k, that Pr(s⃗_k|D_{s⃗_k} ⊆ θ) holds the i-th position in the descending
    ordered Pr(s⃗|D_s⃗ ⊆ θ) list;
end
return order
```

5.4.5 Password Dictionary Generation

The last step in our attack framework is to generate the password dictionary for a previously unseen target picture. First, the PoIs in the previously unseen picture are identified. Then, a dictionary is acquired by applying the LdGSF sequences on the PoIs, following the order created by the BestCover or Unbiased algorithm. Obviously, the passwords generated by an LdGSF sequence that holds a higher position in the LdGSF sequence list will also be in higher positions in the dictionary. However, as addressed earlier, BestCover and Unbiased algorithms do not provide extra information

to rank the passwords generated by the same LdGSF sequence. Inspired by using the click-order patterns as the heuristics for dictionary generation Salehi-Abari *et al.* (2008), we propose to rank such passwords generated by the same LdGSF sequence with gesture-orders. In the training stage, we record the gesture-order occurrence of each LINE and DIAG pattern and rank the patterns in descending order. In the attack stage, for the passwords generated by the same LdGSF sequence, we reorder them with their gesture-orders in the order of LINE and DIAG patterns. Passwords that do not belong to any LINE or DIAG pattern hold lower positions.

5.5 Implementation

In this section, we discuss the implementation details of our proof-of-concept system.

5.5.1 PoI Identification

We chose OpenCV Intel (2014) as the computer vision framework for our implementation and collected several feature detection tools for automatically identifying PoIs in background pictures. The computer vision techniques we adopted include: i) object detection: the goal of object detection is to find the locations and sizes of semantic objects of a certain class in a digital image. Viola-Jones object detection framework Viola and Jones (2004) is the first computationally affordable online object detection framework that utilizes Haar-like features instead of image intensities. Each learned classifier is represented and stored as a haar cascade. We collected 30 proven haar cascades from Reimondo (2008) for 8 different object classes including face (head), eye, nose, mouth, ear, head, body, and clock. ii) low-level feature detection: due to the high positive and high negative rates of object detection, we also resorted to some low-level feature detection algorithms that identify standout

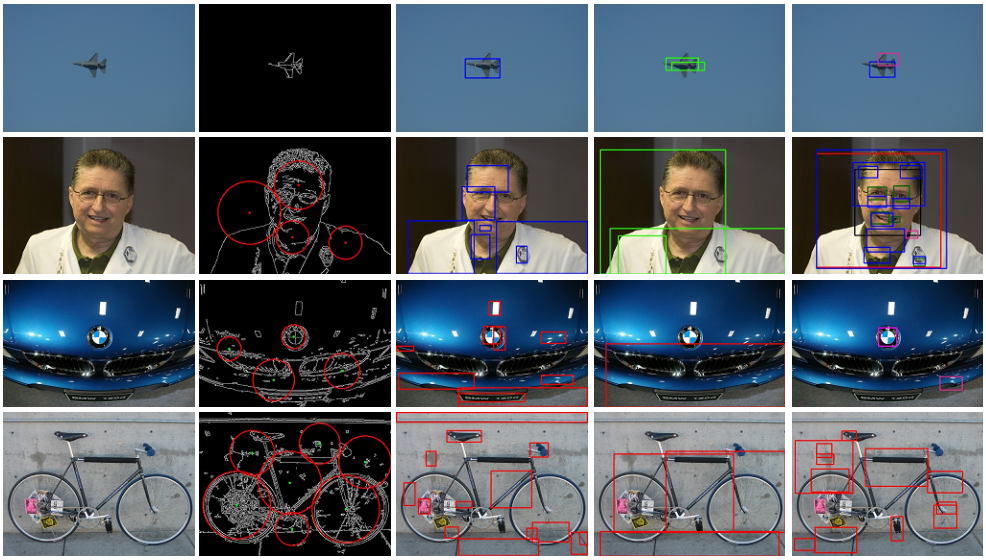

Figure 5.6: PoI Identification on Example Pictures in *Dataset-2*: (a) Original Pictures (b) Circle Detection with Hough Transform (c) Contour Detection (d) Objectness Measure (e) Object Detection

regions without extracting semantics. To identify regions whose colors are different from their surroundings, we first converted the color pictures to black and white, then found the contours using algorithms in Suzuki *et al.* (1985). For the circle detection, we used Canny edge detector Canny (1986) and Hough transform algorithms Ballard (1981). iii) objectness measure: objectness measure Alexe *et al.* (2012) deals with class-generic object detection. Different from detecting objects in a specific class, the objectness measure finds the locations and sizes of class-generic objects whose colors and textures are opposed to the background images. Objectness measure could be considered as a technique combining several low-level feature detectors together. We used an objectness measure library from Alexe *et al.* (2013) that is able to locate objects and give numerical confidence values with its results.

Figure 5.6 displays the PoI detection results on four example pictures in *Dataset-2*. As we can see in Figure 5.6(b), circle detection could identify both bicycle wheels and car badge, but its false positive rate is a little high. Contour detection is the

most robust algorithm with a low false positive rate which could locate regions whose colors are different as shown in Figure 5.6(c). Objectness measure shown in Figure 5.6(d) could also identify regions whose colors and textures are different from their surroundings. Since most haar cascades we used are designed for facial landmarks, they work smoothly on portraits as does the second picture in Figure 5.6(e). However, the results show relatively high false positive rates on pictures from other categories. In order to identify more PoIs as accurate as possible, our approach in PoI identification leveraged two steps. In the first step, all possible PoIs were identified using different kinds of tools. In the second step, we examined all identified PoIs and removed duplicates by comparing their locations, sizes and attributes. Then, our approach generated a PoI set called $P^1_{A\text{-}40}$ and $P^2_{A\text{-}40}$ for each picture in *Dataset-1* and *Dataset-2*, respectively. Those PoI sets consisted of at most 40 PoIs with the highest confidences.

Since our attack algorithms are independent from the PoI identification algorithms, we are also interested in examining how our attack framework performs with ideal PoI annotations for pictures. Besides using the automated PoI identification techniques, we manually annotated pictures in *Dataset-2* for some outstanding PoIs as well. To annotate the pictures, we simply recorded the locations and attributes of at most fifteen most appealing regions in the pictures without referring to any password in the collected dataset. We call this annotated PoI set $P^2_{L\text{-}15}$.

5.5.2 LdGSF Identification

We discuss the identified LdGSFs by linking PoIs and passwords in *Dataset-2* with the help of two PoI sets $P^2_{L\text{-}15}$ and $P^2_{A\text{-}40}$ using our LdGSF identification algorithm discussed in Section 5.4.3. The results from P_L are closer to users' actual selection processes, while the results from P_A are the best approximations to users' selection

processes we could get in a purely automated way with state-of-the-art computer vision techniques.

Table 5.5: Top 10 Identified LdGSFs Using $P^2_{L\text{-}15}$

Rank	$Pr(s_k)$	$Pr(s_k \mid D_{s_k} \subseteq \theta)$
1	$(\mathsf{tap}, \{\mathsf{head}\}, \varnothing)$	$(\mathsf{tap}, \{\mathsf{nose}\}, \varnothing)$
2	$(\mathsf{tap}, \{*_c\}, \varnothing)$	$(\mathsf{tap}, \{\mathsf{mouth}\}, \varnothing)$
3	$(\mathsf{tap}, \{\mathsf{circle}\}, \varnothing)$	$(\mathsf{tap}, \{\mathsf{circle}\}, \varnothing)$
4	$(\mathsf{tap}, \{\mathsf{eye}\}, \varnothing)$	$(\mathsf{tap}, \{\mathsf{eye}\}, \varnothing)$
5	$(\mathsf{circle}, \{\mathsf{head}\}, \varnothing)$	$(\mathsf{tap}, \{*_c\}, \varnothing)$
6	$(\mathsf{tap}, \{\mathsf{nose}\}, \varnothing)$	$(\mathsf{tap}, \{\mathsf{head}\}, \varnothing)$
7	$(\mathsf{circle}, \{\mathsf{circle}\}, \varnothing)$	$(\mathsf{circle}, \{\mathsf{circle}\}, \varnothing)$
8	$(\mathsf{circle}, \{\mathsf{eye}\}, \varnothing)$	$(\mathsf{tap}, \{\mathsf{ear}\}, \varnothing)$
9	$(\mathsf{line}, \{*_c\}, \{*_c\})$	$(\mathsf{line}, \{\mathsf{mouth}\}, \{\mathsf{mouth}\})$
10	$(\mathsf{line}, \{\mathsf{eye}\}, \{\mathsf{eye}\})$	$(\mathsf{tap}, \{\mathsf{forehead}\}, \varnothing)$

The top ten identified LdGSFs using $P^2_{L\text{-}15}$ are shown in Table 5.5 ordered by their $Pr(s_k)$ and $Pr(s_k|D_{s_k} \subseteq \theta)$. It also suggests that 'tap a head' is found the most times in the passwords, while 'tap a nose' is the most popular one when there is a nose in the picture. The result seems unreasonable at the first glance since there is always a nose in a head. Actually, it is because if the head in the picture is really small, we simply annotate the circumscribed rectangle as head instead of marking the inner rectangles with more specific attributes. Table 5.5 indicates that gestures on human organs are the most popular selection functions adopted by subjects.

The top ten identified LdGSFs using $P^2_{A\text{-}40}$ are shown in Table 5.6. By comparing Table 5.5 and Table 5.6, we could notice differences caused by using annotated PoI set and automated detected PoI set. The fact that $s(\mathsf{tap}, \{*\}, \varnothing)$ is among the top ten LdGSFs is an indicator that the automatic PoI identification could not classify

Table 5.6: Top 10 Identified LdGSFs Using $P^2_{A\text{-}40}$

Rank	$Pr(s_k)$	$Pr(s_k \mid D_{s_k} \subseteq \theta)$
1	(tap, {circle}, ∅)	(tap, {clock}, ∅)
2	(tap, {mouth}, ∅)	(circle, {clock}, ∅)
3	(tap, {eye}, ∅)	(tap, {shoulder}, ∅)
4	(tap, {head}, ∅)	(tap, {eye}, ∅)
5	(tap, {$*_c$}, ∅)	(tap, {head}, ∅)
6	(tap, {$*$}, ∅)	(tap, {body}, ∅)
7	(circle, {eye}, ∅)	(tap, {mouth}, ∅)
8	(tap, {body}, ∅)	(tap, {circle}, ∅)
9	(circle, {circle}, ∅)	(tap, {$*$}, ∅)
10	(circle, {head}, ∅)	(tap, {$*_c$}, ∅)

many PoIs and simply mark them as $*$. It is surprising to find out there are two LdGs on clock in top ten ordered by $Pr(s_k|D_{s_k} \subseteq \theta)$ at first, because there is no clock in any picture in *Dataset-2*. The closest guess is OpenCV falsely identified some circle shape objects as clocks, but the number is not very big since there is no LdG on a clock in the top ten ordered by $Pr(s_k)$.

5.6 Attack Evaluation

In this section, we present the evaluation results of our framework for nontargeted attacks and targetted attacks.

5.6.1 Nontargeted Attack Evaluation

In order to attack passwords from a previously unseen picture, the training dataset excluded passwords from the target picture. More specifically, to evaluate *Dataset-1* (58 unique pictures), we used passwords from 57 pictures as the training data and at-

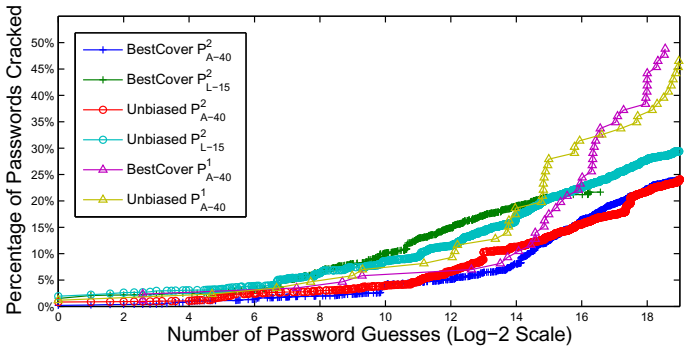

(a)

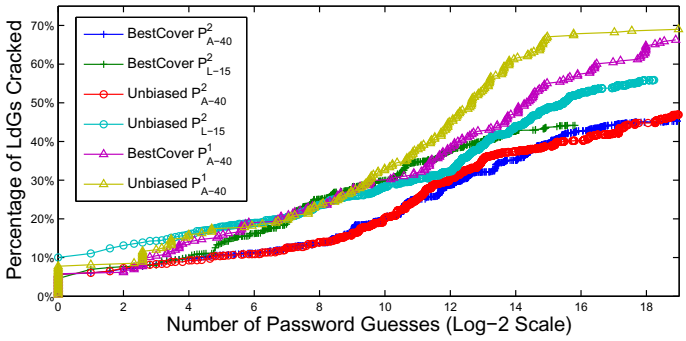

(b)

Figure 5.7: (a) Percentage of passwords cracked vs. number of password guesses, per condition. (b) Percentage of LdGs cracked vs. number of password guesses, per condition. For *Dataset-1*, there are 86 passwords that include 258 LdGs. For *Dataset-2*, there are 10,039 passwords that have 30,117 LdGs.

tacked the passwords for the last picture. To evaluate *Dataset-2* (15 unique pictures), we used passwords for 14 pictures as training data, learned the patterns exhibited in the training data, and generated a password dictionary for the last picture. The same process was carried out 58 and 15 times for *Dataset-1* and *Dataset-2*, respectively, in which the target picture was different in each round. The size of the dictionary was set as 2^{19} which is 11-bit smaller than the theoretical password space. We compared all collected passwords for the target picture with the generated dictionary for the picture, and recorded the number of password guesses.

Nontargeted attacks also require that the training dataset doesnot include previous passwords from the targeted user. However, it turns out very time-consuming to

perform strict nontargeted attacks on our *Dataset-2*. Instead, in our analyses, training password datasets include a very small number of passwords from the targeted subject. More specifically, in our experiment there were around 9,400 training passwords for which only 14 came from the targeted user. Even though this may affect the results, we believe it is less influential. Since all training passwords were treated equally, the influence brought by the 0.14% training data is low.

Offline Attacks

Due to the introduction of a tolerance threshold, picture passwords may be more difficult to store securely compared with text-based passwords that are normally saved after salted hashing. Even though the approach that Windows 8™ is adopting to store picture passwords remains undisclosed, we could consider two attack scenarios where picture passwords are prone to offline attacks. In the first scenario, all passwords which fall into the vicinity (defined by the threshold) of chosen passwords could be stored in a file with salted hashes for comparison. An attacker who has access to this file could perform offline dictionary attacks like cracking text-based password systems. In the second scenario, picture passwords could be used for other purposes besides logging into Windows 8™, where no constraint on the number of attempts is enforced. For example, a registered picture password could be transformed and used as a key to encrypt a file. An attacker who acquires the encrypted file would like to perform an offline attack.

In order to attack passwords from a previously unseen picture, the training dataset excluded passwords from the target picture. More specifically, to evaluate *Dataset-1* (58 unique pictures), we used passwords from 57 pictures as the training data and attacked the passwords for the last picture. To evaluate *Dataset-2* (15 unique pictures), we used passwords for 14 pictures as training data, learned the patterns exhibited in

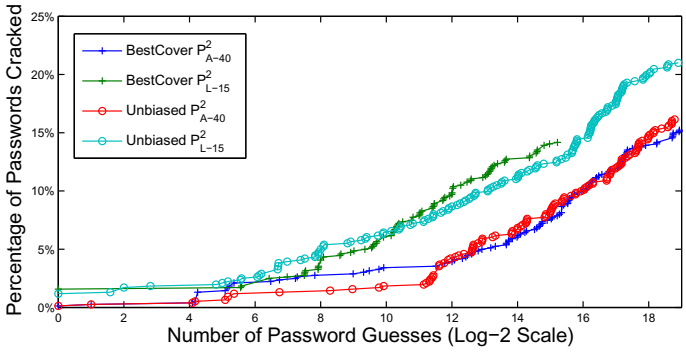

(a)

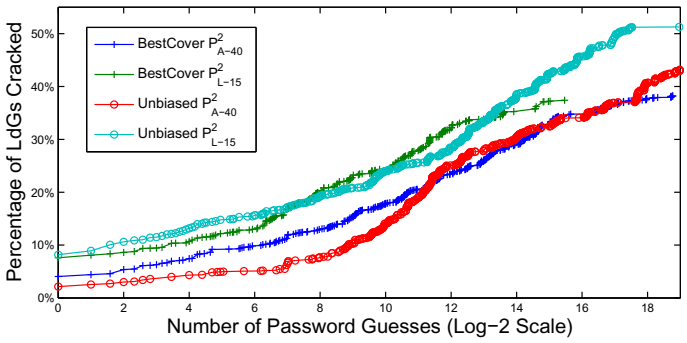

(b)

Figure 5.8: (a) Percentage of passwords cracked vs. number of password guesses, per condition. (b) Percentage of LdGs cracked vs. number of password guesses, per condition. Only the first chosen password by each subject in *Dataset-2* was considered. There are 762 passwords that have 2,286 LdGs.

the training data, and generated a password dictionary for the last picture. The same process was carried out 58 and 15 times for *Dataset-1* and *Dataset-2*, respectively, in which the target picture was different in each round. The size of the dictionary was set as 2^{19} which is 11-bit smaller than the theoretical password space. We compared all collected passwords for the target picture with the generated dictionary for the picture, and recorded the number of password guesses.

The offline attack results within 2^{19} guesses in different settings are shown in Figure 5.7. There are 86 passwords in *Dataset-1*, which have a total of 258 LdGs. And 10,039 passwords were collected in *Dataset-2*, containing a total of 30,117 LdGs. For *Dataset-1*, BestCover cracks 42 (48.8%) passwords out of 86 while Unbiased cracks 40

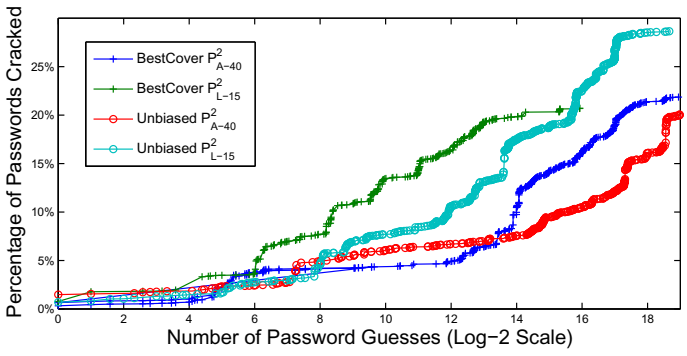

(a)

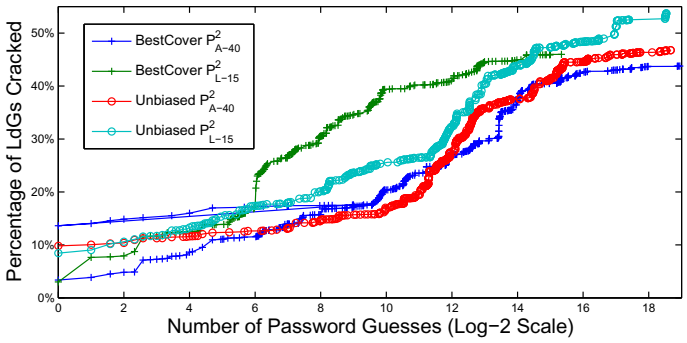

(b)

Figure 5.9: (a) Percentage of passwords cracked vs. number of password guesses, per condition. (b) Percentage of LdGs cracked vs. number of password guesses, per condition. Only passwords for pictures 243, 1116, 2057, 4054, 6467, and 9899 were considered. There are 4,003 passwords that have 12,009 LdGs.

(46.5%) passwords for the same dataset with $P^1_{A\text{-}40}$. For *Dataset-1*, 178 LdGs (68.9%) out of 258 are cracked with Unbiased and 171 (66.2%) are broken with BestCover. On the other hand, Unbiased with $P^2_{L\text{-}15}$ breaks 2,953 passwords (29.4%) out of 10,039 for *Dataset-2*. This implies Unbiased with $P^2_{A\text{-}40}$ cracking 2,418 passwords (24.0%) is the best result for all purely automated attacks on *Dataset-2*. As Figure 5.7 suggests, BestCover outperforms Unbiased slightly when ample training data is available. The better performance of both algorithms on *Dataset-1* is because the password gesture combinations in *Dataset-1* are relatively simpler than the ones in *Dataset-2* as we discussed in Section 5.3.2.

In *Dataset-2*, subjects may not choose all 15 passwords with the same care as

they were eager to finish the process. To reduce this effect, we ran another analysis in which only the first chosen password by each subject was considered. There are 762 passwords that have 2,286 LdGs. Like previous analysis, the training dataset excluded passwords from the target picture. As shown in Figure 5.8, results of this analysis are not as good as previous ones. Unbiased with $P^2_{L\text{-}15}$ breaks 160 passwords (21.0%) out of 762. Unbiased with $P^2_{A\text{-}40}$ cracking 123 passwords (16.1%). BestCover cracks 108 (14.2%) and 116 (15.2%) with $P^2_{L\text{-}15}$ and $P^2_{A\text{-}40}$, respectively.

Since some pictures in *Dataset-2* are similar, we ran an additional analysis in which only passwords for pictures 243 (airplane), 1116 (portrait), 2057 (car), 4054 (wedding), 6467 (bicycle), and 9899 (dog) were considered. There are 4,003 passwords that have 12,009 LdGs. Unbiased with $P^2_{L\text{-}15}$ breaks 1,147 passwords (28.6%) while 803 passwords (20.1%) are cracked by Unbiased with $P^2_{A\text{-}40}$. BestCover cracks 829 (20.7%) and 875 (21.8%) with $P^2_{L\text{-}15}$ and $P^2_{A\text{-}40}$ respectively. Results of this analysis are not as good as results with passwords from all pictures.

Online Attacks

The current Windows 8™ allows five failure attempts before it forces users to enter their text-based passwords. Therefore, breaking a password under five guesses implies the feasibility for launching an online attack. Figure 5.10 shows a refined view of the number of passwords and LdGs cracked with the first five guesses per condition. Purely automated attack Unbiased with $P^2_{A\text{-}40}$ breaks 83 passwords (0.8%) with the first guess and cracks 94 passwords (0.9%) within the first five guesses, while BestCover with $P^2_{A\text{-}40}$ cracked 20 passwords (0.2%) for the first guess and 38 passwords (0.4%) within five guesses. Additionally, Unbiased with $P^2_{A\text{-}40}$ breaks 1,723 LdGs (5.7%) with the first guess. With the help of manually labeled PoI set $P^2_{L\text{-}15}$, the results are even better. For example, Unbiased breaks 195 passwords (1.9%) for the first guess and

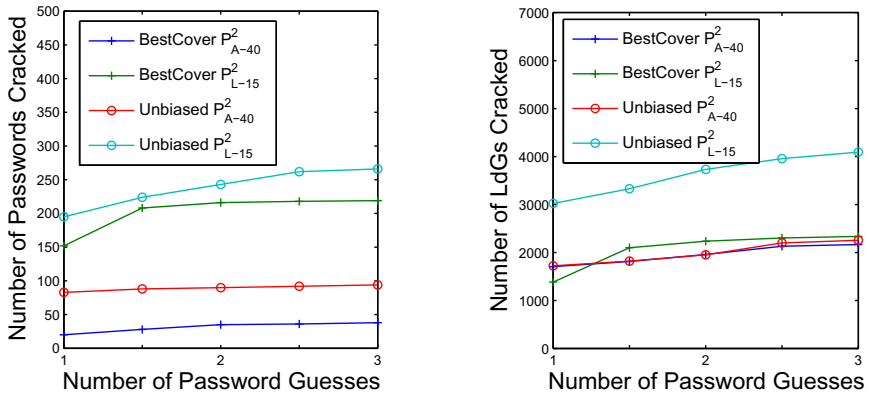

(a) (b)

Figure 5.10: Online attacks. (a) Number of passwords cracked within five guesses, per condition. (b) Number of LdGs cracked within five guesses, per condition.

266 (2.6%) within the first five guesses. In the meantime, Unbiased with $P^2_{L\text{-}15}$ breaks 3,022 LdGs (10.0%) with the first guess and 4,090 LdGs (13.5%) with five guesses.

Effects of Training Data Size

In Figure 5.11, we show the password and LdG cracking results with different sizes of training datasets. For each algorithm, we used $P^2_{A\text{-}40}$ as the PoI set and performed three analyses with 60, 600, and all available passwords (about 9,400) as training data, respectively. The sizes of 60 and 600 represent two cases: i) a training set (60) is ten times smaller than the target set (about 669); and ii) a training set (600) is almost the same size as the target set (about 669). For training datasets with the sizes of 60 and 600, we randomly selected these training passwords and performed each analysis three times to get the averages and standard deviations.

As Figure 5.11 shows, BestCover with 60 training samples could only break an average of 888 passwords (8.8%) out of 10,039. And the standard deviation is as strong as 673. While Unbiased with 60 training samples can crack 2,352 passwords (23.4%) that is almost the same as the results generated from all available training samples. Also, the standard deviation for three trials is as low as 62. The results from

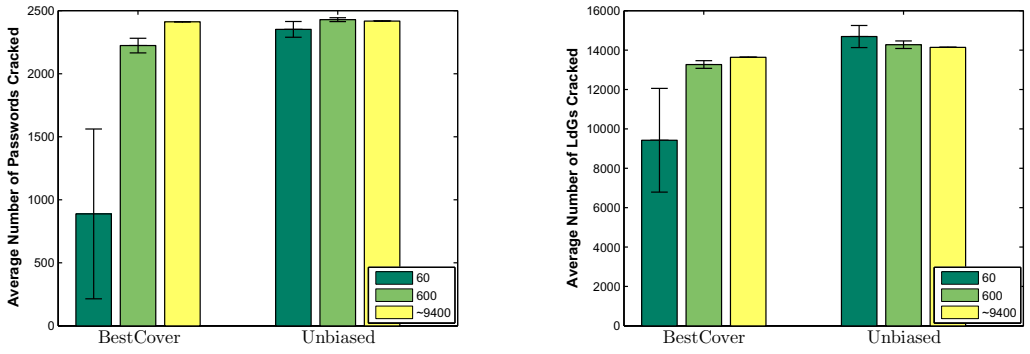

(a) (b)

Figure 5.11: (a) Average number of passwords cracked vs. different training data sizes. (b) Average number of LdGs cracked vs. different training data sizes. $P^2_{A\text{-}40}$ is used for this analysis. Average over 3 analyses, with one standard deviation shown.

BestCover with 600 training samples are much better than the counterparts with 60 training samples. All these observations are expected as Unbiased could eliminate the biases considered in BestCover. The results clearly demonstrate the benefit of using the Unbiased algorithm when a training dataset is small.

Effects on Different Picture Categories

We measured the attack results on different picture categories as shown in Figure 5.12 where each subfigure depicts the number of passwords cracked versus the number of password guesses. Each curve in a subfigure corresponds to a picture as shown in the legend. Our approach cracks more passwords for a picture, if the curve is skewed upward. And the cracking is faster (with fewer guesses), if the curve is leaned toward the left.

Figure 5.12(a) provides a view of the attack results on target pictures 243 and 316, each of which has only one airplane flying in the sky. Fewer PoIs in these two pictures make subjects choose more similar passwords. Unbiased with $P^2_{A\text{-}40}$ breaks 261 passwords (39.0%) for the picture 243 and 209 (31.2%) for the picture 316. The cracking success rates are much higher than the average success rate in *Dataset-2*

under the same condition. Note that the size of generated dictionaries for these two pictures are smaller than 2^{19} due to the number of available PoIs.

In Figure 5.12(b), we show the results on two *portrait* pictures where Unbiased with $P^2_{A\text{-}40}$ cracks 389 passwords (29.0%) for both in total. The attack success rate is much higher than the average success rate in *Dataset-2*. This is due to the fact that state-of-the-art computer vision algorithms work well on facial landmarks and subjects' tendencies of drawing on these features are high. The results show that passwords on simple pictures with fewer PoIs or portraits, for which state-of-the-art computer vision techniques could detect PoIs with high accuracy, are easier for attackers to break.

Figure 5.12(c) shows the attack results on 5 pictures of people. Some of these pictures only have very small figures of people and others have larger figures but not big enough to be considered as a portrait. Unbiased with $P^2_{A\text{-}40}$ cracks 726 passwords (21.7%) for these 5 pictures in total, which is lower than the average success rate in *Dataset-2*.

Figure 5.12(d) shows the attack results on 4 miscellaneous pictures, two of which are bicycle pictures and the other two are car pictures. The picture, 6412.jpg, has a bicycle leaning against the wall. Different colors on the bicycle and wall in this picture make it cluttered and have lots of PoIs. Unbiased with $P^2_{A\text{-}40}$ only cracks 68 passwords (10.1%) for this picture. However, Unbiased with $P^2_{A\text{-}40}$ cracked 458 (17.1%) for all 4 pictures.

Performance

We also evaluated the performance of our attack approach. Our analyses were carried out on a computer with dual-core processor and 4GB of RAM. In Figure 5.13, we show the average runtime for our algorithms to order the LdGSF sequences and

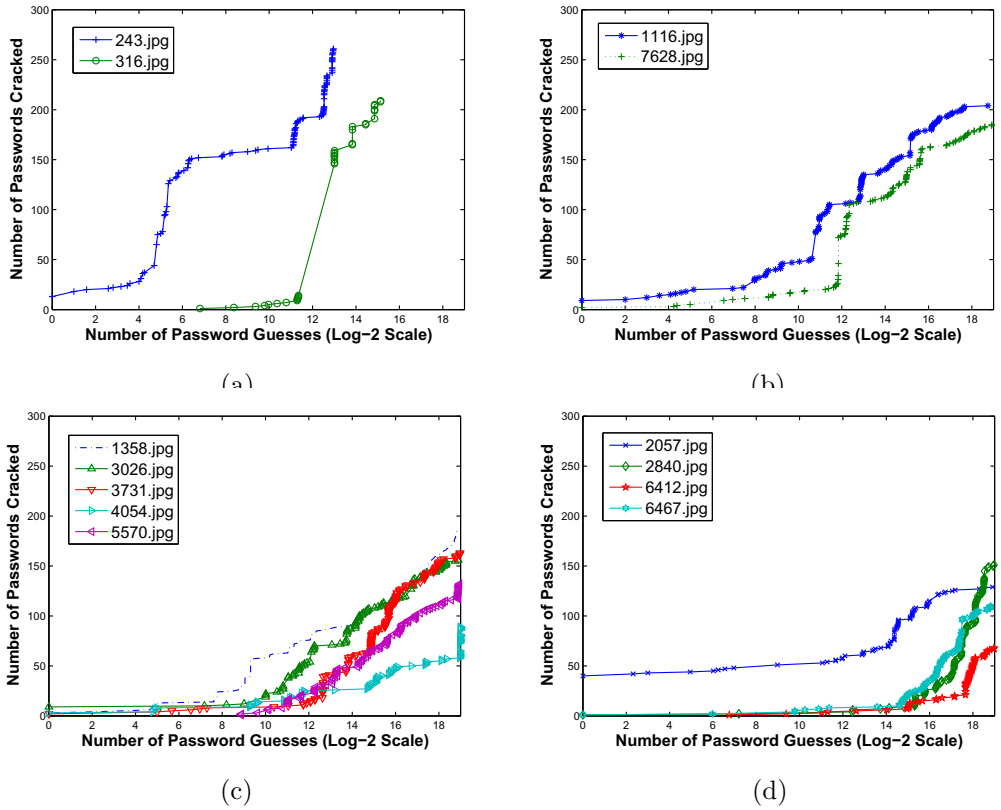

Figure 5.12: (a) pictures with fewer PoIs (b) portraits (c) pictures with people in them (d) pictures with lots of PoIs. Unbiased algorithm on $P^2_{A\text{-}40}$ is used for this analysis.

generate dictionary for a picture in *Dataset-2*. Each bar represents the average time in seconds over 15 pictures with the standard deviation using different algorithms and PoI sets. The results show that BestCover is much faster than Unbiased under the same condition. The average runtime for BestCover on $P^2_{A\text{-}40}$ to order LdGSF sequences is only 0.06 seconds and to generate a dictionary is 2.68 seconds, while Unbiased spends 18.36 and 3.96 seconds, respectively. As we analyzed in Section 5.4.4, such a difference is caused by the complexity of each algorithm. With such a prompt response, BestCover could be used for online queries.

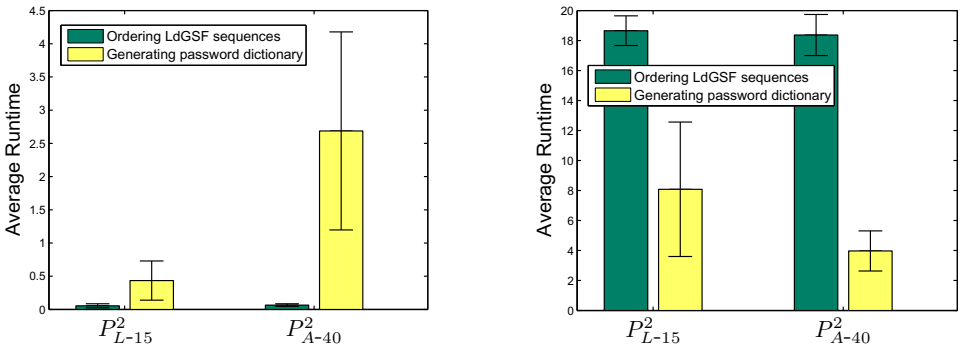

(a) BestCover algorithm (b) Unbiased algorithm

Figure 5.13: Average runtime in seconds to order LdGSF sequences using BestCover and Unbiased. Average over 15 pictures in *Dataset-2* with one standard deviation shown.

5.6.2 Targeted Attack Evaluation

In this section, we present the evaluation results of our framework for targeted attacks. Because most subjects in *Dataset-1* only chose one password, *Dataset-1* was excluded from these experiments. We only use the passwords of the subjects who chose two or more passwords in *Dataset-2* in these experiments. There are 697 subjects who fall into this pattern resulting in 9,974 passwords. For each of the 697 subjects, we use one of her passwords as the target and the rest of her passwords as training data set to build the model. The average size of training data sets is around 13, which is significantly smaller than the size used, which is around 9,400, in nontargeted attacks. A dictionary is generated in this way for each target password per user. Since each subject only chose one password for each picture, a training data set does not include passwords for the target picture. We recorded the number of password guesses when a password is cracked. Then, we cumulated the results for each user and each target password together in a single figure as illustrated in Figure 5.14.

The offline attack results within 2^{19} guesses in different settings are shown in Figure 5.14(a). Unbiased with $P^2_{L\text{-}15}$ breaks 2,233 passwords (22.4%) out of 9,974.

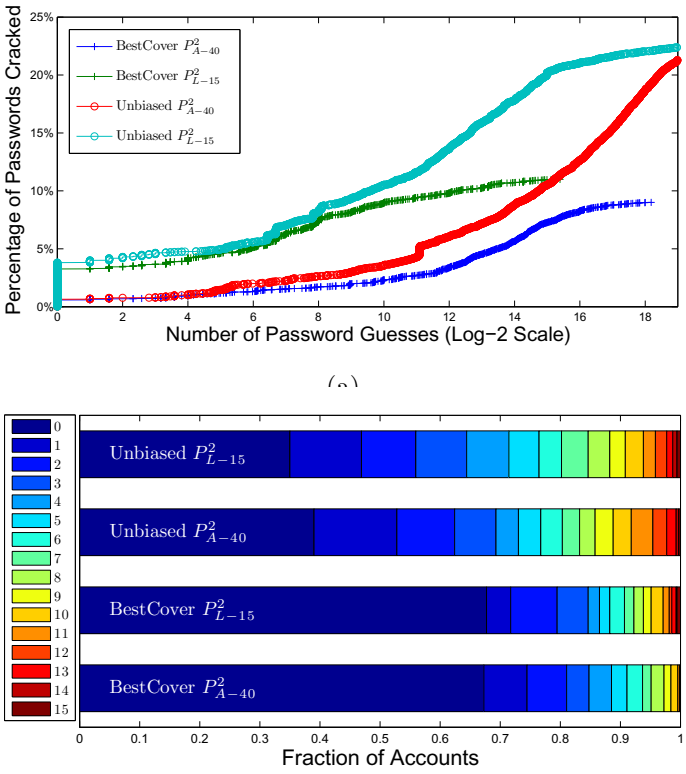

(a)

(b)

Figure 5.14: Offline attacks. There are 9,974 passwords from 697 accounts in this experiment. The average size of training data sets is around 13. (a) Percentage of passwords cracked vs. number of password guesses, per condition. (b) Passwords cracked per account. Each horizontal bar represents a condition. Regions within each bar show the fraction of accounts for which the indicated number of passwords were cracked.

Unbiased with $P^2_{A\text{-}40}$ breaks 2,123 passwords (21.3%) out of 9,974. Even though the results are a little bit lower than nontargeted attacks, we should take the significantly smaller training data set sizes into account. In nontargeted attack, the training data size is around 9,400 passwords. However, in targeted attack, the training data sizes range from at least 1 password to at most 14 passwords with an average of 13. In other word, targeted attacks using Unbiased algorithms with around 100 times smaller training data set could achieve almost the same results as nontargeted attacks. BestCover with $P^2_{L\text{-}15}$ and $P^2_{A\text{-}40}$ breaks 1,096 (10.9%) and 898 (9.0%) passwords,

respectively. Due to the small training data size, the results from BestCover for nontargeted attacks are quite lower than the counterparts for targeted attacks.

For online attacks within 5 guesses that are shown in the left-lower corner of Figure 5.14(a), Unbiased with $P^2_{L\text{-}15}$ breaks 434 passwords (4.4%) out of 9,974, and the first guesses could even break 380 (3.8%) passwords. Unbiased with $P^2_{A\text{-}40}$ breaks 77 passwords (0.7%) out of 9,974. BestCover with $P^2_{L\text{-}15}$ breaks 351 passwords (3.5%), and BestCover with $P^2_{A\text{-}40}$ breaks 70 passwords (0.7%).

Figure 5.14(b) shows the fractions of the accounts for which the indicated number of passwords were cracked. Each bar represents one condition. Unbiased with $P^2_{A\text{-}40}$ crack at least one password for 61.0% accounts, while Unbiased with $P^2_{L\text{-}15}$ could crack 65.0%. Even though BestCover with $P^2_{L\text{-}15}$ crack more passwords in total than with BestCover with $P^2_{L\text{-}15}$, BestCover with $P^2_{L\text{-}15}$ breaks more accounts for at least once. Both Unbiased and BestCover with $P^2_{L\text{-}15}$ cracks all 15 passwords for 4 (5.7%) out of 697 accounts.

5.7 Discussion

In this section, we discuss potential usage of our attack frame work, other attack approaches and the limitations of our work.

5.7.1 Picture-Password-Strength Meter

Our framework could enhance the security of PGA so it would eventually protect users and their devices by providing a picture-password-strength meter. One way to help users choose secure passwords is to enforce some composition policies, such as 'three taps are not allowed'. However, a recent effort Kelley *et al.* (2012) on text-based password found that rule-based password compositions are ineffective because they can allow weak passwords and reject strong ones. The cornerstone of accurate

strength measurement is to quantify the strength of a password. With a ranked password dictionary, our framework, as the first potential picture-password-strength meter, is capable of quantifying the strength of selected picture passwords. More intuitively, a user could be informed of the potential number of guesses for breaking a selected password through executing our attack framework.

5.7.2 Other Attacks on PGA

Besides keyloggers that record users' finger movements, there are some other attack methods that may affect the security of PGA and other background draw-a-secret schemes. Shoulder surfing, an attack where attackers simply observe the user's finger movements, is one of them. In our survey, 54.3% participants believe the picture password scheme is easier for attackers to observe when they are providing their credentials than text-based password. Several new shoulder surfing resistant schemes Forget *et al.* (2010); Zakaria *et al.* (2011) were proposed recently. However, the usability is always a major concern for these approaches. The smudge attack Aviv *et al.* (2010) which recovers passwords from the oily residues on a touch-screen has also been proven feasible to the background draw-a-secret schemes and could pose threats to PGA.

5.7.3 Limitations of Our Study

While we took great efforts to maintain our studies' validity, some design aspects of our studies and developed system may have caused subjects to behave differently from what they do on Windows 8™ PGA. Subjects in *Dataset-2* pretended to access their bank information but did not have anything at risk. Schechter et al. Schechter *et al.* (2007) suggest that role playing like this affects subjects' security behavior, so passwords in *Dataset-2* may not be representative of real passwords chosen by real

users. Besides, we did not record whether a subject used a tablet with touch-screen or a desktop with mouse. The different ways of input may affect the composition of passwords. Moreover, *Dataset-2* includes multiple passwords per user and this may have impacted the results. In our analyses, training password datasets include passwords from the targeted subject. Even though this may have affected the results, we believe it is less influential. Because, for each analysis, there were around 9,400 training passwords for which only 14 came from the targeted user. Since all training passwords were treated equally, the influence brought by the 0.14% training data is low. As discussed in Section 5.6, even though our online attack results showed the feasibility of our approach, it still requires more realistic and significant attack cases. As part of future work, we plan to integrate smudge attacks Aviv *et al.* (2010) into our framework to improve the efficacy of our online attacks.

5.8 Related Work

The security and vulnerability of text-based password have attracted considerable attention because of several infamous password leakage incidents in recent years. Zhang et al. Zhang *et al.* (2010) studied the password choices over time and proposed an approach to attack new passwords from old ones. Castelluccia et al. Castelluccia *et al.* (2012) proposed an adaptive Markov-based password strength meter by estimating the probability of password using training data. Kelley et al. Kelley *et al.* (2012) developed a distributed method to calculate how effectively password-guessing algorithms could guess passwords. Even though the attack framework we presented is dedicated to cracking background draw-a-secret passwords, the idea of abstracting users' selection processes of password construction introduced in this chapter could also be applicable to cracking and measuring text-based passwords.

The basic idea of attacking graphical password schemes is to generate dictionaries

that consist of potential passwords Thorpe and Van Oorschot (2004a). However, the lack of sophisticated mechanisms for dictionary construction affects the attack capabilities of existing approaches. Thorpe et al. Thorpe and van Oorschot (2007) proposed a method to harvest the locations of training subjects' clicks on pictures in click-based passwords to attack other users' passwords on the same pictures. In the same paper Thorpe and van Oorschot (2007), they presented another approach which creates dictionaries by predicting hot-spots using image processing methods. Oorschot et al. Oorschot and Thorpe (2008) cracked DAS using some password complexity factors, such as reflective symmetry and stroke-count. Salehi-Abari et al. Salehi-Abari *et al.* (2008) proposed an automated attack on the PassPoints scheme by ranking passwords with click-order patterns. However, the click-order patterns introduced in their approach could not capture users' selection processes accurately, especially when a background image significantly affects user choice. Nontargeted attacks on PGA passwords were discussed in our previous work Zhao *et al.* (2014).

5.9 Summary

We have presented a novel attack framework against background draw-a-secret schemes with special attention on picture gesture authentication. We have described an empirical analysis of Windows 8™ picture gesture authentication based on our user studies. Using the proposed attack framework, we have demonstrated that our approach was able to crack a considerable portion of picture passwords in various situations. We believe the findings and attack results discussed in this chapter could advance the understanding of background draw-a-secret and its potential attacks.

Chapter 6

DISCOVERING UNDERGROUND INTELLIGENCE

6.1 Introduction

Today's malware-infected computers are deliberately grouped as large scale destructive botnets to steal sensitive information and attack critical net-centric production systems David Anselmi (2010). A recent report by FBI IC3 shows that company losses from the cybercrime rose from 264.6 million dollars to 559.7 million dollars IC3 (2009). The situation keeps getting worse when botnets make use of legitimate social media, such as Facebook and Twitter, to launch botnet attacks Athanasopoulos *et al.* (2008); Thomas (2010). We even recently observed that the well-known social networks, such as Facebook and Twitter, could be used as platforms to launch botnet attacks Thomas (2010). In order to cope with these emerging threats, both proactive and passive approaches are proposed to gather and analyze information from malicious code samples. Previous research efforts on countering botnet attacks could be classified into four categories: (i) capturing malware samples Bächer *et al.* (2005), (ii) collecting and correlating network and host behaviors of malwares Gu *et al.* (2007), (iii) understanding the logic of malwares Chiang (2007); Porras *et al.* (2009), and (iv) infiltrating and taking over botnets Stone-Gross *et al.* (2009); Kanich *et al.* (2008).

Notably, most studies in the area of countering malware and botnets have been focused on detecting bot deployment, capturing and controlling bot behaviors. However, there is little research on examining how these malicious programs are created, rented and sold by adversaries. Even though preventive solutions against thousands of known bots have been deployed on networked systems, and some botnets were

even taken down by law enforcement agencies Mushtaq (2009), the majority of adversaries are still at large and keep threatening the Internet by developing more bots and launching more net-centric attacks. The major reason for this phenomenon is that previous malware-related activities–such as developing, renting and selling bots–were occurred mostly offline, which were way beyond the scope of security analysts.

In recent years, the pursuit of more profit in underground communities leads to the requirement for global collaboration among adversaries, which tremendously changed the division of labor and means of communication among them Dunham and Melnick (2008). (Un)fortunately, adversaries started to communicate with each other, distribute and improve attack tools with the help of the Internet, which leaves security analysts new clues for evidence acquisition and investigation on unwanted program development and trade. Before the widespread use of online social networks (OSNs), adversaries would communicate via electronic bulletin board systems (BBS), forums, and Email systems Goodin (2008).

Content-rich Web 2.0, ubiquitous computing equipments, and newly emerging online social networks provide an even bigger arena for adversaries. In particular, the value of OSNs for adversaries is the capability to cooperate with destructive botnets. The role of OSNs in botnet attacks is twofold: first, OSNs are the platforms to form online black markets, release bots, and coordinate attacks Dunham and Melnick (2008); Bächer *et al.* (2005); Holt and Bossler. (2010); second, OSN profiles act as bots to perform malicious actions Athanasopoulos *et al.* (2008) or C&C server nodes coordinates other networked bots Thomas (2010). Although our efforts in this chapter are mainly concerned about the former case, our proposed model for online underground social dynamics and corresponding social metrics can be also utilized to identify compromised and suspicious OSN profiles.

In the former role of OSNs for botnet attacks, a recent study Dunham and Mel-

nick (2008) reveals that many of these online black markets operate out of eastern Europe and Russia, and allow skilled programmers to create and profit from the sale of new malicious codes. These markets even use eBay-style feedback systems to help the suppliers of these services establish good business reputations. Individuals who control existing botnets also sell access to their infected machines for a variety of attacks including spamming and DDoS. As a consequence, these markets enable a great deal of unskilled adversaries and innocent computer users to engage in cybercrime.

Given the great amount of valuable information in online social dynamics, the investigation of the relationships between online underground social communities and network attack events are imperative to tactically cope with net-centric threats. In this chapter, we propose a novel solution using social dynamics analysis to counter malware and botnet attacks as a complement to existing research investments. In order to demonstrate the feasibility and applicability of our mechanism, we describe a proof-of-concept prototype with a case study on real-world data archived from Internet. We formally model online underground social dynamics and propose SocialImpact which is a suite of measures to help identify adversarial evidence by examining social dynamics.

The rest of this chapter is organized as follows. Section 6.3 presents our online underground social dynamics model and addresses SocialImpact, which is a systematic ranking analysis suite for mining adversarial evidence based on the model. In Section 6.4, we discuss the design and implementation of our proof-of-concept system. Section 6.5 presents the results of applying our model and metrics on synthetic social dynamics data. Section 6.6 presents the evaluation of our approach on real-world underground social dynamics data followed by the related work in Section 6.7. Section 6.8 concludes this chapter.

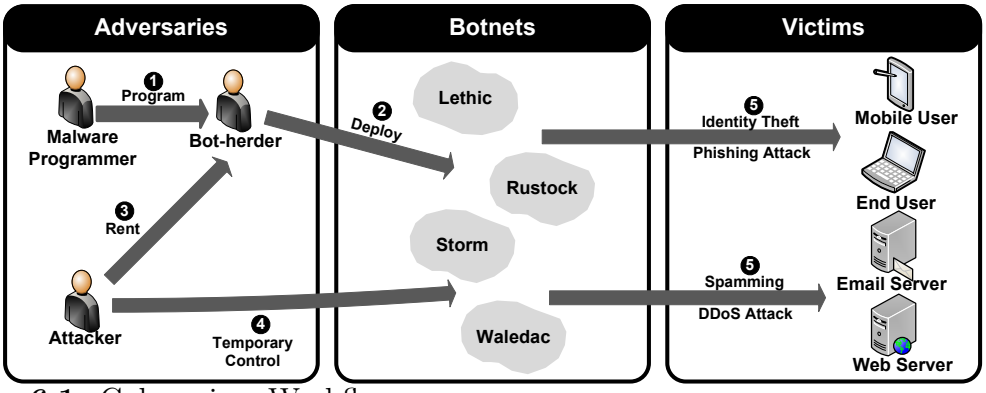

Figure 6.1: Cybercrime Workflow

6.2 Patterns in Cybercrime

Figure 6.1 shows a typical workflow of cybercrime. In *Step 1*, malware programmers develop crafted attack tools. The most prevalent and destructive tool developed to carry out various attacks is a set of bots. Malware programmers turn bots to bot-herders through online black markets or offline channels. In *Step 2*, bot-herders deploy a botnet through social engineering, drive-by-download or other possible vectors. In *Step 3*, bot-herders rent a botnet out to other adversaries, from which bot-herders and malware programmers profit, who have targets in mind but do not have the technological expertise to design or administer the botnet. In *Step 4*, attackers, such as spammers, take control of the botnet. A rented botnet may result in a variety of attacks launched by multiple adversaries who might have different intents. In *Step 5*, attackers coordinate bot nodes to perform multiple attacks such as spamming, identity theft, DDoS, phishing attacks, etc.

The power of botnets relies on their coordination and the volume of the responses from the bot nodes. In a typical botnet, hundreds to thousands of bot nodes respond to botmaster's commands. When these nodes are instructed to connect to one webpage at the same time, the aggregated volume of the network traffic would be tremendous for most companies to handle, causing denial-of-service to the targeted

servers. When these nodes are instructed to download banking credentials, the botmaster receives credentials from each bot which can be thousands or even millions in some botnets. Another critical problem caused by botnets is e-mail spamming. Nowadays a spam causes not only a network-clogging problem, but also a means for adversaries to distribute additional malwares.

Most significant botnets today are constantly changing. They are evolved by adding bots, deleting bots, changing to new channels, being upgraded, etc. Attempting to discover their C&C servers may bring immediate benefits but also stimulate the evolution of botnets. Park and Reeves pointed out Park and Reeves (2009), it is also important to monitor botnets for an extended time to learn the purpose of the botnets to develop more effective countermeasures. A good example of this is what happened after the takedown of the largest spamming botnet in the world, the McColo botnet. In November 2008, the major spamming botnet command and control, McColo was shut down. The next day the spam volume was nearly cut in half, but by the end of 2009 the volume was increased higher than ever. Experts agree that the explosion in spamming is a result of the botmasters in charge of McColo regrouping and creating other botnets in which they could spread their spam once again Security (2010).

In other words, existing approaches concentrate on *Step 2*, *Step 4* and *Step 5* in Figure 6.1 and largely overlook *Step 1* and *3*. Furthermore, since malware authors have adopted protection approaches to hide malware-related data from analysis, research results on *Step 2*, *Step 4* and *Step 5* which may work smoothly for prior malwares are ineffective to accommodate the new trend of malware evolution. Therefore, we also propose to systematically examine social dynamics to bridge the gap of research efforts on *Step 1* and *Step 3* and automatically extract internal ciphertext data from malware to complement existing efforts on *Step 2*, *Step 4* and *Step 5*.

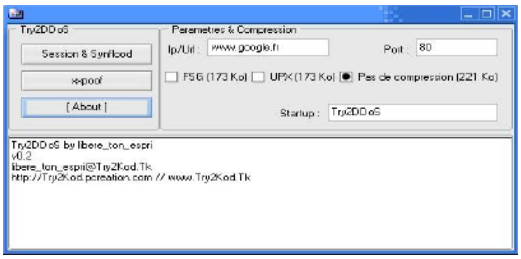

(a) First Version by *libere_ton_espri* posted on *Underground konnekt* (June 17, 2005)

(b) Appearance in Chinese site *andyx.cn* (June 17, 2005)

(c) Spanish Version by *Polifemo* posted on *indice del foro Indetectables* (Nov 24, 2006)

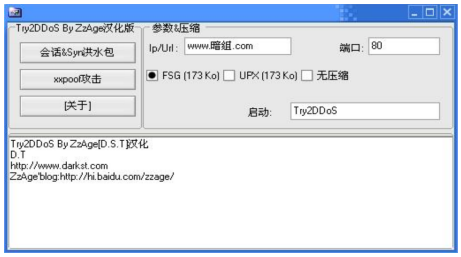

(d) Chinese Version by *ZzAge* posted on *521bbs.yi.org* (May 26, 2007)

Figure 6.2: Motivating Example of Malware Distribution and Evolution in Social Dynamics (All screenshots taken from Holt (2008))

A recent study reveals that rogue programs are sold in black markets built on top of online platforms Holt and Bossler. (2010). Individuals who control existing botnets also sell access to their infected machines for a variety of attacks including spamming and denial of service. As a consequence, these markets enable a great deal of unskilled adversaries and innocent computer users to engage in cybercrime. Before the advent of OSNs, adversaries would communicate via electronic bulletin board systems (BBS), forums and Email systems. More seriously, newly-emerging OSNs provide an even big arena for high-tech criminals.

In Holt (2008), researchers describe a good motivating example to show the value of examining social dynamics for analysis of malware distribution and evolution. *Try2DDos* is a standalone attack tool for distributed denial of service attack (DDos) which was named one of top 30 DDos tools in 2008 Vaqxine (2008). As shown in

Figure 6.2a, *Try2DDos* was first released on a French forum *Underground konnekt* by *libere_ton_espri* in June, 2005. On the same day, it appeared in a Chinese hacker site without any modification as shown in Figure 6.2b. More than one year later, the first public variant of this tool in Spanish appeared on an Argentina hacker forum as shown in Figure 6.2c. Almost another year later, a Chinese variant of this tool developed by *ZzAge* was announced as shown in Figure 6.2d. From 2005 to 2008, this tool and its variants spread to China, Russia, Guatemala, and Argentina and caused damages to a large number of networked systems Holt (2008).

6.3 Using Social Interaction Patterns to Discover Intelligence

In this section, we first address the modeling approach we utilized to represent online underground social dynamics (OUSDs). Unlike existing OSN models Zheleva and Getoor (2009); Hu *et al.* (2014c); Li *et al.* (2012); Zhao *et al.* (2012a); Hu *et al.* (2012) which emphasize on user profile, friendship link, and user group, our model also gives attention to user-generated contents due to the fact that a wealth of information resides in online adversarial conversations. We also elaborate the design principles of social metrics to identify adversarial behaviors in OUSDs. Then, we present SocialImpact, which consists of nine indices, to bring order to underground social dynamics based on our OUSD model.

Adversaries choose online social networks which meet their special requirements to form online underground social communities. Online Underground Social Networks (OUSNs) are used to share technical articles and trade malicious tools, rather than photo-sharing or video-sharing, making them different from normal OSNs in the following aspects:

- OUSNs provide a blog-like article-sharing mechanism, which has less constraints on the length of articles a user can post. Length limitation of posts adopted

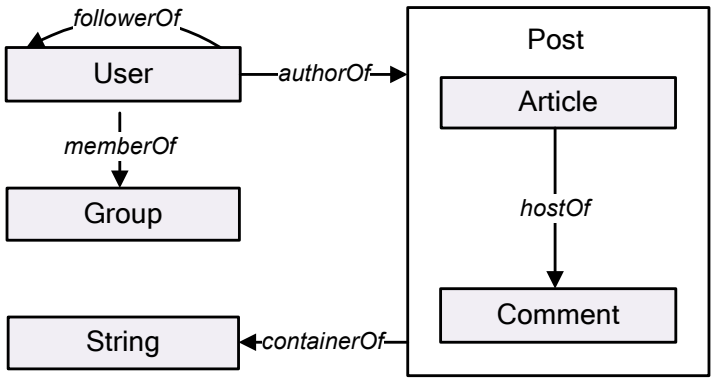

Figure 6.3: Online Underground Social Dynamics Model: Entities and Relationships

in traditional OSNs, such as Twitter and Facebook, is unlikely suitable for well-explained technical articles in OUSNs.

- OUSNs have less access and write constraints on posted articles. For instance, Facebook adopts strict policies to protect its users' privacy, in which one user has to be in the others' circle of trust to access and comment on their posts. However, in OUSNs, a user does not need to be a friend of the article author to read the article or give comments on it. This characteristic allows OUSNs to disseminate more knowledge and technical discussions than OSNs.

- OUSNs do not require users to provide their real-world identities. Adversaries prefer not to associate their real-world identities with their online profiles, therefore OUSNs do not claim themselves as *real* social networks. However, OSNs such as Facebook require users to provide their real names, education backgrounds, and relationship statuses.

6.3.1 Online Underground Social Dynamics Model

As shown in Figure 6.3, an OUSD can be represented by six fundamental entities and five basic types of unidirectional relationships between them.

Users are those who have profiles in the network and have the rights to join

groups, post articles, and give comments to others. *Groups* are those to which users can belong. In an OUSD, groups are mainly formed based on common interests. *Articles* are posted by users who want to share them with the society. In an OUSD, articles might introduce the latest technologies, analyze recent vulnerabilities, call for participation of network attacks, and trade newly developed and deployed botnets. In terms of the form of articles, they do not have to be literary. They could also contain multimedia contents, such as photos and melodies. *Comments* are the subsequent posts to articles. *Posts* are the union of articles and comments. *Strings* are the elementary components of articles and comments. Strings are not necessarily meaningful words. They could be names, URLs, and underground slangs. A user has a relationship *authorOf* with each post s/he creates. A user has a relationship *followerOf* with each user s/he follows. A user has a relationship *memberOf* with each group s/he joins. An article has a relationship *hostOf* with each comment it receives. A post has a relationship *containerOf* with each string it consists of.

The following formal description summarizes the above-mentioned entities and relationships.

Definition 6.1. *Online Underground Social Dynamics. A* ***OUSD*** *is modeled with the following components:*

- U *is a set of users;*
- G *is a set of user groups;*
- A *is a set of articles;*
- C *is a set of comments;*
- P *is a set of posts.* $P = A \cup C$*;*

- *S is a set of strings;*
- *$UP = \{(u, p)|\ u \in U, p \in P$ and u has an* authorOf *relationship with $p\}$ is a one-to-many user-to-post relation denoting a user and her posts;*
- *$FL = \{(u, y)|\ u \in U, y \in U$ and u has a* followerOf *relationship with $y\}$ is a many-to-many user-to-user follow relation;*
- *$MB = \{(u, g)|\ u \in U, g \in G$ and u has a* memberOf *relationship with $g\}$ is a many-to-many user-to-group membership relation;*
- *$AC = \{(a, c)|\ a \in A, c \in C$ and a has a* hostOf *relationship with $c\}$ is a one-to-many article-to-comment relation denoting an article and its following comments; and*
- *$PS = \{(p, s)|\ p \in P, s \in S$ and p has a* containerOf *relationship with $s\}$ is a many-to-many post-to-string relation.*

We focus on the main structure and activities in online underground society and overlook some sophisticated features & functionalities, such as online chatting, provided by specific OSNs and BBS. Hence, our OUSD model is generic and can be a reference model for most real-world OSNs and BBS. As a result, security analysts could easily map real-world social dynamics data archived from any OSNs and BBS to our model for further analysis and investigation.

6.3.2 Principles of Metric Design and Definitions

We also address the following critical issues related to evidence mining in underground society: How can we identify adversaries among the crowd of social users? Given the additional evidence acquired from other sources, how can we correlate

them with underground social dynamics? How can we measure the evolution in underground community? To answer these questions, we articulate several *principles* that the measures for underground social dynamics analysis should follow: 1) The measures should support identifications of interesting adversaries and groups based on both their social relationships and online conversations; 2) The measures should be able to take external evidence into account and support interactions with security analysts; and 3) The measures should support temporal analysis for the better understanding of the evolution in adversarial society.

To this end, we introduce several feature vectors to achieve aforementioned goals. For the mathematical notations, we use lower case bold roman letters such as $\mathbf{x}$ to denote vectors, and uppercase bold roman letters such as $\mathbf{V}$ to denote matrices. We assume all vectors to be column vectors and a superscript T to denote the transposition of a matrix or vector. We also define $max()$ as a function to return the maximum value of a set.

Definition 6.2. *Article Influence Vector. Given an article $a \in A$, the article influence vector of a is defined as $\mathbf{v}_a^T = (v_1, v_2, v_3)$, where v_1 is the length of the article, $v_2 = |\{c \mid c \in C \text{ and } (a, c) \in AC\}|$ is the number of comments received by a, and v_3 is the number of outlinks it has.*

When stacking all articles' influence vector together, we get the **article influence matrix V**. We assess an article's influence by its activity generation, novelty and eloquence Agarwal *et al.* (2008). More comments an article receives, more influential it is. The number of outlinks and length is used to approximately represent article's novelty and eloquence without extracting its semantics. More outlinks an article has, less novelty it has. Also, a longer article is assumed to be more eloquent.

Definition 6.3. *Article Relevance Factor. Given a set of strings $\mathbf{s} = \{s_1, s_2, ..., s_n\} \subseteq$*

S and an article $a \in A$, article relevance factor, denoted as $r(a, \mathbf{s})$, is defined as the number of occurrence of strings $\mathbf{s}$ *in the article* a.

The strings $\mathbf{s}$ could represent an external evidence that security analysts acquired from other sources and query keywords in which security analysts are interested. The given strings $\mathbf{s}$ could represent an external evidence that security analysts acquired from other sources and query keywords in which security analysts are interested.

Definition 6.4. *User Activeness Vector. The user activeness vector of u is defined as $\mathbf{z}_u^T = (z_1, z_2, z_3)$, where $z_1 = |\{p \mid p \in P \text{ and } (u,p) \in UP\}|$ is the number of articles and comments u posted, $z_2 = |\{y \mid y \in U \text{ and } (u,y) \in FL\}|$ is the number of users u follows, and $z_3 = |\{g \mid g \in G \text{ and } (u,g) \in MB\}|$ is the number of groups u joins.*

We measure a user's activeness by the number of posts s/he sends, users s/he follows, and groups s/he joins. By aggregating all users' $\mathbf{z}_u$, we get **user activeness matrix Z**.

Definition 6.5. *Social Matrix. Social matrix, denoted as $\mathbf{Q}$, is defined as a $|U| \times |U|$ square matrix with rows and columns corresponding to users. Let v be a user and N_v be the number of users v follows. $\mathbf{Q}_{u,v} = 1/N_v$, if $(v,u) \in FL$ and $\mathbf{Q}_{u,v} = 0$, otherwise.*

Social matrix is similar to transition matrix for hyperlinked webpages in PageRank. The sum of each column in social matrix is either 1 or 0, which depends on whether the vth column user follows any other user.

Definition 6.6. *δ-n Selection Vector. A δ-n selection vector, denoted as $\mathbf{y}_\delta^n$, is defined as a boolean vector with n components and $\|\mathbf{y}_\delta^n\|_1 = \delta$.*

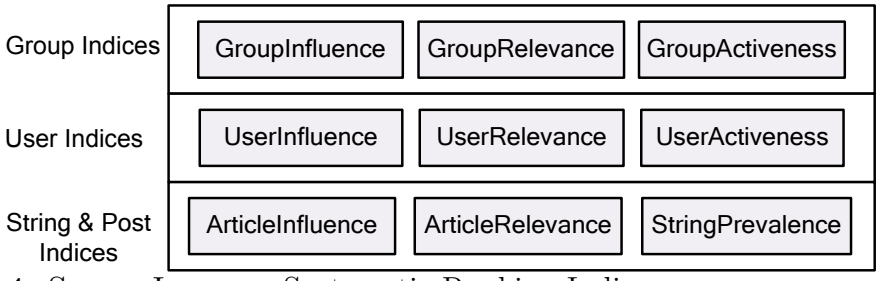

Figure 6.4: SocialImpact: Systematic Ranking Indices

A δ-n selection vector is used to select a portion of elements for one set. For example, the top 10 influential articles of a user a could be represented by a selection vector $\mathbf{y}_{10}^{|A|}$ over the article set A. By stacking all users' δ-n selection vectors over the same set together, we get the δ-n **selection matrix** $\mathbf{Y}_{\delta}^{n}$.

6.3.3 Ranking Metrics

As shown in Figure 6.4, SocialImpact consists of nine indices, which are classified into three categories: string & post indices, user indices, and group indices. Each index in upper categories is computed by the indices from lower categories. For instance, UserInfluence that indicates a user's influence in the community is calculated based on the ArticleInfluence of user's articles and the social metrics $\mathbf{Q}$ of this community.

To fulfill *Principle 1*, user and group indices are devised to identify influential, active, and relevant users and groups. We devise personalized PageRank models Chakrabarti (2007) to calculate UserInfluence and UserRelevance, since it could capture the characteristics of both user-to-user relationships and user-generated contents in social dynamics. To accommodate *Principle 2*, ArticleRelevance, UserRelevance and GroupRelevance are designed to take external strings as inputs, combine them with existing data in social dynamics, and generate more comprehensive results. To fulfill *Principle 3*, all feature vectors and indices could be calculated for a given time win-

dow and StringPrevalence could indicate the topic evolution in the society. Moreover, we believe the combination of UserActiveness and UserInfluence could also be used to identify suspicious spam profiles in online social networks.

We consider a weighted additive model Keeney and Raiffa (1993) when there exist several independent factors to determine one index. To reduce the bias introduced by different size of sets, we use δ-n selection vector to choose a portion of data in calculation. The followings are the detailed descriptions of indices.

ArticleInfluence, *denoted as $x_1(a)$, represents the influence of article a. $x_1(a)$ is computed as $\mathbf{v}_a^T\mathbf{w_1}$, where $\mathbf{w_1}$ denotes the weight vector.*

By normalizing $x_1(a)$ to $[0, 1]$ and stacking $x_1(a)$ from all articles together, we get a vector $\mathbf{x_1}$.

$$\mathbf{x_1} = \frac{\mathbf{V}^T\mathbf{w_1}}{max_{b\in A}(x_1(b))} \tag{6.1}$$

ArticleRelevance, *denoted as $x_2(a, \mathbf{s})$, represents the relevance of the article a to given strings $\mathbf{s}$. $x_2(a, \mathbf{s})$ is proportional to the occurrence of the given strings in the article and the influence of the article.*

$$x_2(a, \mathbf{s}) = \frac{r(a,\mathbf{s})x_1(a)}{max_{b\in A}(r(b,\mathbf{s})x_1(b))} \tag{6.2}$$

By stacking $x_2(a, \mathbf{s})$ from all users together, we get a vector $\mathbf{x_2}(\mathbf{s})$ denoting all articles' relevance to $\mathbf{s}$.

UserInfluence, *denoted as x_3, represents the influence of a user. x_3 can be measured by two parts. One is the impact of the user's opinions, which is modeled by* ArticleInfluence. *The other is the user's social relationships, which is modeled by $\mathbf{Q}$. x_3 is devised as a personalized PageRank function to capture both parts.*

By stacking x_3 from all users together, we get a vector $\mathbf{x_3}$.

$$\mathbf{x_3} = d_3\mathbf{Q}\mathbf{x_3} + (1 - d_3)\mathbf{Y}_\alpha^{|A|}\mathbf{x_1} \tag{6.3}$$

Where $d_3 \in (0,1)$ is the decay factor which makes the linear system stable and convergent. $\mathbf{Y}_{\alpha}^{|A|}$ is the $\delta - n$ selection matrix corresponding to all users's top α influential articles.

UserRelevance, *denoted as $x_4(\mathbf{s})$, represents the relevance of a user to strings* $\mathbf{s}$.

By stacking $x_4(\mathbf{s})$ from all users together, we get a vector $\mathbf{x_4}$.

$$\mathbf{x_4}(\mathbf{s}) = d_4 \mathbf{Q} \mathbf{x_4}(\mathbf{s}) + (1 - d_4)(\mathbf{Y}_{\alpha}^{|A|} \mathbf{x_2}(\mathbf{s})) \tag{6.4}$$

Where $d_4 \in (0,1)$ is the decay factor. $\mathbf{Y}_{\alpha}^{|A|}$ is a $\delta - n$ selection matrix corresponding to all users's top α relevant articles to $\mathbf{s}$.

UserActiveness, *denoted as x_5, represents the activeness of a user.*

$$\mathbf{x_5} = \mathbf{Z}^T \mathbf{w_5} \tag{6.5}$$

We use the addition of a group's top α members' influence, relevance, and activeness to model its influence, relevance, and activeness, respectively. As mentioned before, this model can reduce the bias caused by the number of members.

GroupInfluence, *denoted as x_6, represents the influence of a group.*

By stacking all x_6 together, we get $\mathbf{x_6}$.

$$\mathbf{x_6} = \mathbf{Y}_{\alpha}^{|U|} \mathbf{x_3} \tag{6.6}$$

Where $\mathbf{Y}_{\alpha}^{|U|}$ is the δ-n selection matrix corresponding to all groups' top α influential users.

GroupRelevance, *denoted as x_7, represents the relevance of a group to strings* $\mathbf{s}$.

By stacking all x_7 together, we get $\mathbf{x_7}$.

$$\mathbf{x_7} = \mathbf{Y}_{\alpha}^{|U|} \mathbf{x_4} \tag{6.7}$$

Where $\mathbf{Y}_{\alpha}^{|U|}$ is the δ-n selection matrix corresponding to all groups' top α relevant users.

GroupActiveness, *denoted as x_8, represents the activeness of a group.*

By stacking all x_8 together, we get $\mathbf{x_8}$.

$$\mathbf{x_8} = \mathbf{Y}_{\alpha}^{|U|}\mathbf{x_5} \tag{6.8}$$

Where $\mathbf{Y}_{\alpha}^{|U|}$ is the δ-n selection matrix corresponding to all groups' top α active users.

StringPrevalence, *denoted as $x_9(s)$, represents the popularity of string s.*

$$x_9(s) = \sum_{p_j \in P} ti_{s,p_j} \tag{6.9}$$

where ti_{s,p_j} is the term frequency-inverse document frequency Salton and Buckley (1988) of string s in post p_j.

The computations for UserInfluence and UserRelevance are proven to be convergent Bianchini *et al.* (2005). And the corresponding time complexity is $O(|H|log(1/\epsilon))$, where $|H|$ is the number of $followerOf$ relationships in the social dynamics and ϵ is a given degree of precision Bianchini *et al.* (2005). The time complexity for calculating StringPrevalence is $O(|P||S|)$, where $|P|$ is the number of posts and $|S|$ is the size of string set. The complexities for all other indices are linear if the underlying indices are calculated.

6.4 System Design and Implementation

In this section, we describe the challenges in analyzing real-world underground social dynamics data. We address our efforts to cope with these challenges and present the design and implementation of our proof-of-concept system.

6.4.1 Challenges from Real-world Data

The first challenge of real-world data is its multilingual contents. The most effective way to coping with this challenge is to take advantage of machine translation

systems. Our tool utilizes Google Translate to detect the language of the contents and translate them into English. However, machine translation systems may fail to generate meaningful English interpretations for the following cases: i) adversaries may use cryptolanguages that no machine translation system could understand. For instance, *Fenya*, a Russian cant language that is usually used in prisons, is identified in online underground society Yarochki (2009); and ii) both intentional and accidental misspellings are common in online underground society Raymond (1996). In order to cope with this challenge, our tool maintains a dictionary of known jargons, such as *c4n* as *can* and *sUm1* as *someone*.

Another challenge is that the social dynamics data may not be in a consistent format. Different OSNs use different styles in web page design. Even in one OSN, in order to make the web page more personalized, the OSN allows users to customize the format of their posts. Since HTML is not designed to be machine-understandable in the first place, extracting structural information from HTML is a tedious and heavy-labor work. To address this problem, we first cluster data, and then devise an HTML parser for each cluster. We also design a light-weight semi-structure language to store the information extracted from HTML.

Since one major component in social dynamics is the relationships between entities, storing and manipulating social dynamics data in a relational database is relatively time-consuming. We choose graph database Angles and Gutierrez (2008) which employs the concepts from graph theory, such as node, property, and edge, to realize faster operations for associative data sets.

6.4.2 System Architecture and Implementation

Figure 6.5 shows a high level architecture of our tool. The upper level of our tool includes several visualization modules and provides query control for security

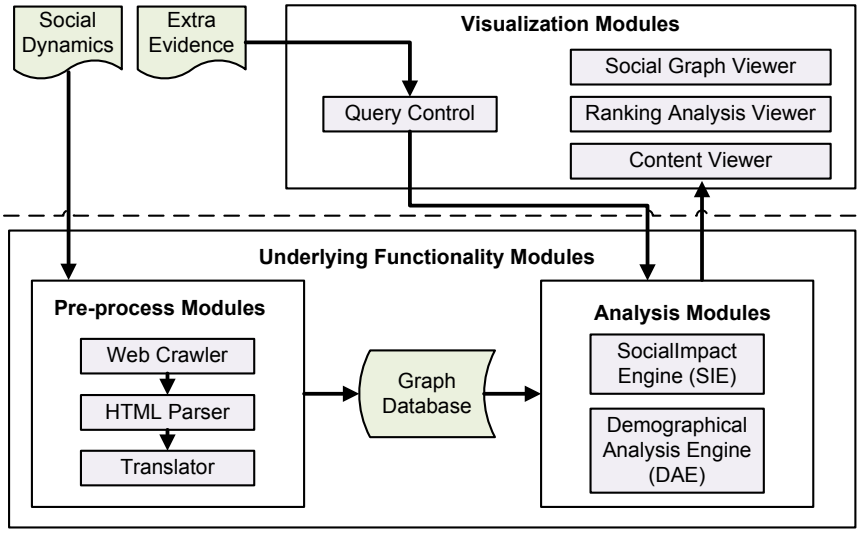

Figure 6.5: System Architecture of Our Tool

analysts to provide the additional evidence. In reality, such evidence could be in the format of text, picture, video, audio or any other forms. Yet, representing multimedia contents like pictures and videos in a machine-understandable way is still a difficult challenge. Our tool acts like a modern web search engine in response to keyword queries. Social graph viewer is designed to show social relationships among users and groups. Ranking analysis viewer is used to list the ranking results based on security analysts' queries. Content viewer can show both original and translated English web resources.

The lower level of the architecture realizes underlying functionalities addressed in our framework. After underground community data is crawled from Internet, the HTML parser module extracts meaningful information from it. If the content is not in English, our translator takes over and generates English translation. All extracted information is stored in a graph database for the rapid retrieval. Analysis modules have two working modes: offline and online. The offline mode generates demographical information with demographical analysis engine (DAE) and intelligence, such as user influence and activeness, with SocialImpact engine (SIE). When security

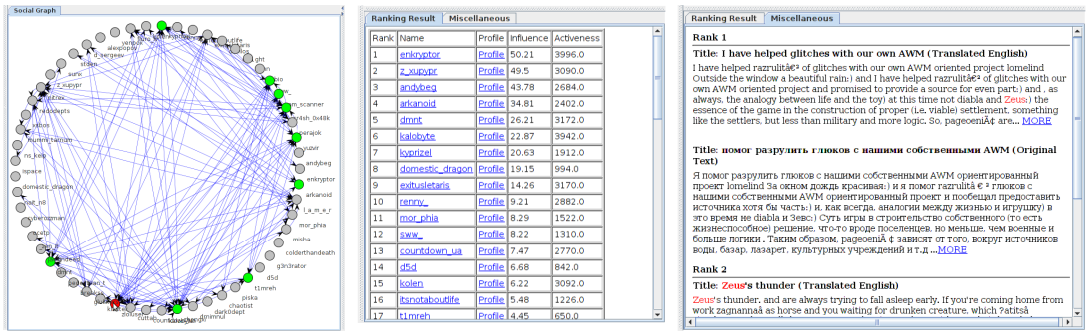

(a) Social Graph (b) User Ranking (c) Article Ranking

Figure 6.6: Screenshots of Our Tool

analysts provide the additional evidence, SocialImpact engine switches to online mode and generates analysis results, such as user relevance, based on data in graph database and additional evidence provided by security analysts.

Our tool was implemented in Java programming language. We took advantage of Java swing and JUNG to realize graphical user interfaces and graph visualization. As we mentioned before, our tool uses Google Translate API to translate texts. In most cases, Google Translate could output acceptable translations from original texts. Our tool stores user profiles, user-generated contents, and social relationships among users in a Neo4j graph database. For each group, user, article, and comment, our tool creates a node in the database, stores associated data–such as the birthday of user and the content of article–in each node's properties, and assigns the relationships among nodes.

6.4.3 Visualization Interfaces of Our Tool

Figure 6.6 depicts interfaces of our tool. As illustrated in Figure 6.6a, all users in the social group are displayed by a circle. And their *followerOf* relationships are displayed with curved arrows. It is clear to view that some users have lots of followers while others do not. By clicking any user in the group, our tool has the ability to

highlight this user in red and all his followers in green. In this way, our tool helps analysts understand the social impact of any specific user. Another windows as shown in Figure 6.6b displays the ranking results. Analysts can specify the ranking metric, such as UserInfluence and UserActiveness, to reorder the displayed rank. Clicking a user's name which is the second column in Figure 6.6b would bring the analysts to the list of all posted articles by the user in descending order of ArticleInfluence. Clicking the user's profile link which is the third column in Figure 6.6b would bring the analysts to the webpage of the user's profile archived from the Internet. Analysts could also specify some keywords in query control and our tool would display the results in descending order of ArticleRelevance. As shown in Figure 6.6c, our tool displays both the original and translated texts and highlights the input keywords in red.

6.5 Experiments on Synthetic Social Dynamics Data

We first compared our social ranking approach with a PageRank-based solution Page *et al.* (1999a) to evaluate the effectiveness of our social ranking mechanism. PageRank uses numerical weights of elements that are linked together to measure their relative importance. Although PageRank is successfully deployed in commercial search engines, as discussed in Agarwal *et al.* (2008), it is not very suitable to rank sparsely linked elements.

For simplicity, we only included a synthetic case study considering user influence and activeness, as shown in Figure 6.7. In this scenario with five users, the left-hand figure shows the relationships between users and the right-hand tables show information from user-generated contents in five different stages. *David* and *Carl* are two of most popular users with four and three followers, respectively. While *Edward* seems the most eloquent user in the stage one with six articles and twenty posted

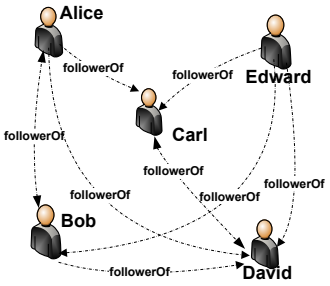

Alice					
Stage→	1	2	3	4	5
Articles	4	3	0	1	2
Comments Received	19	13	0	4	9
Comments Posted	5	5	5	10	3
Follows	3				
Followers	1				

Bob					
Stage→	1	2	3	4	5
Articles	2	4	4	2	1
Comments Received	6	13	23	8	2
Comments Posted	13	6	12	20	9
Follows	2				
Followers	2				

Carl					
Stage→	1	2	3	4	5
Articles	2	5	3	5	3
Comments Received	5	15	9	19	9
Comments Posted	7	8	13	18	7
Follows	1				
Followers	3				

David					
Stage→	1	2	3	4	5
Articles	2	1	3	4	2
Comments Received	4	6	18	12	11
Comments Posted	11	10	15	2	5
Follows	1				
Followers	4				

Edward					
Stage→	1	2	3	4	5
Articles	6	1	4	5	4
Comments Received	2	1	19	13	5
Comments Posted	20	19	5	6	12
Follows	3				
Followers	0				

Figure 6.7: An OUSD Scenario

comments. Figure 6.8(a) shows the user influence index sorted in descending order in the stage one. *Alice* is ranked as the most influential user, mainly because her four articles received nineteen comments from the society. Note that, although *David* has four followers in the society, his influence is limited due to the fact that he initiated few attractive conversations. Although, *Edward* has no followers, our model considers he still has some influence in the community because his contributions have attracted other's attention. Figure 6.8(b) shows the user activeness index in the stage one. The least influential user *Edward* is ranked as the most active user not only because he is eloquent, but also because he follows everyone in the community. *Bob* is ranked as the second most active member since he contributed to many conversations. We notice that the most influential user *Alice* is ranked as the second least active user which verifies that a user does not need to speak much to make a difference. Figure 6.8(c) shows the PageRank-based ranking analysis results. Note that PageRank ignores user-generated contents, and only considers user relationships for ranking analysis. One reason for *Carl* being more influential than *David*, even if in the case that *David* has more followers than *Carl*, is because in PageRank analysis the value of link-votes is divided among all outbounds. The fact that *David* only follows *Carl* indicates *Carl*'s influence in this model. PageRank fails to identify *Edward*'s influence as well merely because he has no follower. Another drawback of PageRank analysis is that it

Rank	Name	Index
1	Alice	69.3
2	Bob	23.9
3	Carl	21.5
4	David	13.6
5	Edward	5.1

(a) UII according to our solution

Rank	Name	Index
1	Edward	29
2	Bob	17
3	David	14
4	Alice	12
5	Carl	10

(b) UAI according to our solution

Rank	Name	Index
1	Carl	1.111
2	David	0.371
3	Alice	0.075
4	Bob	0.024
5	Edward	0.000

(c) PageRank Index

Figure 6.8: Indices According to Our Solution and PageRank

cannot generate temporal patterns of the influential users since relationships do not change.

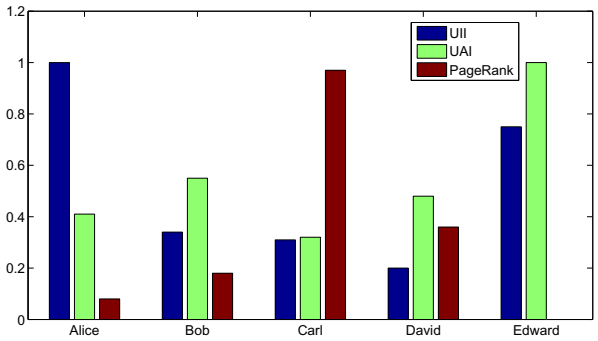

Figure 6.9: Comparison of Normalized Indices for Each User

We normalize three different indices calculated for each adversary and show their comparison in Figure 6.9. The significant difference between our solution and PageRank-based solution shows the importance of considering user-generated contents as well as social relationships.

6.6 A Case Study on Real-world Online Underground Social Dynamics

In this section, we present our evaluation on real-world social dynamics. We evaluated our tool on 4GB of data crawled from *Livejournal.com* which is a popular

online social network especially in the Russian-speaking countries. We anonymized the group names and user names in this OSN for preserving privacy.

All webpages in this OSN could be roughly divided into two categories in terms of content: i) profile and ii) article. The profile webpage contains basic information of a user or a group, which includes name, biography, location, birthday, friends, and members. Every article has title, author, posted time, content, and several comments by other users. The webpages are mainly *.html* files, along with some *.jpeg*, *.gif*, *.css*, and *.js* files. Our solution only considers text data from *.html* files.

We started to crawl group profiles from six famous underground groups in this OSN. Then we crawled all members' profiles and articles of these six groups. We also collected one-hop friends' articles of these members. Therefore, we ended up with 29,614 articles posted by 6,364 users which are from 4,220 groups. Based on the information in user profiles, we noticed that about 32.7% and 52.7% users were born in early and mid-late 80's. This clearly illustrates the age distribution of active users in this community.

6.6.1 Post, User and Group Analysis

Our tool calculated all articles' ArticleInfluence and identified top 50 articles over a time window of 48 months. Since not all of these articles are related to computer security, we checked these articles in descending order of their influences and picked five articles that are highly related to malware. We could observe some popular words related to malware, such as PE (the target and vehicle for Windows software attacks), exploits (a piece of code to trigger system vulnerabilities), hook (a technique to hijack legitimate control flow) and so on.

Our tool also generated each user's UserInfluence and UserActiveness and group's GroupInfluence and GroupActiveness over a time window of 48 months. And, Table 6.2

Top Five Influential Users		Top Five Active Users	
User	UserInfluence	User	UserActiveness
z_xx_ur	49.5020	xsbxx_ur	4024
andxx_ur	43.7800	enkxx_ur	3942
arkxx_ur	34.8074	kalxx_ur	3936
_moxx_ur	26.7700	exixx_ur	3170
kyp_ur	20.6292	kolxx_ur	3092

Table 6.1: Top Five Influential/Active Users

Top Five Influential Groups		Top Five Active Groups	
Group	GroupInfluence	Group	GroupActivenss
b_gp	344.4807	b_gp	57798
c_gp	79.7781	d_gp	28644
d_gp	45.5222	demxx_gp	20846
murxx_gp	26.2094	beaxx_gp	20290
chrxx_gp	18.6487	_hoxx_gp	19486

Table 6.2: Top Five Influential/Active Groups

shows the top five influential/active users/groups for the entire period of our observation. We can notice that there is no overlap between the top five *influential* users and the top five *active* users, while there exists similarity for the top five *influential* groups and the top five *active* groups.

We calculated the correlation coefficient ($corrcoef$) for the pairs of UserInfluence and UserActivenss, GroupInfluence and GroupActivenss based on the results generated from our tool. Similar to the phenomenon we identified in Table 6.2, in Figure 6.10(a) we observed that the correlation coefficient between UserInfluence and UserActivenss is around 0.52 (the maximum value for correlation coefficient is 1 indicating a perfect positive correlation between two variables), which means one user's influence is not

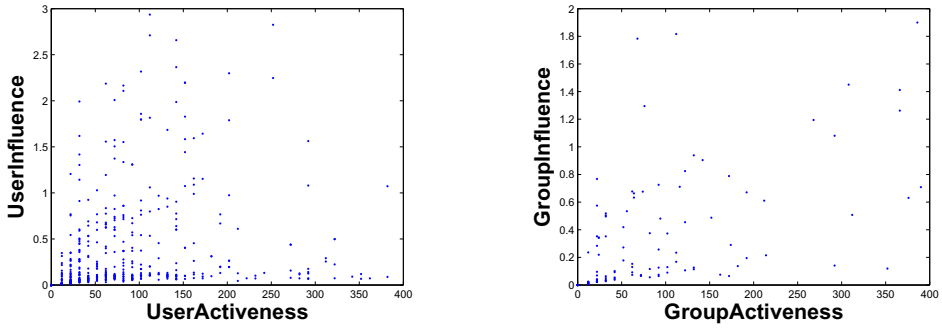

(a) $corrcoef = 0.5204$ (b) $corrcoef = 0.9094$

Figure 6.10: Correlation Coefficient of UserActiveness & UserInfluence and GroupActiveness & GroupInfluence

highly correlated to her/his activeness. This phenomenon indicates that talking more does not make a user more influential in a community. On the other hand, as shown in Figure 6.10(b) we observed that the correlation coefficient between GroupInfluence and GroupActivenss is around 0.90, which indicates a very strong positive correlation between the influence and the activeness of a group. The application of influence and activeness indices is not limited to identify such a social phenomenon. We could also leverage the high UserActivenss and the low UserInfluence as indicators for the analysis of social spammers in any OSN.

The temporal patterns of the influential/active users/groups could be observed in Figure 6.11, where x-axis denotes the users/groups who were identified as the most influential/active ones for each month. For example, $x = 1$ denotes the most influential/active user/group of the first month in our time window and $x = 48$ denotes the most influential/active user/group of the last month in our time window; y-axis denotes the entire 48 months in the time window; and z-axis denotes user/group's influence/activeness value. As shown in Figure 6.11(a), some users maintain their influence status for several months. The large plain area in the right part of this figure indicates most users come as the most influential ones suddenly. This observation implies that a user does not need to be a veteran to be an influential one in the

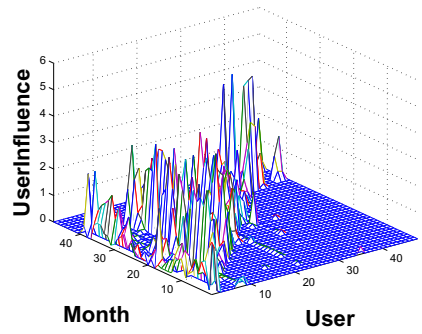

(a) UserInfluence over 48 months

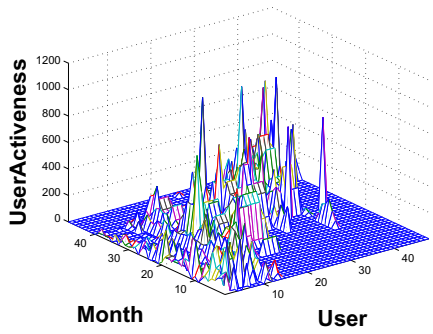

(b) UserActiveness over 48 months

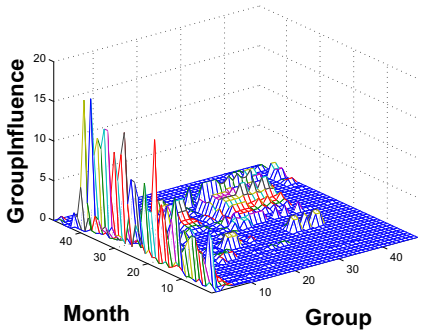

(c) GroupInfluence over 48 months

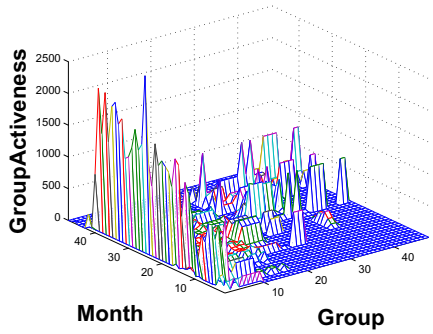

(d) GroupActiveness over 48 months

Figure 6.11: Temporal Pattern Analysis

community. On the other side, we can see from Figure 6.11(b) that most active users remain active before they became the most active ones. The plain area in the left portion of Figure 6.11(b) implies that most users do not always keep active. Normally they keep active for 15-30 months, then get relatively silent. While the smaller plain area in the left part of Figure 6.11(a) shows once a user becomes influential, s/he keeps the status for a long period of time. Figure 6.11(c) shows that there are 2 or 3 groups who maintain the status of influence during the whole 48 months and get even more influential as time goes on. While, other groups only keep influential for a relatively short period of time and just fade out. Figure 6.11(d) shows the similar phenomenon.

6.6.2 Evidence Mining by Correlating Social Dynamics with Adversarial Events

We present our finding with keyword queries on the same dataset in our tool. Those keywords and attack patterns could also be automatically generated from the approaches proposed in Zhao *et al.* (2011a); Zhao and Ahn (2013). For each query, our tool returns the lists of articles, users, and groups in descending order of ArticleRelevance, UserRelevance and GroupRelevance, respectively. The results we present in this section are with regard to three major adversarial activities: i) botnet; ii) identity theft and credit card fraud; and iii) vulnerability analysis and malicious code development.

Botnet

As we mentioned before, botnet is a serious threat to all networked computers. In order to identify adversaries and their conversations in our dataset related to botnet, we queried the keywords shown in Table 6.3(a) in our tool. Our tool was able to identify 490 articles related to 'spam', 44 articles related to 'botnet', 9 articles related to 'zeus' and 1 article about 'rustock'.

Then, we checked the results returned by our tool carefully and Table 6.4 shows several interesting articles and their information including the number of comments they received, ArticleRelevance of each article, and authors of these articles. We first noticed one article titled 'Rustock.C' with very high ArticleRevelance and ArticleInfluence. This article presented an original analysis of the C variant of Rustock that once accounted for 40% of the spam emails in the world.

Another article titled 'On startup failure to sign the drivers in Vista x64' returned by our tool as top relevant article to 'botnet' attracting our attention as well. In this article, the author crx_ur discussed about how to load unsigned driver to Windows

Keywords	Relevant Articles #
spam	490
botnet	44
zeus	9
rustock	1
mega-d	0

(a) Results for Botnet

Keywords	Relevant Articles #
pin	129
credit card	93
carding	1
credit card sale	0
ssn	0

(b) Results for Identity Theft and Credit Card Fraud

Keywords	Relevant Articles #
vulnerability	418
shellcode	169
polymorphic	12
zero-day	11
cve	2

(c) Results for Vulnerability Discovery and Malicious Code Development

Table 6.3: Results from Our Tool for Queries

Translated Article Title	# Comments Received	x_2[1]	Author
Rustock.C	13	135.3	swx_ur
On startup failure to sign the drivers in Vista x64	5	59.8	crx_ur
video	3	35.6	zlx_ur
sleepy	3	32.3	crx_ur
FireEye Joins Internet2	2	27.8	eax_ur

[1] ArticleRelevance

Table 6.4: Selected Top Relevant Articles

Vista x64 by modifying PE file header. The corresponding author claimed that malware vendors would use this technique to build bot and infect thousands of computers. A further investigation on this user shown in Table 6.5 reveals that s/he authored several security-related articles. Her/his profile indicated that s/he was very active in malicious code development and interested in several cybercrime topics, such as rootkit, exploits, and shellcode.

Identity Theft and Credit Card Fraud

Identity theft and credit card fraud are both serious issues in nowadays Internet transactions. Online identity theft includes stealing usernames, passwords, social security numbers (ssn), personal identification numbers (PINs), account numbers, and other credentials. Credit card fraud also consists of phishing (the process to steal credit card information), carding (the process to verify whether a stolen credit card is still valid), and selling verified credit card information.

Table 6.3(b) shows results that our tool returned when these keywords are queried. Our tool identified one article that was authored by a user dx_ur related to 'carding'

Translated Article Title	# Comments Received	x_1[1]	Translated Interests
The old tale about security	7	79.6	malware, ring0,
Malcode statistics	6	68.9	rootkit, botnets,
Cold boot attacks on encryption keys	2	37.6	asm, exploits,
Wanted Cisco security agent	2	28.1	cyber terrorism,
Antirootkits bypass	1	18.7	shellcode, viruses,
Syser debugger	0	8.9	underground,
Termorektalny cryptanalysis	0	7.8	Kaspersky, paintball

[1] ArticleInfluence

Table 6.5: Selected Articles by crx_ur and Her/His Information

Translated Interests	carding, banking, shells, hacking, freebie, web hack, credit card fraud, security policy, system administrators, live in computer bugs
# Articles Posted	1295
# Comments Posted	7294
# Comments Received	2693

Table 6.6: Information about dx_ur

in the dataset. A further investigation on this user revealed that s/he was a member of a carding interest group, which had more than 20 members around the world. Table 6.6 shows some basic information of dx_ur. Compared to crx_ur, it is obvious that dx_ur has more interests in financial security issues, such as credit card fraud, web hack, and banking. We could also notice that dx_ur was very active in posting articles and replying others' posts.

Vulnerability Analysis and Malicious Code Development

We analyzed several keywords related to vulnerability analysis and malicious code development, such as polymorphism (a technique widely used in malware to change the appearance of code, but keep the semantics), cve (a reference-method for publicly-known computer vulnerabilities), shellcode (small piece of code used as the payload in the exploitation of software vulnerabilities), and zero-day (previously-unknown computer vulnerabilities, viruses and other malwares).

As shown in Table 6.3(c), the community is very active in these topics. More than 400 articles related to vulnerabilities were found. However, we noticed most of these articles have low-ArticleInfluence. We checked these low-ArticleInfluence articles and discovered that most of them were articles copied from other research blogs and kept the links to original webpages. Our ArticleInfluence index successfully identified these articles were not very novel, thus calculated low ArticleInfluence for them.

At the same time, as shown in Table 6.7, our tool also identified several high-ArticleInfluence vulnerability analysis articles. For example, the article entitled 'Blind spot' authored by arx_ur which analyzed a new Windows Internet Explorer vulnerability even attracted 79 replies.

6.6.3 Comparison with HITS Algorithm

In order to evaluate the effectiveness of our approach, we implemented HITS algorithm Kleinberg (1999) in our tool and compared the results with our SocialImpact metrics. HITS algorithm is able to calculate the authorities and hubs in a community by examining the topological structure where *authority* means the nodes that are linked by many others and *hub* means the nodes that point to many others. Note that the fundamental difference between SocialImpact and HITS is that SocialImpact

Translated Article Title	# Comments Received	x_2[1]	Author
Blind spot	79	793.2	arx_ur
Seven thirty-four pm PCR	14	146.4	tix_ur
HeapLib and Shellcode generator under windows	1	15.6	eax_ur
Who fixes vulnerabilities faster, Microsoft or Apple?	0	5.6	bux_ur
FreeBSD OpenSSH Bugfix	0	4.2	sux_ur

[1] ArticleRelevance

Table 6.7: Selected Top Relevant Articles

takes more parameters, such as user-generated content and activity, into account, therefore ranking results are based on a more comprehensive set of social features.

Top Five Authorities		Top Five Hubs	
User	auth	User	hub
zhengxx_ur	0.506	zlo_xx_ur	0.265
crx_xx_ur	0.214	zhengxx_ur	0.237
yuz_ur	0.163	crx_xx_ur	0.234
t1mxx_ur	0.148	yuz_ur	0.205
rst_ur	0.143	t1mxx_ur	0.183

Table 6.8: Top Five Authorities and Hubs by HITS

Comparing the results for authorities and hubs (HITS) shown in Table 6.8 with UserInfluence and UserActiveness (SocialImpact) in Table 6.2, we can observe that the authorities and hubs have much overlap with HITS algorithm when online conversations are ignored and the results generated by SocialImpact are different from HITS counterparts.

6.7 Related Work

Computer-aided crime analysis (CACA) utilizes the computation and visualization of modern computer to understand the structure and organization of traditional adversarial networks Xu and Chen (2005). Although CACA is not designed for the analysis of cybercrime, its methods of relation analysis, and visualization of social network are adopted in our work. Zhou et al. Zhou *et al.* (2005) studied the organization of United State domestic extremist groups on web by analyzing their hyperlinks. Chau et al. Chau and Xu (2007) mined communities and their relationships in blogs for understanding hate group. Lu et al. Lu *et al.* (2010) used four actor centrality measures (degree, betweenness, closeness, and eigenvector) to identify leaders in hacker community. In contrast, our proposed solution in this dissertation and previous papers Zhao *et al.* (2011b, 2012b) considers both social relationships and user-generated contents in identifying interesting posts and users for cybercrime analysis.

Systematically bringing order to a dataset has plenty of applications in both social and computer science. With the development of web, ranking analysis in hyperlinked environment received much attention. Kleinberg Kleinberg (1999) proposed a hubs and authorities approach (HITS) by calculating the eigenvectors of a certain matrices associated with the link graph. Almost at the same time, Page and Brin Page *et al.* (1999b) developed PageRank that uses a page's backlinks' sum as its importance index. However, both HITS and PageRank only consider the topological structure of given dataset but ignore its contents Bianchini *et al.* (2005). Therefore, we devised a ranking system based on personalized PageRank, which is proposed to efficiently deal with ranking issues in different situations Chakrabarti (2007).

In order to provide a safer platform for net-centric business and secure the internet experience for end users, huge research efforts have been invested in defeating malware

and designing defense systems. Hu et al. Hu *et al.* (2014b,a) proposed systems to enhance firewalls to make sure malicious packets can not bypass existing detecting systems. Gu et al. analyzed botnet C&C channels for identifying malware infection and botnet organization Gu *et al.* (2007). Zhang et al. Zhang *et al.* (2013) investigated using high-entropy detectors to detect botnet traffics that employ encryption. Stone-Gross et al. Stone-Gross *et al.* (2009) took over *Torpig* for a period of ten days and gathered rich and diverse set of data from this infamous botnet.

6.8 Summary

In this chapter, we have presented a novel approach to help identify adversaries by analyzing social dynamics. We formally modeled online underground social dynamics and proposed SocialImpact as a suite of measures to highlight interesting adversaries, as well as their conversations and groups. The evaluation of our proof-of-concept system on real-world social data has shown the effectiveness of our approach. As part of future work, we would further test the effectiveness and the usability of our system with subject matter experts.

Chapter 7

CONCLUSION

In this dissertation, we have proposed a pattern-based approach framework, whose goal is to handle previously unknown security events by considering their root causes, randomness and uncertainty and at the same time quantify the confidence of decision making. Different from pre-determined pattern-based approaches, our approach does not rely on fixed bit sequences, but considers randomness and uncertainty. We have shown our approach can cope with previously unknown security events. Different from statistical pattern-based approaches that leave the feature discovery to statistical methods, our pattern-based approaches focuses on using the domain knowledge in each security problem to discover regularities and tackle root causes directly. Therefore, the reasons for such regularities to occur are explainable and interpreted in a security-related way. We have applied our framework to discover and use patterns in code, network, choices, and communities to counter security challenges.

7.1 Contributions

The contributions of this dissertation are as follows:

1. We proposed a framework to discover and use patterns for countering security challenges. We have demonstrated that such a methodology can be used for both defending and attacking in several different stages of the security cycle.

2. We have proposed instruction sequence abstraction as a coarse-grained approach to extract distinguishable features from binary code. We have proposed opcode mnemonic sequence and binary finite-dimensional representation to represent

arbitrary shellcode sample. We have proposed a shellcode detection approach based on Markov model and a shellcode attribution approach with support vector machines. We have investigated the feature selection methods and demonstrate its effectiveness with our collected large set of shellcode samples. With our developed tool, we have demonstrated the identified top opcode transition patterns. We have evaluated the effectiveness of our shellcode detection and attribution approaches with collected real-world shellcode samples. In addition, we have compared the strengths of real-world shellcode engines with several metrics.

3. We have proposed using routing table changes as evidence to measure the risk of node isolation in mobile ad hoc networks. We have identified several categories of routing table change patterns and measure the impact of each routing table change category. We have proposed an extended Dempster-Shafer evidence model with importance factors and articulate expected properties for Dempster's rule of combination with importance factors. Our Dempster's rule of combination with importance factors is nonassociative and weighted. We have proposed an adaptive risk-aware response mechanism with the extended D-S evidence model, considering damages caused by both attacks and countermeasures. The evaluation has shown the effectiveness of our approach in multiple MANET attack scenarios.

4. We have performed an empirical analysis on collected PGA passwords to understand user choice patterns in background picture, gesture location, gesture order, and gesture type. We have proposed a selection function model which models the thinking process of users when they choose picture passwords. We have demonstrated our approach to automatically extract picture password compo-

sition processes with this model. We have implemented our attack framework and evaluated its effectiveness on the collected dataset in several different attack models which includes targeted attack, nontargetted attack, online attack and offline attacks.

5. We have studied the role of underground social dynamics in the whole underground economy and collected a dataset of the user interactions of an underground social network. We have presented an online underground social network model which takes users and their interactions into account. based on this model, we have demonstrated our approaches to identify influential players and to associate security events with their behind-scene players in underground social networks. We have evaluated our approaches on a real-world underground social network dataset and discovered intelligences of underground society from this dataset and linked existing attack events with discussions in this social data.

7.2 Future Work

For future work, we plan to use the proposed pattern-based framework to counter more security challenges. For each challenge we tried to tackle in this dissertation, we plan to explore more sophisticated models by considering more factors.

REFERENCES

Agarwal, N., H. Liu, L. Tang and P. Yu, "Identifying the influential bloggers in a community", in "Proceedings of the 1st International Conference on Web Search and Web Data Mining (WSDM)", (ACM, 2008).

Akritidis, P., E. Markatos, M. Polychronakis and K. Anagnostakis, "Stride: Polymorphic sled detection through instruction sequence analysis", in "Proceedings of the IFIP International Information Security and Privacy Conference (SEC)", pp. 375–391 (2005).

Al-Saleh, M. I. and J. R. Crandall, "Application-level reconnaissance: Timing channel attacks against antivirus software", in "Proceedings of the 4th USENIX Workshop on Large-Scale Exploits and Emergent Threats (LEET)", (USENIX, 2011).

Alexe, B., T. Deselaers and V. Ferrari, "Measuring the objectness of image windows", IEEE Transactions Pattern Analysis and Machine Intelligence (2012).

Alexe, B., T. Deselaers and V. Ferrari, "Objectness measure v1.5", http://groups.inf.ed.ac.uk/calvin/objectness/objectness-release-v1.5.tar.gz (2013).

Angles, R. and C. Gutierrez, "Survey of graph database models", ACM Computing Surveys (CSUR) **40**, 1, 1–39 (2008).

Athanasopoulos, E., A. Makridakis, S. Antonatos, D. Antoniades, S. Ioannidis, K. Anagnostakis and E. Markatos, "Antisocial networks: Turning a social network into a botnet", in "Proceedings of the 11th International Conference on Information Security (ISC)", (Springer, 2008).

Aviv, A., K. Gibson, E. Mossop, M. Blaze and J. Smith, "Smudge attacks on smartphone touch screens", in "Proceedings of the 4th USENIX conference on Offensive technologies", pp. 1–7 (USENIX Association, 2010).

Awerbuch, B., R. Curtmola, D. Holmer, C. Nita-Rotaru and H. Rubens, "Odsbr: An on-demand secure byzantine resilient routing protocol for wireless ad hoc networks", ACM Transactions on Information and System Security (TISSEC) **10**, 4, 1–35 (2008).

Bächer, P., T. Holz, M. Kötter and G. Wicherski, "Know your Enemy: Tracking Botnets–Using honeynets to learn more about Bots", (2005).

Ballard, D., "Generalizing the hough transform to detect arbitrary shapes", Pattern recognition **13**, 2, 111–122 (1981).

Barrantes, E., D. Ackley, T. Palmer, D. Stefanovic and D. Zovi, "Randomized instruction set emulation to disrupt binary code injection attacks", in "Proceedings of the ACM Conference on Computer and Communications Security (CCS)", pp. 281–289 (2003).

Bianchini, M., M. Gori and F. Scarselli, "Inside pagerank", ACM Transactions on Internet Technology (TOIT) **5**, 1, 92–128 (2005).

Bicakci, K., N. Atalay, M. Yuceel, H. Gurbaslar and B. Erdeniz, "Towards usable solutions to graphical password hotspot problem", in "Proceedings of the 33rd Annual IEEE International on Computer Software and Applications Conference", vol. 2, pp. 318–323 (IEEE, 2009).

Biddle, R., S. Chiasson and P. Van Oorschot, "Graphical passwords: Learning from the first twelve years", ACM Computing Surveys **44**, 4, 2012 (2011).

Bishop, C. M. and N. M. Nasrabadi, *Pattern recognition and machine learning*, vol. 1 (Springer New York, 2006).

Bonneau, J., S. Preibusch and R. Anderson, "A birthday present every eleven wallets? the security of customer-chosen banking pins", Proceedings of the Financial Cryptography and Data Security pp. 25–40 (2012).

Borders, K., A. Prakash and M. Zielinski, "Spector: Automatically analyzing shell code", in "Proceedings of the Annual Computer Security Applications Conference (ACSAC)", pp. 501–514 (2007).

Boser, B., I. Guyon and V. Vapnik, "A training algorithm for optimal margin classifiers", in "Proceedings of the fifth annual workshop on Computational learning theory (COLT)", pp. 144–152 (1992).

Brostoff, S. and M. Sasse, "Are passfaces more usable than passwords? a field trial investigation", People And Computers pp. 405–424 (2000).

Brumley, D., J. Newsome, D. Song, H. Wang and S. Jha, "Towards automatic generation of vulnerability-based signatures", in "Proceedings of the IEEE Symposium on Security and Privacy", (2006).

Caballero, J., P. Poosankam, C. Kreibich and D. Song, "Dispatcher: Enabling active botnet infiltration using automatic protocol reverse-engineering", in "Proceedings of the ACM Conference on Computer and Communications Security (CCS)", pp. 621–634 (2009).

Canny, J., "A computational approach to edge detection", IEEE Transactions on Pattern Analysis and Machine Intelligence , 6, 679–698 (1986).

Castelluccia, C., M. Dürmuth and D. Perito, "Adaptive password-strength meters from markov models", in "Proceedings of the 19th Network and Distributed System Security Symposium", vol. 2012 (2012).

Chakrabarti, S., "Dynamic personalized pagerank in entity-relation graphs", in "Proceedings of World Wide Web (WWW)", (2007).

Chang, C.-C. and C.-J. Lin, "LIBSVM: A library for support vector machines", ACM Transactions on Intelligent Systems and Technology (TIST) **2**, 27:1–27:27 (2011).

Chau, M. and J. Xu, "Mining communities and their relationships in blogs: A study of online hate groups", International Journal of Human-Computer Studies **65**, 1, 57–70 (2007).

Cheng, P., P. Rohatgi, C. Keser, P. Karger, G. Wagner and A. Reninger, "Fuzzy multi-level security: An Experiment on quantified risk-adaptive access control", in "Proceedings of the 28th IEEE Symposium on Security and Privacy", (2007).

Chiang, L. L., K., "A case study of the rustock rootkit and spam bot", in "Proceedings of Usenix Workshop on Hot Topics in Understanding Botnets", (2007).

Chiasson, S., A. Forget, R. Biddle and P. van Oorschot, "User interface design affects security: Patterns in click-based graphical passwords", International Journal of Information Security **8**, 6, 387–398 (2009).

Chiasson, S., E. Stobert, A. Forget, R. Biddle and P. Van Oorschot, "Persuasive cued click-points: Design, implementation, and evaluation of a knowledge-based authentication mechanism", IEEE Transactions on Dependable and Secure Computing **9**, 2, 222–235 (2012).

Chiasson, S., P. van Oorschot and R. Biddle, "Graphical password authentication using cued click points", pp. 359–374 (Springer, 2007).

Chinchani, R. and E. Van Den Berg, "A fast static analysis approach to detect exploit code inside network flows", in "Proceedings of the International Symposium on Research in Attacks, Intrusions and Defenses (RAID)", pp. 284–308 (2006).

Christodorescu, M., S. Jha, S. Seshia, D. Song and R. Bryant, "Semantics-aware malware detection", in "Proceedings of the IEEE Symposium on Security and Privacy", pp. 32–46 (2005).

Chung, S. and A. Mok, "Advanced allergy attacks: Does a corpus really help?", in "Proceedings of the International Symposium on Research in Attacks, Intrusions and Defenses (RAID)", pp. 236–255 (2007).

Cifuentes, C. and A. Fraboulet, "Intraprocedural static slicing of binary executables", in "Software Maintenance", pp. 188–195 (1997).

Clausen, T. and P. Jacquet, "Optimized Link State Routing Protocol", Network Working Group (2003).

Cortes, C. and V. Vapnik, "Support-vector networks", Machine learning **20**, 3, 273–297 (1995).

David Anselmi, N. S., Jimmy Kuo, *Microsoft Security Intelligence Report Volume 9* (Microsoft, 2010).

Davis, D., F. Monrose and M. Reiter, "On user choice in graphical password schemes", in "Proceedings of the 13th conference on USENIX Security Symposium", pp. 11–11 (USENIX Association, 2004).

Deng, H., W. Li and D. Agrawal, "Routing security in wireless ad hoc networks", IEEE Communications Magazine **40**, 10, 70–75 (2002).

Denning, D. E., "An intrusion detection model", pp. 119–131 (IEEE, 1986).

Detristan, T., "Polymorphic shellcode engine using spectrum analysis", in "Phrack Magazine", (2003).

Dhamija, R. and A. Perrig, "*Déjà* vu: A user study using images for authentication", in "Proceedings of the 9th conference on USENIX Security Symposium", (USENIX Association, 2000).

Dirik, A. E., N. Memon and J.-C. Birget, "Modeling user choice in the passpoints graphical password scheme", in "Proceedings of the 3rd symposium on Usable privacy and security", pp. 20–28 (ACM, 2007).

Dunham, K. and J. Melnick, *Malicious bots: an inside look into the cyber-criminal underground of the internet* (Auerbach Pub, 2008).

Dunphy, P. and J. Yan, "Do background images improve draw a secret graphical passwords?", in "Proceedings of the 14th ACM conference on Computer and communications security", pp. 36–47 (ACM, 2007).

Everingham, M., L. Van Gool, C. K. I. Williams, J. Winn and A. Zisserman, "The PASCAL Visual Object Classes Challenge 2007 (VOC2007) Results", http://www.pascal-network.org/challenges/VOC/voc2007/workshop/index.html (2007).

Fall, K. and K. Varadhan, "The ns Manual", (2010).

Feige, U., L. Lovász and P. Tetali, "Approximating min sum set cover", Algorithmica **40**, 4, 219–234 (2004).

Felix, J., C. Joseph, B.-S. Lee, A. Das and B. Seet, "Cross-layer detection of sinking behavior in wireless ad hoc networks using svm and fda", IEEE Transactions on Dependable and Secure Computing (TDSC) **8**, 2, 233–245 (2011).

Fogla, P., M. Sharif, R. Perdisci, O. Kolesnikov and W. Lee, "Polymorphic blending attacks", in "Proceedings of the USENIX Security Symposium", pp. 241–256 (2006).

Foley, M. J., "Microsoft: 60 million windows 8 licenses sold to date", http://www.zdnet.com/microsoft-60-million-windows-8-licenses-sold-to-date-7000009549/ (2013).

Forget, A., S. Chiasson and R. Biddle, "Shoulder-surfing resistance with eye-gaze entry in cued-recall graphical passwords", in "Proceedings of the 28th international conference on Human factors in computing systems", pp. 1107–1110 (ACM, 2010).

Gao, H., X. Guo, X. Chen, L. Wang and X. Liu, "Yagp: Yet another graphical password strategy", in "Proceedings of the 24th Annual Computer Security Applications Conference", pp. 121–129 (IEEE, 2008).

Goodin, D., "Online crime gangs embrace open source ethos, http://www.theregister.co.uk/2008/01/17/globalization_of_crimeware/", (2008).

Gu, B., X. Bai, Z. Yang, A. Champion and D. Xuan, "Malicious shellcode detection with virtual memory snapshots", in "Proceedings of the International Conference on Computer Communications (INFOCOM)", pp. 1–9 (2010).

Gu, G., P. Porras, V. Yegneswaran, M. Fong and W. Lee, "Bothunter: Detecting malware infection through ids-driven dialog correlation", in "Proceedings of USENIX Security Symposium", (USENIX Association, 2007).

Holt, G. W. B., Thomas J. and A. M. Bossler., "Social Learning and Cyber Deviance: Examining the Importance of a Full Social Learning Model in the Virtual World", Journal of Crime and Justice p. 33 (2010).

Holt, T. J., "Social Networks in the Computer Underground", URL `http://www.theregister.co.uk/2008/01/17/globalizationofcrimeware` (2008).

Horspool, R. and N. Marovac, "An approach to the problem of detranslation of computer programs", The Computer Journal **23**, 3, 223 (1980).

Hu, H., G.-J. Ahn, W. Han and Z. Zhao, "Flowguard: Building robust firewalls for software-defined networks", in "Proceedings of ACM SIGCOMM Workshop on Hot Topics in Software Defined Networking (HotSDN)", (ACM, 2014a).

Hu, H., G.-J. Ahn, W. Han and Z. Zhao, "Towards a reliable sdn firewall", in "Proceedings of the Open Networking Summit 2014 (ONS)", (USENIX, 2014b).

Hu, H., G.-J. Ahn and J. Jorgensen, "Enabling collaborative data sharing in google+", in "Proceedings of the 2012 IEEE Global Communications Conference (GLOBECOM)", pp. 720–725 (IEEE, 2012).

Hu, H., G.-J. Ahn, Z. Zhao, J. Jorgensen and D. Yang, "Game theoretic analysis of multiparty privacy control in online social networks.", in "Proceedings of the ACM Symposium on Access Control Models and Technologies", (2014c).

Hu, Y., D. Johnson and A. Perrig, "SEAD: Secure efficient distance vector routing for mobile wireless ad hoc networks", Ad Hoc Networks **1**, 1, 175–192 (2003).

Hu, Y. and A. Perrig, "A survey of secure wireless ad hoc routing", IEEE Security and Privacy magazine **2**, 28–39 (2004).

Hu, Y., A. Perrig and D. Johnson, "Packet leashes: a defense against wormhole attacks in wireless networks", in "Proceedings of the 23nd Annual IEEE International Conference on Computer Communications (INFOCOM)", vol. 3, pp. 1976–1986 (2004).

Hu, Y., A. Perrig and D. Johnson, "Ariadne: A secure on-demand routing protocol for ad hoc networks", Wireless Networks **11**, 1, 21–38 (2005).

IC3, "Internet Crime Report 2009. http://www.ic3.gov/media/annualreport/2009-ic3report.pdf", (2009).

Intel, "Intel 8086 family user's manual", (1979).

Intel, "Opencv", http://opencv.willowgarage.com (2014).

Jermyn, I., A. Mayer, F. Monrose, M. Reiter and A. Rubin, "The design and analysis of graphical passwords", in "Proceedings of the 8th USENIX Security Symposium", pp. 1–14 (Washington DC, 1999).

Jing, Y., G.-J. Ahn, Z. Zhao and H. Hu, "Riskmon: Continuous and automated risk assessment for mobile applications", in "Proceedings of 4th ACM Conference on Data and Applications Security (CODASPY)", pp. 99–110 (ACM, 2014).

Johnson, J., "Picture gesture authentication", (US Patent 163201, 2012).

Kanich, C., C. Kreibich, K. Levchenko, B. Enright, G. Voelker, V. Paxson and S. Savage, "Spamalytics: An empirical analysis of spam marketing conversion", in "Proceedings of the 15th ACM conference on Computer and Communications Security (CCS)", pp. 3–14 (ACM, 2008).

Kannhavong, B., H. Nakayama, Y. Nemoto, N. Kato and A. Jamalipour, "A survey of routing attacks in mobile ad hoc networks", IEEE Wireless Communications Magazine **14**, 5, 85–91 (2007).

Karlof, C. and D. Wagner, "Secure routing in wireless sensor networks: Attacks and countermeasures", Ad hoc networks **1**, 2-3, 293–315 (2003).

Keeney, R. and H. Raiffa, "Decisions with multiple objectives", Cambridge Books (1993).

Kelley, P., S. Komanduri, M. Mazurek, R. Shay, T. Vidas, L. Bauer, N. Christin, L. Cranor and J. Lopez, "Guess again (and again and again): Measuring password strength by simulating password-cracking algorithms", in "Proceedings of the IEEE Symposium on Security and Privacy", pp. 523–537 (IEEE, 2012).

Kleinberg, J., "Authoritative sources in a hyperlinked environment", Journal of the ACM (JACM) **46**, 5, 604–632 (1999).

Kolter, J. and M. Maloof, "Learning to detect and classify malicious executables in the wild", The Journal of Machine Learning Research **7**, 2721–2744 (2006).

Kong, D., D. Tian, P. Liu and D. Wu, "Sa3: Automatic semantic aware attribution analysis of remote exploits", in "International Conference on Security and Privacy in Communication Networks", pp. 1–19 (2011).

Kruegel, C., E. Kirda, D. Mutz, W. Robertson and G. Vigna, "Polymorphic worm detection using structural information of executables", in "Proceedings of the International Symposium on Research in Attacks, Intrusions and Defenses (RAID)", pp. 207–226 (2006).

Kurosawa, S., H. Nakayama, N. Kato and A. Jamalipour, "Detecting blackhole attack on AODV-based mobile ad hoc networks by dynamic learning method", International Journal of Network Security **105**, 627, 65–68 (2006).

Landi, W., "Undecidability of static analysis", ACM Letters on Programming Languages and Systems (LOPLAS) **1**, 4, 323–337 (1992).

Levine, B., C. Shields and E. Belding-Royer, "A secure routing protocol for ad hoc networks", in "Proceedings of 10th IEEE International Conference on Network Protocols (ICNP)", pp. 78–88 (2002).

Li, L., X. Zhao and G. Xue, "Searching in the dark: A framework for authenticating unknown users in online social networks", in "Proceedings of the 2012 IEEE Global Communications Conference (GLOBECOM)", pp. 714–719 (IEEE, 2012).

Li, L., X. Zhao and G. Xue, "A lightweight system to authenticate smartphones in the near field without nfc chips", in "Proceedings of the IEEE International Conference on Communications (ICC)", pp. 6391–6395 (IEEE, 2013a).

Li, L., X. Zhao and G. Xue, "Near field authentication for smart devices", in "Proceedings of the IEEE INFOCOM", pp. 375–379 (IEEE, 2013b).

Li, L., X. Zhao and G. Xue, "Unobservable reauthentication for smart phones", in "Proceedings of the 20th Network and Distributed System Security Symposium (NDSS)", vol. 13 (2013c).

Li, Z., M. Sanghi, Y. Chen, M. Kao and B. Chavez, "Hamsa: Fast signature generation for zero-day polymorphicworms with provable attack resilience", in "Proceedings of the IEEE Symposium on Security and Privacy", (2006).

Li, Z., L. Wang, Y. Chen and Z. Fu, "Network-based and attack-resilient length signature generation for zero-day polymorphic worms", in "Proceedings of the IEEE International Conference on Network Protocols (ICNP)", pp. 164–173 (2007).

Linn, C. and S. Debray, "Obfuscation of executable code to improve resistance to static disassembly", in "Proceedings of the ACM Conference on Computer and Communications Security (CCS)", pp. 290–299 (2003).

Lu, Y., M. Polgar, X. Luo and Y. Cao, "Social Network Analysis of a Criminal Hacker Community", Journal of Computer Information Systems pp. 31–42 (2010).

Marti, S., T. Giuli, K. Lai and M. Baker, "Mitigating routing misbehavior in mobile ad hoc networks", in "Proceedings of the 6th ACM International Conference on Mobile Computing and Networking (MOBICOM)", pp. 255–265 (2000).

Mason, J., S. Small, F. Monrose and G. MacManus, "English shellcode", in "Proceedings of the ACM Conference on Computer and Communications Security (CCS)", pp. 524–533 (2009).

Microsoft, "Data Execution Prevention (DEP) feature in Windows XP", (2006).

Microsoft, "Microsoft by the numbers", http://www.microsoft.com/en-us/news/bythenumbers/ms_numbers.pdf (2013).

Mitre, "2011 CWE/SANS Top 25 Most Dangerous Software Errors. http://cwe.mitre.org/top25/", (2011).

Mohammed, N., H. Otrok, L. Wang, M. Debbabi and P. Bhattacharya, "Mechanism design-based secure leader election model for intrusion detection in manet", IEEE Transactions on Dependable and Secure Computing (TDSC) **8**, 1, 89–103 (2011).

Moore, H., "The metasploit project. http://www.metasploit.com/", (2009).

Mu, C., X. Li, H. Huang and S. Tian, "Online risk assessment of intrusion scenarios using D-S evidence theory", in "Proceedings of the 13th European Symposium on Research in Computer Security (ESORICS)", pp. 35–48 (2008).

Mushtaq, A., "Smashing the Mega-d/Ozdok botnet in 24 hours, http://blog.fireeye.com/research/2009/11/smashing-the-ozdok.html", (2009).

Newsome, J., B. Karp and D. Song, "Polygraph: Automatically generating signatures for polymorphic worms", in "Proceedings of the IEEE Symposium on Security and Privacy", pp. 226–241 (2005).

Newsome, J. and D. Song, "Dynamic taint analysis for automatic detection, analysis, and signature generation of exploits on commodity software", in "Proceedings of the Network and Distributed System Security Symposium (NDSS)", (2005).

One, A., "Smashing the stack for fun and profit", Phrack magazine **7**, 49 (1996).

Oorschot, P. and J. Thorpe, "On predictive models and user-drawn graphical passwords", ACM Transactions on Information and system Security (TISSEC) **10**, 4, 5 (2008).

Ovide, S., "Microsoft's windows 8 test: Courting consumers", (2012).

Pace, Z., "Signing in with a picture password", http://blogs.msdn.com/b/b8/archive/2011/12/16/signing-in-with-a-picture-password.aspx (2011a).

Pace, Z., "Signing into windows 8 with a picture password", http://www.youtube.com/watch?v=Ek9N2tQzHOA (2011b).

Page, L., S. Brin, R. Motwani and T. Winograd, "The pagerank citation ranking: Bringing order to the web.", Technical Report 1999-66, Stanford InfoLab, URL `http://ilpubs.stanford.edu:8090/422/`, previous number = SIDL-WP-1999-0120 (1999a).

Page, L., S. Brin, R. Motwani and T. Winograd, "The PageRank Citation Ranking: Bringing Order to the Web.", (1999b).

Park, Y. and D. Reeves, "Identification of Bot Commands by Run-Time Execution Monitoring", in "Proceedings of the 25th Annual Computer Security Applications Conference (ACSAC)", pp. 321–330 (IEEE, 2009).

Perkins, C., E. Belding-Royer and S. Das, "Ad hoc on-demand distance vector routing", Mobile Ad-hoc Network Working Group **3561** (2003).

Polychronakis, M., K. Anagnostakis and E. Markatos, "Emulation-based detection of non-self-contained polymorphic shellcode", in "Proceedings of the International Symposium on Research in Attacks, Intrusions and Defenses (RAID)", pp. 87–106 (2007).

Porras, P., H. Saidi and V. Yegneswaran, "A foray into Conficker logic and rendezvous points", in "Proceedings of the 2nd USENIX Workshop on Large-Scale Exploits and Emergent Threats (LEET)", (2009).

Raymond, E., *The new hacker's dictionary* (The MIT press, 1996).

Refaei, M., L. DaSilva, M. Eltoweissy and T. Nadeem, "Adaptation of reputation management systems to dynamic network conditions in ad hoc networks", IEEE Transactions on Computers pp. 707–719 (2010).

Reimondo, A., "Haar cascades", http://alereimondo.no-ip.org/OpenCV/34 (2008).

Rescue, D., "IDA Pro Disassembler. http://www.datarescue.com/idabase", (2006).

Ros, F., "UM-OLSR implementation (version 0.8.8) for NS2", (2007).

Rosenblum, N., B. Miller and X. Zhu, "Extracting compiler provenance from program binaries", in "Proceedings of the 9th ACM SIGPLAN-SIGSOFT workshop on Program analysis for software tools and engineering (PASTE)", pp. 21–28 (2010).

Salehi-Abari, A., J. Thorpe and P. Van Oorschot, "On purely automated attacks and click-based graphical passwords", in "Proceedings of the 24th Annual Computer Security Applications Conference", pp. 111–120 (IEEE, 2008).

Salton, G. and C. Buckley, "Term-weighting approaches in automatic text retrieval", Information processing & management **24**, 5, 513–523 (1988).

Schechter, S. E., R. Dhamija, A. Ozment and I. Fischer, "The emperor's new security indicators", in "Proceedings of the 2007 IEEE Symposium on Security and Privacy", pp. 51–65 (IEEE, 2007).

Security, M., "Security Labs Report January - June 2010 Recap", (2010).

Sentz, K. and S. Ferson, "Combination of evidence in Dempster-Shafer theory", Tech. rep., Sandia National Laboratories (2002).

Shacham, H., M. Page, B. Pfaff, E. Goh, N. Modadugu and D. Boneh, "On the effectiveness of address-space randomization", in "Proceedings of the ACM Conference on Computer and Communications Security (CCS)", pp. 298–307 (2004).

Shafer, G., *A mathematical theory of evidence* (Princeton university press, 1976).

Song, Y., M. Locasto, A. Stavrou, A. Keromytis and S. Stolfo, "On the infeasibility of modeling polymorphic shellcode", in "Proceedings of the ACM Conference on Computer and Communications Security (CCS)", pp. 541–551 (2007).

Stone-Gross, B., M. Cova, L. Cavallaro, B. Gilbert, M. Szydlowski, R. Kemmerer, C. Kruegel and G. Vigna, "Your botnet is my botnet: Analysis of a botnet takeover", in "Proceedings of Computer and Communications Security (CCS)", (ACM, 2009).

Strasburg, C., N. Stakhanova, S. Basu and J. Wong, "Intrusion response cost assessment methodology", in "Proceedings of the 4th ACM Symposium on Information, Computer, and Communications Security (ASIACCS)", pp. 388–391 (2009).

Sun, L., R. Srivastava and T. Mock, "An information systems security risk assessment model under the Dempster-Shafer theory of belief functions", Journal of Management Information Systems **22**, 4, 109–142 (2006a).

Sun, Y., W. Yu, Z. Han and K. Liu, "Information theoretic framework of trust modeling and evaluation for ad hoc networks", IEEE Journal on Selected Areas in Communications (JSAC) **24**, 2, 305–317 (2006b).

Suo, X., Y. Zhu and G. Owen, "Graphical passwords: A survey", in "Proceedings of the 21st Annual Computer Security Applications Conference", pp. 10–19 (IEEE, 2005).

Suzuki, S. *et al.*, "Topological structural analysis of digitized binary images by border following", Computer Vision, Graphics, and Image Processing **30**, 1, 32–46 (1985).

Tan, P.-N. *et al.*, *Introduction to data mining* (Pearson Education India, 2007).

Teo, L., G. Ahn and Y. Zheng, "Dynamic and risk-aware network access management", in "Proceedings of the 8th ACM Symposium on Access Control Models and Technologies (SACMAT)", p. 230 (2003).

Theodoridis, S. and K. Koutroumbas, *Pattern Recognition* (Academic Press, 2008).

Thomas, K., "The Koobface botnet and the rise of social malware", in "Proceedings of the 5th IEEE International Conference on Malicious and Unwanted Software (MALWARE)", pp. 1–8 (2010).

Thorpe, J. and P. Van Oorschot, "Graphical dictionaries and the memorable space of graphical passwords", in "Proceedings of the 13th conference on USENIX Security Symposium", pp. 10–10 (USENIX Association, 2004a).

Thorpe, J. and P. Van Oorschot, "Towards secure design choices for implementing graphical passwords", in "Proceedings of the 20th Annual Computer Security Applications Conference", pp. 50–60 (IEEE, 2004b).

Thorpe, J. and P. van Oorschot, "Human-seeded attacks and exploiting hot-spots in graphical passwords", in "Proceedings of 16th USENIX Security Symposium", p. 8 (USENIX Association, 2007).

Toth, T. and C. Kruegel, "Accurate buffer overflow detection via abstract payload execution", in "Proceedings of the International Symposium on Research in Attacks, Intrusions and Defenses (RAID)", pp. 274–291 (2002a).

Toth, T. and C. Kruegel, "Evaluating the impact of automated intrusion response mechanisms", in "Proceedings of the 18th Annual Computer Security Applications Conference (ACSAC)", pp. 9–13 (2002b).

Tseng, C., T. Song, P. Balasubramanyam, C. Ko and K. Levitt, "A specification-based intrusion detection model for OLSR", in "Proceedings of the 9th international symposium on recent advances in intrusion detection (RAID)", pp. 330–350 (2006a).

Tseng, C., S. Wang, C. Ko and K. Levitt, "Demem: Distributed evidence-driven message exchange intrusion detection model for manet", in "Proceedings of the 9th International Symposium on Recent Advances in Intrusion Detection (RAID)", pp. 249–271 (2006b).

van Oorschot, P. and J. Thorpe, "Exploiting predictability in click-based graphical passwords", Journal of Computer Security **19**, 4, 669–702 (2011).

Vaqxine, "30 of the hottest DoS tools", (2008).

Viola, P. and M. Jones, "Robust real-time face detection", International journal of computer vision **57**, 2, 137–154 (2004).

Vogt, P., F. Nentwich, N. Jovanovic, E. Kirda, C. Kruegel and G. Vigna, "Cross site scripting prevention with dynamic data tainting and static analysis", in "Proceedings of the Network and Distributed System Security Symposium (NDSS)", (2007).

Wang, K., G. Cretu and S. Stolfo, "Anomalous payload-based worm detection and signature generation", in "Proceedings of the International Symposium on Research in Attacks, Intrusions and Defenses (RAID)", pp. 227–246 (2006a).

Wang, S., C. Tseng, K. Levitt and M. Bishop, "Cost-sensitive intrusion responses for mobile ad hoc networks", in "Proceedings of the 10th International Symposium on Recent Advances in Intrusion Detection (RAID)", pp. 127–145 (2007).

Wang, X., Y. Jhi, S. Zhu and P. Liu, "Still: Exploit code detection via static taint and initialization analyses", in "Proceedings of the Annual Computer Security Applications Conference (ACSAC)", pp. 289–298 (2008).

Wang, X., C. Pan, P. Liu and S. Zhu, "Sigfree: a signature-free buffer overflow attack blocker", in "Proceedings of the USENIX Security Symposium", (2006b).

Wartell, R., Y. Zhou, K. Hamlen, M. Kantarcioglu and B. Thuraisingham, "Differentiating code from data in x86 binaries", in "Proceedings of the European Conference on Machine Learning and Principles and Practice of Knowledge Discovery in Databases", pp. 522–536 (2011).

Weinberger, J., P. Saxena, D. Akhawe, M. Finifter, R. Shin and D. Song, "A systematic analysis of xss sanitization in web application frameworks", in "Proceedings of the European Symposium on Research in Computer Security (ESORICS)", (2011).

Wiedenbeck, S., J. Waters, J. Birget, A. Brodskiy and N. Memon, "Authentication using graphical passwords: effects of tolerance and image choice", in "Proceedings of the Symposium on Usable privacy and security", pp. 1–12 (ACM, 2005).

Wu, H., M. Siegel, R. Stiefelhagen and J. Yang, "Sensor fusion using Dempster-Shafer theory", in "Proceedings of IEEE Instrumentation and Measurement Technology Conference", vol. 1, pp. 7–12 (2002).

Wu, Z., S. Gianvecchio, M. Xie and H. Wang, "Mimimorphism: a new approach to binary code obfuscation", in "Proceedings of the ACM Conference on Computer and Communications Security (CCS)", pp. 536–546 (2010).

Xu, J. and H. Chen, "CrimeNet explorer: a framework for criminal network knowledge discovery", ACM Transactions on Information Systems (TOIS) **23**, 2, 201–226 (2005).

Yager, R., "On the dempster-shafer framework and new combination rules", Information sciences **41**, 2, 93–137 (1987).

Yamada, M. and M. Kudo, "Combination of weak evidences by D-S theory for person recognition", in "Knowledge-Based Intelligent Information and Engineering Systems", pp. 1065–1071 (2004).

Yarochki, F. V., "From Russia with love.exe, http://www.seacure.it/archive/2009/stuff/Seacure2009FyodorYarochkin-FromRussiaWithLove.pdf", (2009).

Yuille, J. C., *Imagery, memory, and cognition* (Lawrence Erlbaum Assoc Inc, 1983).

Zadeh, L., "Review of A Mathematical Theory of Evidence", AI Magazine **5**, 3, 81 (1984).

Zakaria, N., D. Griffiths, S. Brostoff and J. Yan, "Shoulder surfing defence for recall-based graphical passwords", in "Proceedings of the 7th Symposium on Usable Privacy and Security", p. 6 (ACM, 2011).

Zhang, H., C. Papadopoulos and D. Massey, "Detecting encrypted botnet traffic", in "Proceedings of the 2013 IEEE Conference on Computer Communications Workshops (INFOCOM WKSHPS)", pp. 163–168 (IEEE, 2013).

Zhang, Q. and B. Li, "Discriminative k-svd for dictionary learning in face recognition", in "Proceedings of the 2010 IEEE Conference on Computer Vision and Pattern Recognition (CVPR)", pp. 2691–2698 (IEEE, 2010).

Zhang, Q. and B. Li, "Mining discriminative components with low-rank and sparsity constraints for face recognition", in "Proceedings of the 18th ACM SIGKDD international conference on Knowledge discovery and data mining", pp. 1469–1477 (ACM, 2012).

Zhang, Y., F. Monrose and M. Reiter, "The security of modern password expiration: An algorithmic framework and empirical analysis", in "Proceedings of the 17th ACM conference on Computer and communications security", pp. 176–186 (ACM, 2010).

Zhao, X., L. Li and G. Xue, "Keeping identity secret in online social networks", in "Proceedings of the 7th ACM Symposium on Information, Computer and Communications Security (ASIACCS)", pp. 55–56 (ACM, 2012a).

Zhao, Z., G.-J. Ahn, , J. Seo and H. Hu, "On the security of picture gesture authentication.", in "Proceedings of the 22nd USENIX Security Symposium", pp. 383–398 (2014).

Zhao, Z. and G.-J. Ahn, "Using instruction sequence abstraction for shellcode detection and attribution", in "Proceedings of 2013 IEEE Conference on Communications and Network Security (CNS)", pp. 323–331 (IEEE, 2013).

Zhao, Z., G.-J. Ahn and H. Hu, "Automatic extraction of secrets from malware", in "Proceedings of 18th Working Conference on Reverse Engineering (WCRE)", pp. 159–168 (IEEE, 2011a).

Zhao, Z., G.-J. Ahn and H. Hu, "Examining social dynamics for countering botnet attacks", in "Proceedings of 2011 IEEE Global Telecommunications Conference (GLOBECOM)", pp. 1–5 (IEEE, 2011b).

Zhao, Z., G.-J. Ahn, H. Hu and D. Mahi, "Socialimpact: systematic analysis of underground social dynamics", in "Proceedings of European Symposium on Research in Computer Security (ESORICS)", pp. 877–894 (Springer, 2012b).

Zhao, Z., H. Hu, G.-J. Ahn and R. Wu, "Risk-aware response for mitigating manet routing attacks", in "Proceedings of 2010 IEEE Global Telecommunications Conference (GLOBECOM)", pp. 1–6 (IEEE, 2010).

Zhao, Z., H. Hu, G.-J. Ahn and R. Wu, "Risk-aware mitigation for manet routing attacks", IEEE Transactions on Dependable and Secure Computing pp. 250–260 (2012c).

Zheleva, E. and L. Getoor, "To join or not to join: the illusion of privacy in social networks with mixed public and private user profiles", in "Proceedings of the 18th International Conference on World Wide Web (WWW)", pp. 531–540 (ACM, 2009).

Zhou, Y., E. Reid, J. Qin, H. Chen and G. Lai, "US domestic extremist groups on the Web: link and content analysis", IEEE intelligent systems pp. 44–51 (2005).